# Silane Bridge Deck Rating

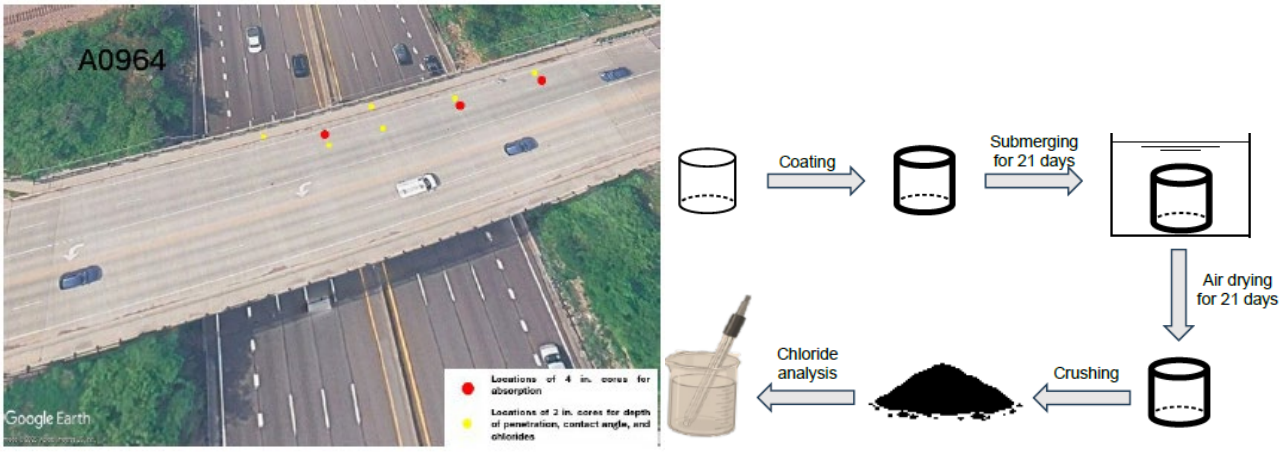



July 2026
Final Report

Project number TR202413
MoDOT Research Report number cmr 26-010



**PREPARED BY:**

Ahmed I. Ghazal

John J. Myers

Mohamed A. ElGawady

Missouri University of Science and Technology


**PREPARED FOR:**

Missouri Department of Transportation

Construction and Materials Division Research Section

# Technical Report Documentation Page

| | | |
|---|---|---|
| 1. Report No. | 2. Government Accession No. ] | 3. Recipient's Catalog No. |
| 4. Title and Subtitle<br>Silane Bridge Deck Rating | | 5. Report Date<br>July 2026 |
| | | 6. Performing Organization Code |
| 7. Author(s)<br>Ahmed I. Ghazal<br>John J. Myers<br>Mohamed A. ElGawady | | 8. Performing Organization Report No. |
| 9. Performing Organization Name and Address<br>Missouri University of Science and Technology<br>1401 N. Pine st.<br>Rolla MO 65401 | | 10. Work Unit No. (TRAIS) |
| | | 11. Contract or Grant No.<br>MoDOT project #TR202413 |
| 12. Sponsoring Agency Name and Address<br>Missouri Department of Transportation<br>1617 Missouri Boulevard<br>Jefferson City, MO 65102 | | 13. Type of Report and Period Covered<br>Final Report |
| | | 14. Sponsoring Agency Code |
| 15. Supplementary Notes | | |

16. Abstract

Bridge decks are among the most vulnerable components of bridge structures due to the combined effects of multiple deterioration mechanisms, including traffic-induced abrasion, repeated freeze-thaw cycling, and chloride ingress. Surface impregnation using silane sealers has proven to be an effective method for mitigating concrete deterioration in bridge decks. In this study, the performance of various silane sealers and silane-nanoclay composite systems was extensively evaluated to assess their ability to protect bridge decks against deterioration mechanisms such as freeze-thaw cycling, capillary absorption, chloride ingress, and surface scaling. In addition, the service life of silane and silane-nanoclay composite systems was estimated. A field evaluation was conducted on bridge decks that had been in service for approximately 8 years. The evaluation included measurements of depth of penetration, static contact angle, chloride ingress, and rate of absorption. The results demonstrate that silane treatments represent a viable option for protecting bridge decks against deterioration. However, silane-nanoclay composites exhibited increased chloride ingress under aggressive exposure conditions and greater surface scaling under exposure to deicing chemicals. The field investigation demonstrated a wide range of performance among the bridge decks evaluated. Nevertheless, following early-age applications, silane treatments can be successfully reapplied at intervals of approximately 5 years to maintain long-term protective performance.

| | | | |
|---|---|---|---|
| 17. Key Words<br>Bridge decks, Silanes, Silane-nanoclay composites, Cracked and uncracked concrete, Electrical resistivity, Chloride penetration, Freeze-thaw cycling, Frost scaling, Capillary suction, Service life. | | 18. Distribution Statement<br>[Leave blank] | |
| 19. Security Classification (of this report)<br>Unclassified | 20. Security Classification (of this page)<br>Unclassified | 21. No. of Pages<br>91 | 22.<br>Price |

Form DOT F 1700.7 (8-72) Reproduction of completed page authorized

# Silane Bridge Deck Rating

*By*
Ahmed I. Ghazal, John J. Myers, and Mohamed A. ElGawady
Missouri University of Science and Technology

*Prepared for*
Missouri Department of Transportation

July 2026

**Final Report**

[Report Number, If Applicable]

[Agency Logo, If Applicable]

# Copyright

Authors herein are responsible for the authenticity of their materials and for obtaining written permissions from publishers or individuals who own the copyright to any previously published or copyrighted material used herein.

# Disclaimer

The contents of this report reflect the views of the author(s) who is (are) responsible for the facts and accuracy of the data presented herein. The contents do not necessarily reflect the official views or policies of the Missouri Department of Transportation or the Federal Highway Administration. This report does not constitute a standard, specification, or regulation.

# Declaration of Generative Artificial Intelligence (AI), and AI Assisted Technologies

The use of unapproved, **open AI systems** (such as ChatGPT, Bing Chat, and other publicly available AI systems) for research report writing **is prohibited.** Open AI systems such as these, capture data that is entered into it and then uses that data for training their systems to respond to all users of the system. **This is the equivalent of publishing information onto a public website – a violation of MoDOT policy.** Researchers inputting data and information into an AI tool are prohibited from disclosing confidential data or information belonging to MoDOT or MoDOT's partners. Researchers must comply with MoDOT's policies concerning data and record retention, and the proper storage, handling and sharing of sensitive information.

# Acknowledgments

The authors wish to express their gratitude to the numerous individuals and organizations that contributed to the success of this research project. A heartfelt thank you is extended to the Missouri Department of Transportation (MoDOT) for their financial support, vision, and commitment to innovative concepts that pushed the boundaries of current practices. The authors would also like to sincerely acknowledge Jen Harper and Scott Breeding for their valuable guidance, support, and contributions throughout the project. The project's success was largely due to MoDOT's support, encouragement, and the collaborative efforts of all those involved.

Furthermore, the authors acknowledge Missouri University of Science and Technology for its significant contributions to this research. The dedicated efforts of the staff from the Department of Civil, Architectural, and Environmental Engineering and the Center for Infrastructure Engineering Studies were invaluable to the successful completion of this work. Special appreciation is extended to John Whitchurch for his extensive assistance with the experimental testing program, and to Jason Cox for his valuable technical support throughout the experimental phase of the study. The authors also gratefully acknowledge the contributions of the many undergraduate students who assisted with the experimental work. Finally, sincere appreciation is extended to Kayley Bozarth from the Missouri Center for Transportation Innovation for her assistance with the linguistic editing and formatting of the report.

# Executive Summary

This report presents an evaluation of the performance and service life of silanes for surface impregnation of bridge decks, based on both laboratory and field investigations. The propriety available silane sealers evaluated in this study included Protectosil SH100, Protectosil S300, Protectosil CIT, and SIL-ACT-ATS 200, all of which are listed on the Missouri Department of Transportation (MoDOT) Approved Products List. In addition, surface-modified organophilic montmorillonite nanoclay, containing 25–30% by weight trimethyl octadecyl ammonium chloride, was used to prepare silane-nanoclay composites for concrete surface treatment at loading ratios of 2.5% and 5.0%. The performance of the silane products and silane-nanoclay composites was evaluated using MoDOT Grade B2 and Grade B1 concrete, respectively. Evaluation methods included static contact angle, depth of penetration, salt absorption and vapor transmission, chloride ion penetration, surface and bulk resistivity, resistance to rapid freeze-thaw cycling, surface scaling under deicing chemicals, sorptivity, and water permeability. Characterization of the silane-nanoclay composites was conducted using scanning electron microscopy (SEM), X-ray diffraction (XRD), and Fourier transform infrared spectroscopy (FTIR).

The results demonstrate that silane impregnation provides an effective barrier against chloride ingress, reduces water absorption by capillary suction, mitigates surface scaling and associated mass loss under deicing-salt exposure, and limits the development of critical saturation during freeze–thaw cycling. Among the products evaluated, Protectosil SH100 and SIL-ACT-ATS 200 exhibited the best overall performance, followed by Protectosil S300. In comparison, Protectosil CIT was less effective as a surface impregnation treatment for bridge-deck concrete under the conditions investigated. Surface resistivity measurements of silane-treated concrete also correlated well with resistance to chloride-ion penetration.

Silane–nanoclay composites improved resistance to freeze–thaw deterioration and chloride ingress under the moderate chloride-exposure conditions investigated, including solutions containing up to 3% chloride. At the higher chloride concentrations evaluated, however, the silane–nanoclay composites exhibited increased chloride ingress, more extensive surface scaling, and greater capillary absorption. FTIR analysis indicated that the nanoclay may have experienced loss or alteration of its organic modifier under conditions of high ionic strength, which may have contributed to the observed reduction in performance. Further investigation is therefore recommended to evaluate silane–nanoclay systems incorporating alternative organic modifiers and smaller nanoclay particle sizes.

Using the service-life estimation approach adopted in this study and a 3% NaCl exposure condition consistent with the AASHTO T259 ponding procedure used within the SHRP C-103 research program, the estimated service lives of Protectosil SH100 and SIL-ACT-ATS 200 were approximately 5.4 and 5.0 years, respectively. The corresponding estimated service lives of the silane–nanoclay composites were 5.8 and 6.1 years for nanoclay loading ratios of 2.5% and 5.0%, respectively.

The field investigation revealed considerable variability in performance among the bridge decks evaluated. Bridge A8380 exhibited the best overall performance, demonstrating low water absorption and minimal chloride ingress. Although Bridge A0964 showed favorable absorption characteristics, significant chloride accumulation was measured in the near-surface region. In contrast, Bridge A8499 exhibited a higher rate of water absorption while maintaining a chloride profile comparable to that of Bridge A8380. Bridge A8495 demonstrated the poorest performance, with elevated chloride concentrations penetrating deeper into the concrete, and a high rate of water absorption. These findings indicate that Bridge A8495 requires rehabilitation to prevent further deterioration.

# Table of Contents

# List of Figures

# List of Tables

# List of Equations

# List of Abbreviations and Acronyms

| | |
|---|---|
| AASHTO | American Association of State Highway and Transportation |
| ARTBA | American Road and Transportation Builders Association (ARTBA) |
| ASCE | American Society of Civil Engineers |
| ASTM | American Society for Testing and Materials |
| FHWA | Federal Highway Administration |
| FTIR | Fourier Transform Infrared Spectroscopy |
| HR-XRD | High-Resolution X-Ray Diffraction |
| MoDOT | Missouri Department of Transportation |
| NCHRP | National Cooperative Highway Research Program |
| NDT | Non-Destructive Testing |
| SEM | Scanning Electron Microscopy |
| US | United States of America |
| XRD | X-Ray Diffraction |

# Chapter 1: Introduction

## 1.1 Background

Bridge structures, including bridge decks which are a focus of this investigation, are vulnerable to deterioration caused by chloride ingress from the extensive use of deicing chemicals used in cold climates, repeated freeze-thaw cycles, and surface scaling. The durability of concrete is largely governed by its inherent porosity and pore structure, which control the transport of fluids and aggressive agents into the interior of the material. In addition, concrete surfaces are susceptible to cracking due to shrinkage and applied loads, which further facilitates the ingress of deleterious substances, particularly chloride ions, and accelerate reinforcement corrosion. As deterioration progresses, the structural capacity of bridge components may be compromised, leading to increased maintenance demands and associated economic costs. According to the 2021 report by the American Society of Civil Engineers (ASCE), approximately 7.5% of bridges in the United States (US) is considered structurally deficient and estimated cost $125 billion needed for rehabilitation. According to 2025 report by American Road and Transportation Builders Association (ARTBA), 8.8% of bridges in Missouri are classified as structurally deficient. The Federal Highway Administration (FHWA) identifies corrosion of reinforcing steel in concrete decks and substructures as the primary deterioration mechanism.

Concrete bridge decks are among the most vulnerable components of bridge structure, as they are exposed to synergetic deterioration mechanisms, including freeze-thaw cycling, carbonation, and chloride ingress (Kuosa et al., 2014). This vulnerability is further exacerbated by intensive microcracking arising from early-age shrinkage particularly in elements with high surface-to-volume ratios.

To address these challenges, surface treatment of concrete has emerged as an effective strategy to modify transport properties and enhance durability, particularly in cold climates. Surface treatments are generally classified into four categories based on their mechanism of action: (a) hydrophobic pore lining, (b) pore blocking, (c) surface coating, and (d) multifunctional systems (Zheng et al., 2024; Pen et al., 2017). Although surface coatings can provide effective protection, they present several limitations, including higher cost, susceptibility to cracking and delamination, reduced fire resistance, and limited-service life. Consequently, surface impregnation using silicone-based materials has gained significant attention and has been widely adopted by the Missouri Department of Transportation (MoDOT) and other agencies for bridge deck protection. Silicone-based compounds offer advantages such as high thermal stability, hydrophobicity, vapor permeability (breathability), and resistance to biological and chemical attack. In addition, these materials can be modified or combined with other constituents to enhance their performance for cementitious surface treatments (Zheng et al., 2024).

## 1.2 Problem Statement and Research Significance

Bridge decks are exposed to aggressive environments characterized by freeze-thaw cycling and chloride-laden conditions. These exposures lead to progressive deterioration, cracking, and reduced structural integrity. Cracking further accelerates the ingress of harmful agents, exacerbating corrosion and durability issues. Collectively, these factors pose safety concerns and result in significant economic impacts due to increased maintenance and rehabilitation costs.

This research investigates alternative surface treatment approaches based on organosilanes for enhancing the durability of concrete bridge decks. The study evaluates and compares key durability-related properties of concrete treated with different sealing systems. In addition, the study examines the potential use of nondestructive testing (NDT) techniques as practical tools for quality control and in-situ performance assessment. Laboratory findings are further validated through field testing to demonstrate the effectiveness of organosilane-based treatments under real service conditions. The outcomes of this research are intended to support MoDOT engineers and practitioners by providing guidance on the selection, application, and performance evaluation of silane-based surface treatments for bridge deck protection.

## 1.3 Research Tasks

The primary objective of this study is to evaluate organosilane-based surface treatment systems for bridge deck applications and to develop best practices for their implementation and performance monitoring. The specific research tasks are as follows:

- Compare the durability-related properties of treated (sealed) and untreated (control) concrete.
- Assess the applicability of nondestructive testing methods for evaluating the effectiveness of surface treatments for in-situ applications.
- Investigate the efficacy of silane-nanoclay composites for sealing of concrete
- Estimate the service life of organosilane treatments as a critical factor in sealer selection and reapplication planning.
- Validate laboratory findings through field testing to assess the practical applicability and performance of organosilane treatments for bridge deck protection.

## 1.4 Report Content

This report comprises the following chapters:

Chapter 1: presents the introduction, including background information, the problem statement, research significance, research objectives, and the overall report structure.

Chapter 2: provides a comprehensive literature review. It covers the chemistry of organosilanes, distinguishes between water-based and solvent-based systems. In addition, the electrical properties of silane-treated concrete are reviewed, as well as their effectiveness in protecting cracked concrete and pavement joints. The potential benefits of incorporating nanoparticles, particularly nanoclay, into silane systems are also discussed.

Chapter 3: evaluates the performance of four commercially available silane products from the Missouri Department of Transportation (MoDOT) approved products list. The evaluation includes chloride penetration, salt scaling, capillary suction, and water permeation. The influence of silane treatments on surface resistivity is also assessed in an effort to correlate electrical properties with durability performance.

Chapter 4: examines the effect of incorporating nanoclay into the silane matrix on key durability properties, including chloride diffusion, freeze-thaw resistance, salt-frost scaling, capillary suction, and water permeation. This chapter also includes material characterization of silane-nanoclay composites to better understand the mechanisms associated with nanoclay incorporation.

Chapter 5: estimates the service life of neat silanes and silane-nanoclay composites adopted in chapter 4.

Chapter 6: presents the field evaluation of silane treatments applied to selected bridge decks in Missouri, focusing on in-service performance.

Chapter 7: summarizes the key findings of the study and provides recommendations for the selection, application, and performance evaluation of silane-based surface treatments.

# Chapter 2: Literature Review

## 2.1 Chemistry of Organosilanes

Silanes, including alkoxy silanes or organoalkoxy silanes, have the ability to form polymeric resin for treatment of surfaces through hydrolysis and polycondensation reactions as shown in Figure 2.1. Silanes are usually manufactured from organochlor silane to form a variety of structures that are commonly referred to as Q, T, D, and M structures (Nguyen, 1996). Each type can be completely defined by the specific arrangement around the silicon atoms to unhydrolyzed, hydrolyzed, and siloxane bondage.

It is of practical relevance to understand the reaction kinetics of the hydrolysis and condensation reaction. The reaction of silanes to form siloxane resin is dependent on the nature of silane, the type and percentage of the solvent, the catalyst, the water/silane ratio, temperature, pH, and ionic strength. It is well known that the reactions involved are proton transfer reactions.

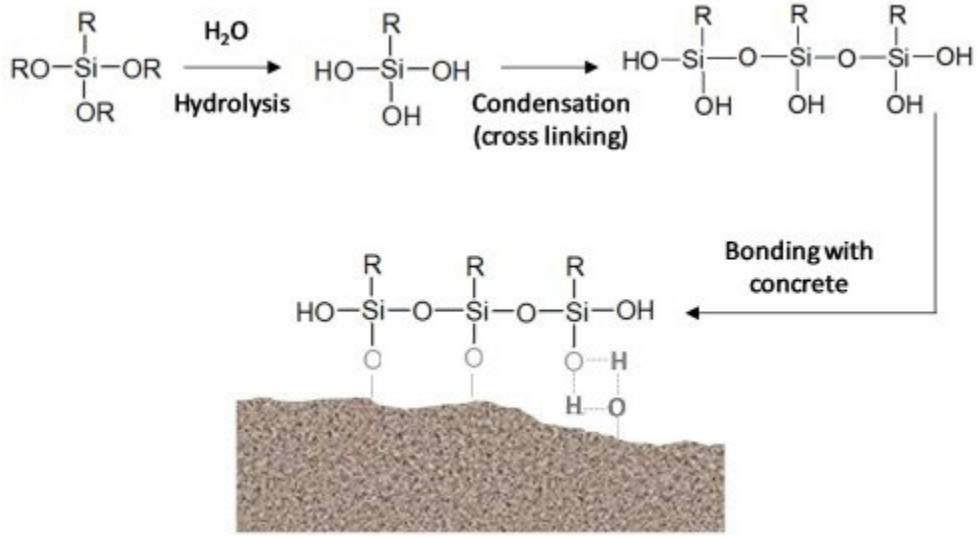


**Figure 2.1. Hydrolysis and condensation reactions of silanes with the cementious substrate (adopted from Mundo et al., 2020)**

Regarding the order of reaction, hydrolysis is first order with the silane concentration and range between 0.8 and 4.4 with respect to water based on the carrier. However, the condensation reaction is a second order with respect to the concentration of organosilanetriol. The condensation of silicic ester ranged between 1 and 5 with the order decreased in the presence of catalyst (Issa and Luyt, 2019).

Silane sealers are commonly classified as solvent-based or water-based, depending on the type of carrier used. Solvent-based formulations typically use alcohols, mineral spirits, or low-volatile organic compound solvents as carriers. In contrast, water-based formulations use water as the carrier in the form of emulsions, microemulsions, or water-dispersed silane systems. Solvent-

based silane systems achieve greater penetration depths and provide higher durability compared with water-based systems (Cady, 1994). Furthermore, the use of neat (carrier-free) silane has been reported to provide superior performance by allowing greater penetration of the active ingredient into the concrete substrate. Carter evaluated the performance of silane formulations containing 40% and 98% active ingredient with respect to damp-proofing effectiveness and penetration depth. After successive cycles of surface abrasion, concrete specimens treated with the 98% silane formulation retained a damp-proofing effectiveness of 89% after the second abrasion cycle, compared with only 49% for specimens treated with the 40% silane formulation (Carter, 1994).

## 2.2 Electrical resistivity of silane-treated concrete

The durability of concrete is largely governed by the mobility of ions within its pore structure, which controls the transport of aggressive species and influences the rate of deterioration. Azarsa and Gupta reported that the electrical resistivity of concrete is inversely related to permeability, reinforcement corrosion, and other durability-related properties (Azarsa and Gupta, 2017). However, for surface-treated concrete, these correlations are not as well established as they are for untreated concrete. McCarter evaluated the surface resistivity of silane-treated concrete following exposure to water and a 1 M sodium chloride (NaCl) solution. For specimens exposed to water, the surface resistivity of the treated concrete was approximately 15 times greater than that of the corresponding untreated specimens. Exposure to the chloride solution resulted in a significant reduction in resistivity and a smaller difference between treated and untreated concrete. Nevertheless, the treated specimens consistently exhibited higher resistivity than the untreated specimens (McCarter, 1996).

Nagaoka et al. (2023) investigated the protective effect of silane impregnation using spectroscopy. They reported an inverse power-law relationship between electrical resistivity and the effective chloride diffusion coefficient, except for oven-dried specimens, which exhibited high electrical resistivity but relatively high chloride diffusion coefficients. The authors also demonstrated that the electrical resistance of the silane-treated layer could be distinguished from that of the untreated concrete by interpreting the Nyquist plots obtained from the electrochemical impedance measurements (Nagaoka et al., 2023). Using both accelerated chloride migration and natural diffusion tests, Coppola et al. demonstrated a strong correlation between electrical conductivity and the chloride diffusion coefficient. This relationship was found to depend primarily on the water-to-cement ratio and the cement type. In contrast, varying the cement content at a constant water-to-cement ratio did not produce significant changes in the observed correlation (Coppola,2020).

At this point, it seems reasonable to discuss the electrical resistivity of integral hydrophobic concrete. Carette et al., investigated the early-age electrical behavior of bulk hydrophobic mortars prepared with CEM I and CEM III/A cements. The authors reported that the incorporation of a silane/silicone emulsion decreased the electrical resistivity of CEM I mortar but significantly increased the resistivity of CEM III/A mortar after approximately 200 h of curing. This behavior was attributed, at least in part, to differences in pore structure

development. In particular, the total porosity of the CEM I mortar increased by approximately 9% after one day, whereas a much smaller increase was observed for the CEM III/A mortar (Carette et al., 2020). Similarly, Wong et al. (2015) investigated the electrical conductivity of hydrophobic concrete incorporating wastepaper sludge ash. Prior to testing, the specimens were vacuum-saturated and subsequently immersed in water for 40 days. The electrical conductivity decreased with increasing wastepaper sludge ash content, which the authors attributed to a reduction in the amount of free water within the concrete pore structure (Wong et al., 2015).

## 2.3 Performance of Silane Sealers for Cracked Concrete and Pavement Joints

Chloride ion penetration in salt-laden environments presents a significant risk for corrosion of steel reinforcement in concrete structures. The ingress of chloride ions disrupts the passive oxide layer formed by the high alkalinity of concrete, thereby initiating corrosion of embedded steel. Several mitigation strategies are commonly employed, including increasing concrete cover, using cement with higher aluminate content to enhance chloride binding capacity, and incorporating corrosion inhibitors. Cracking in concrete is permitted within limits by most design codes. Surface cracks may also develop due to early-age shrinkage associated with rapid moisture loss. These cracks can serve as expedited pathways for chloride ingress in aggressive environments.

Dai et al. experimentally investigated the effect of silane impregnation applied before and after cracking on chloride penetration and reinforcement corrosion. The study reported that a penetration depth greater than 0.2 in. is required to achieve effective protection against chloride ingress. When silane was applied after cracking, effective protection was limited to crack widths up to approximately 0.003 in. In contrast, when applied prior to cracking, crack widths up to 0.008 in. could be tolerated. The authors recommended deep impregnation and reapplication after crack stabilization to extend the service life of reinforced concrete structures in marine environments (Dai et al., 2010). The influence of silane treatment applied before and after crack formation was also examined by Whittmann et al. Concrete prisms with crack widths of 0.004, 0.008, and 0.016 in. were exposed to a 3% NaCl solution for 28 days. Results showed increased chloride concentration ahead of the crack tip, attributed to microcracking within the fracture process zone. Surface impregnation with silane after crack formation was found to effectively reduce chloride ingress, largely independent of crack width. However, for specimens treated prior to cracking, effective protection was observed primarily for crack widths up to 0.004 in. (Whittmann et al., 2008).

In NCHRP Report 244, Pfeifer et al. evaluated the durability of cracked and uncracked concrete treated with various coating materials under accelerated weathering conditions simulating both northern and southern climates. Silane-treated specimens demonstrated excellent resistance to chloride penetration and reinforcement corrosion. However, under northern climate exposure involving freeze-thaw cycles, some deep surface deterioration was observed. This deterioration was attributed to the presence of sulfonic acid formation in the salt solution (NCHRP 244, 1981).

Tittarelli and Moriconi assessed the performance of silane as a water-repellent treatment in both cracked and uncracked concrete, with embedded steel plates used to monitor corrosion. At a water-to-cement ratio (w/c) of 0.8, silane treatment in uncracked concrete effectively prevented corrosion. However, in cracked specimens, corrosion rates were higher than those observed in untreated control samples. This behavior was attributed to increased oxygen diffusion through air-filled pores in hydrophobic (silane-treated) concrete, compared to water-filled pores in untreated concrete. It should be noted that, in this study, silane was incorporated into the concrete mixture rather than applied as a surface treatment, and specimens were totally submerged in a 3.5% NaCl solution and the oxygen availability was controlled by adequate recycling (Tittarelli and Moriconi, 2008).

In a field study, Xiao et al. evaluated the long-term performance of silane-treated pavement joints. After 8.2 yr of service, the silane layer remained effective, as evidenced by measurable penetration depth, increased surface contact angle, and reduced water absorption (Xiao et al., 2021). These results should not be directly extrapolated to bridge decks, as pavement joints are not subjected to tire-induced abrasion and are generally less exposed to ultraviolet (UV) degradation. In a laboratory investigation by the same authors, they confirmed significant reductions in water absorption and chloride ingress. Chloride reduction was reported as 27% in the near-surface layer (0.063–0.5 in.) and 15% in the deeper layer (0.5–1.0 in.) for ordinary Portland cement concrete. For fly ash-modified concrete, reductions reached 46% in the surface layer and 30% in the deeper layer. The authors recommended application under dry substrate conditions and the use of multiple applications at reduced coverage rates to ensure adequate penetration and performance (Adil et al., 2021).

## 2.4 Performance Evaluation of Silane-Nanocomposites

Silane-nanocomposites have recently emerged as a promising technology for the surface treatment of concrete, offering reduced permeability, improved resistance to ultraviolet (UV) degradation, and enhanced durability under aggressive environmental exposure. In these systems, silane primarily acts as a pore-lining agent, while nanoparticles penetrate the near-surface region and partially occlude capillary pores, thereby reducing transport properties (Li et al., 2018).

Compared to other nanomaterials commonly used in polymer-based coatings, nanoclay represents a cost-effective alternative (Piyush et al., 2025). Nanoclay consists of layered aluminosilicate structures that provide cation exchange sites, enabling organic modification of interlayer surfaces and improved compatibility with organic matrices (Ganguly et al., 2011; Uddin, 2008).

Due to these characteristics, nanoclay has gained considerable attention in polymer composite applications. Sakr and Bassuoni incorporated organically modified nanoclay, containing methyl tallow bis(2-hydroxyethyl) quaternary ammonium, and nanosilica into silane and methyl methacrylate matrices at loading levels of 5% and 10% by mass to develop nanocomposite

coatings for concrete exposed to freeze-thaw cycling and physical salt attack. The inclusion of nanoclay improved performance by forming interwoven barrier within the silane matrix, which limited salt crystal deposition and growth near the surface. However, higher loading levels resulted in reduced effectiveness, likely due to nanoparticle agglomeration. Overall, silane-based nanocomposites demonstrated superior resistance to salt-frost scaling compared to methyl methacrylate-based systems, particularly for lower-quality concrete (Sakr and Bassuoni, 2021).

Scarfato et al. developed nanocomposite coatings by intercalating montmorillonite nanoclay into two systems: (1) a blend of acrylic polymer and vinylidene fluoride, and (2) a siloxane-based formulation. The performance of these systems was evaluated in terms of transport properties, hydrophobicity, and resistance to sulfate attack. The addition of 6% nanoclay increased vapor barrier resistance by approximately 30%. Furthermore, the siloxane-based nanocomposite exhibited superior performance due to its hydrophobic characteristics combined with the pore-blocking effect of nanoclay, as evidenced by a 40% reduction in weight loss during sulfate exposure, compared to 20% for the acrylic/vinylidene fluoride system (Scarfato et al., 2012).

Woo et al. evaluated the barrier performance of silane-nanoclay composites incorporating two types of nanoclay: Cloisite 20A (modified with dimethyl dehydrogenated tallow quaternary ammonium) and I.30P (modified with primary octadecyl amine), dispersed in a mixture of octyltriethoxysilane and isooctyltriethoxysilane. Cloisite 20A demonstrated improved moisture barrier performance. In contrast, I.30P provided only marginal improvement in moisture resistance and significantly reduced performance under salt spray exposure. The average chloride reduction was approximately 92% for neat silane and 60% for the silane-nanocomposite system relative to untreated concrete.

# Chapter 3: Experimental Investigation of Silane Sealers

This experimental investigation was conducted to evaluate the effectiveness of selected concrete sealers from the Missouri Department of Transportation (MoDOT) Approved Products List. Performance was assessed in terms of capillary suction, chloride diffusion, and resistance to surface scaling caused by de-icing chemicals under repeated freezing-and-thawing cycles. In addition, the electrical resistivity/conductivity of silane-impregnated concrete surfaces was measured to characterize changes in the electrical properties of the concrete associated with the presence of a silane treatment layer and to examine potential relationships between these electrical properties and durability-related performance measures. For this investigation, four commercially available silane formulations were selected and applied as surface treatments to concrete specimens prepared using a MoDOT Grade B2 concrete mixture (Missouri standard specifications for highway construction,2025).

## 3.1 Overview of the Experimental Investigation

In this investigation, commercially produced ready-mixed concrete conforming to MoDOT Grade B2 specifications was supplied by Rolla Ready Mixed Concrete. The compressive strength of the concrete was 3,960 psi after 28 days of moist curing. To evaluate the performance of silane-based surface impregnation treatments for reinforced concrete bridge decks, four commercially available formulations of aliphatic alkyl trialkoxy silanes were selected. Manufacturer-provided information for each product, including chemical formulation, percentage of active ingredients, density, viscosity, and recommended coverage rate, is presented in Table 3.1.

A total of 120 concrete specimens were cast and consolidated by rodding in accordance with ASTM C31-25b. After 24 h, the specimens were demolded and transferred to a controlled moist curing chamber maintained at a temperature of 70 °F and a relative humidity of approximately 95%. Unless otherwise mentioned, all specimens were cured for a period of 28 days. Prior to silane application, the concrete surfaces were prepared using hydro-jet pressure washing in accordance with the manufacturer's recommendations to remove surface laitance and expose near-surface pores. This surface preparation was intended to enhance silane penetration depth and improve adherence of silane reaction products with the concrete substrate. Following surface preparation, the specimens were allowed to dry for seven days under laboratory conditions at a temperature of 70 °F and a relative humidity of approximately 65%. After the drying period, silane treatments were applied in three successive coats using a low-pressure sprayer, with a 20-min interval between coats. An application rate of 175 $ft^2$/gal per coat was maintained to ensure consistency across all products. Following treatment, the specimens were stored under standard laboratory conditions and were tested no earlier than seven days after silane application.

**Table 3.1. Manufacturer's data for silanes used in this study**

| | SIL1 | SIL2 | SIL3* | SIL4 |
|---|---|---|---|---|
| Formulation | Silicic acid ester silane | Iso-butyl-triethoxy silane | – | Iso-butyl-triethoxy silane |
| Active ingredients | 100 | 100 | 100 | 100 |
| Density (oz/in.$^3$) | 0.613 | 0.509 | 0.510 | 0.514 |
| Viscosity** (CPS) | 2.5 | 1.67 | 2.085 | 2.085 |
| Coverage rate (ft$^2$/gallon) | Flooding | Flooding | 2-3 coats each at 145 – 200 | 150 – 400 |

*SIL3 is described as a corrosion inhibitor. The chemical formulation was not disclosed by the manufacturer.

** Viscosity was measured in the laboratory using rotational viscometer.

## 3.2 Performance Tests

### 3.2.1 Salt Absorption/Vapor Transmission Test

#### 3.2.1.1 Procedure of the Test

The test procedure is illustrated schematically in Figure 3.1. Three 4 in. × 8 in. cylindrical specimens were prepared for each silane treatment, along with three untreated control specimens. All specimens were moist cured for 21 days. Following curing, the upper 4 in. portion of each cylinder was cut using a water-cooled diamond saw. After surface drying and silane impregnation (as described in 3.1.), all specimens were immersed in a 15% NaCl solution by weight for 21 days, followed by a drying period of equal duration. During both the immersion and drying phases, specimen mass changes relative to the initial mass prior to salt immersion were recorded at three-day intervals, in accordance with National Cooperative Highway Research Program (NCHRP) Series II procedures. At the end of the drying period, the specimens were split into halves along the longitudinal axis using a universal testing machine. One half of each specimen was crushed and tested for chloride content in accordance with AASHTO T260 using the acid digestion-potentiometric titration method. The crushed material was ground to pass a 300 µm sieve. A 0.1 oz (3 g) powder sample was completely digested in an acidic solution using a glass stirring rod and subsequently boiled on a hot plate for 60 seconds. The resulting suspension was filtered through Whatman No. 40 filter paper and rinsed with boiled water to achieve a total filtrate volume between 6.73 and 9.154 in.$^3$ (125 and 150 mL). The filtrate was then titrated with a 0.01 M silver nitrate solution. The equivalence point was identified as the point corresponding to the maximum change in electrical potential during titration. The chloride ion content (percent by mass of concrete) was calculated using Equation 3.1.

$$Cl^- \text{ percent} = \frac{(3.5453\ (V_1N_1 - V_2N_2)}{W}$$

Where:

$V_1$ = Endpoint in mL of $AgNO_3$

$N_1$ = Normality of $AgNO_3$

W = Mass of original sample in grams

$V_2$ = Volume of NaCl added, in mL

$N_2$ = Normality of NaCl

**Equation 3.1. Chloride ion content as per AASHTO T260**

#### 3.2.1.2 Discussion of the Results

Figure 3.2 presents the absorption and vapor transmission behavior of both silane-treated and untreated concrete specimens. The untreated (control) specimens exhibited high initial absorption rate, which decreased after approximately nine days and approached a nearly constant rate with continued immersion. All silane-treated specimens demonstrated a substantial reduction in water absorption, with measured reductions ranging from approximately 85 to 90% relative to the untreated specimens. No significant differences were observed among the silane formulations; however, SIL2 and SIL4 exhibited slightly lower absorption values. This behavior is attributed to the branched alkyl group structure of these formulations, which enhances water-repellent performance and further limit capillary absorption.

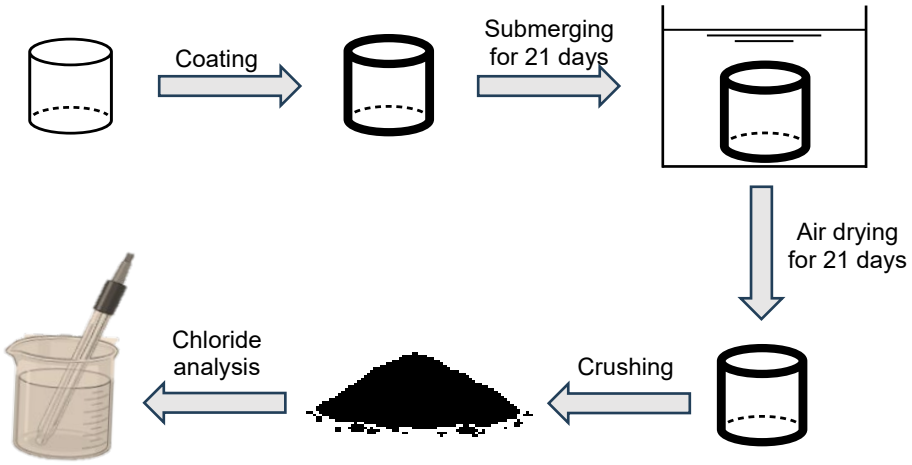


**Figure 3.1. The sequence of salt absorption/desorption test**

Both treated and untreated cylinders exhibited a similar trend of decreasing vapor loss over time. However, the rate of vapor loss was lower for silane-treated specimens, primarily due to their lower degree of saturation at the onset of the drying phase. In contrast to absorption behavior, vapor transmission did not appear to be significantly influenced by the chemical

composition of the hydrophobic silane layer, as indicated by the comparable vapor loss rates observed for all silane types.

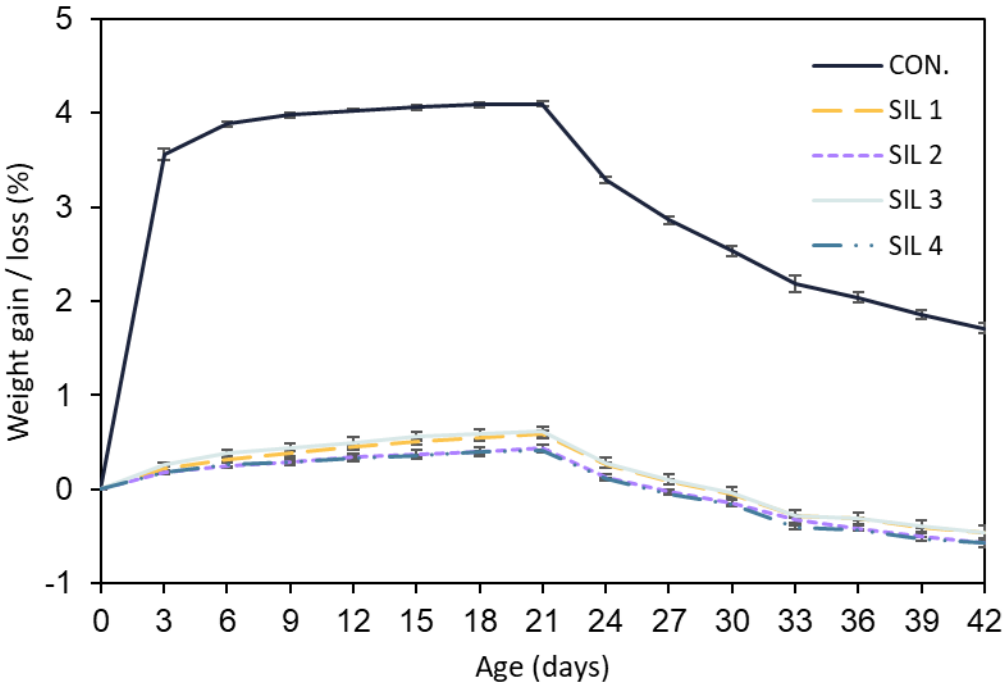


**Figure 3.2. Weight gain/loss (%) vs. time (days)**

The results of ion chloride content by percentage are given in Table 3.2. Similarly, the different silanes were capable of lowering chloride ion penetration into concrete effectively by 83-88%. It is clearly noticed that chloride ion contents show a similar pattern to absorption except for Sil1 which shows the highest chloride ion content.

**Table 3.2. The ion chloride content for untreated and silane treated concrete**

| Type | $Cl^-$ (%) |
|---|---|
| Control | 1.027 ± 0.036 |
| SIL1 | 0.171 ± 0.014 |
| SIL2 | 0.147 ± 0.004 |
| SIL3 | 0.165 ± 0.005 |
| SIL4 | 0.119 ± 0.007 |

### 3.2.1.3 Conclusions

According to the acceptance criteria outlined in NCHRP Report 209 for approving silane treatments for field implementation, both absorption and chloride ion penetration should be reduced by at least 75% relative to untreated control concrete. Based on these criteria, all evaluated silane products meet the acceptance requirements. Among the tested formulations, SIL2 and SIL4 exhibited the best overall performance, while SIL1 and SIL3 demonstrated comparatively lower, yet still acceptable, effectiveness. Vapor transmission was not significantly

impeded by any of the silane treatments, as evidenced by the similar rates of mass loss observed during the drying period for all products.

### 3.2.2 Long Term Ion Chloride Penetration (AASHTO T259)

#### 3.2.2.1 Procedure of the Test

The long-term chloride ion penetration test was conducted in accordance with AASHTO T259. The test procedure is summarized as follows: 1) Triplicate concrete slab specimens with nominal dimensions of 12 in. × 12 in. × 3 in. were cast and moist-cured for 14 days in a controlled curing chamber. 2) Following drying and surface impregnation, the slab surfaces were lightly abraded using a steel wire brush and cleaned to remove loose material. A perimeter dam approximately 1 in. high was then placed around the edges of each. 3) The treated surface of each specimen was continuously ponded with a 3% NaCl solution by weight for a duration of 90 days. 4) At the end of the ponding period, the specimens were dried, and the exposed surface was ground to a depth of 0.063 in. 5) Powdered concrete samples were collected at the specified locations and depths, as illustrated schematically in the referenced figure (Figure 3.3). Chloride content was determined using the acid digestion–potentiometric titration method, as described in Section 3.2.1.1.

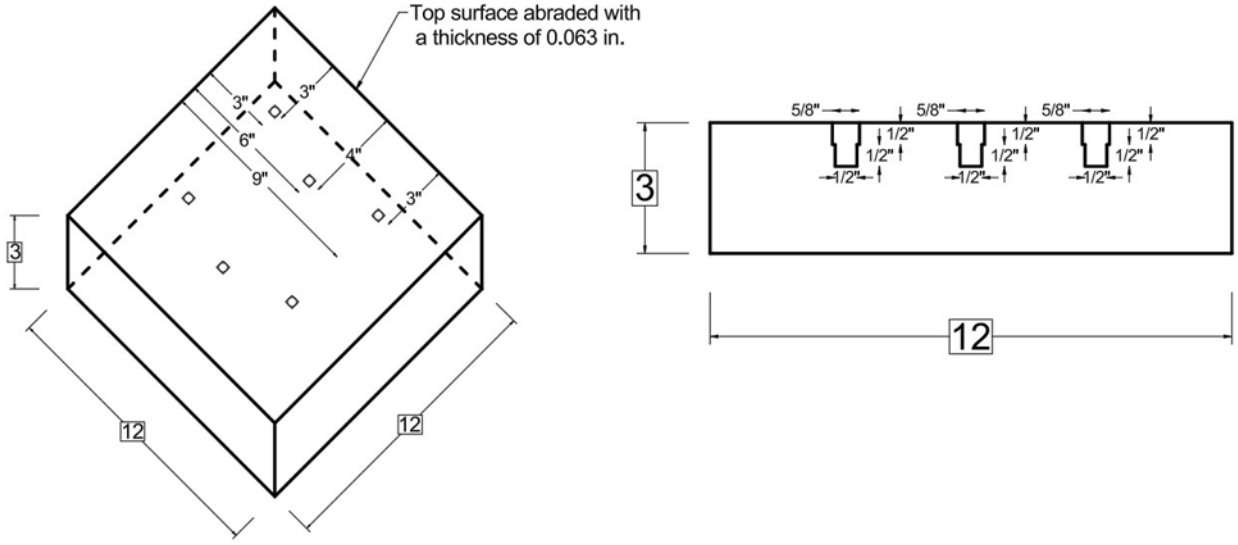


**Figure 3.3. The pattern adopted for chloride sampling (All dimensions are in inches)**

#### 3.2.2.2 Discussion of the Results

The chloride ion content as a function of depth from the concrete surface is summarized in Table 3.3. Silane-treated specimens consistently exhibited reduced chloride penetration compared to the untreated control specimens. Among the silane formulations, SIL1 demonstrated the lowest overall chloride content, indicating superior performance in this long-term ponding test. This result contrasts with the findings reported in Section 3.2.1, where SIL1 showed relatively lower performance. SIL4 continued to perform well and produced chloride penetration values comparable to SIL1 due to its higher degree of hydrophobicity. SIL2, which

shares similar functional groups with SIL4, exhibited slightly higher chloride content in the near-surface layer compared to SIL4; however, this difference was not statistically significant. SIL3 demonstrated the lowest performance overall. At depths of 0.063–0.5 in. and 0.51–1.0 in., the chloride content in SIL3 specimens increased by approximately 100% and 70%, respectively, relative to SIL1 concrete.

**Table 3.3. Chloride content profile vs. depth as per AASHTO T259**

| Depth | Control | SIL1 | SIL2 | SIL3 | SIL4 |
|---|---|---|---|---|---|
| 1.6–13 mm | 0.79 ± 0.008 | 0.073 ± 0.015 | 0.103 ± 0.016 | 0.151 ± 0.034 | 0.080 ± 0.009 |
| 13–25 mm | 0.39 ± 0.037 | 0.043 ± 0.004 | 0.043 ± 0.003 | 0.073 ± 0.004 | 0.050 ± 0.008 |

#### 3.2.2.3 Conclusions

In conclusion, silane surface-treated concrete exhibited lower chloride content relative to untreated concrete, indicating the potential for extended service life of bridge decks. Among the silane formulations evaluated, SIL1 was the most effective in limiting chloride ion penetration, with SIL4 demonstrating comparable performance. SIL2 showed a slight increase in chloride content relative to SIL4, while SIL3 exhibited the lowest effectiveness of the silanes tested.

### 3.2.3 Scaling Resistance of Concrete

#### 3.2.3.1 Procedure of the Test

The scaling resistance test was conducted following the procedure described in (Sakr and Bassuoni, 2021). A total of 15 concrete slabs, each measuring 12 in. × 12 in. × 3 in., were prepared, with three slabs left untreated to serve as reference controls. During the drying period, a 0.5 in.-high perimeter dike was formed around the top surface of each slab. After compound curing, a calcium chloride solution with concentration 0.14 oz per 6.1 $in.^3$ (4 g per 100 mL of water) was applied to pond the top surface of each specimen. The slabs were then placed in a freezing-thawing chamber, where each cycle consisted of 18 h of freezing followed by 6 h of thawing. After every five cycles, the scaled material was collected, oven-dried at 230 ± 9 °F to constant mass, and weighed. Surface scaling was evaluated using a visual rating scale from 0 to 5, where a higher rating indicates increased deterioration.

#### 3.2.3.2 Discussion of the Results

The cumulative mass loss ($oz/yd^2$) and visual surface ratings of the concrete specimens are summarized in Table 3.4. The progression of surface scaling after each set of five freeze-thaw cycles is illustrated in Figure 3.4. Silane surface treatments significantly mitigated deterioration caused by deicing salts under frost exposure. For the untreated specimens, cumulative mass loss reached 212.9 $oz/yd^2$ after 10 cycles, whereas no scaling was observed for silane-coated specimens. The hydrophobic layer formed by silane treatment reduces surface energy, thereby

limiting capillary suction and inhibiting the formation and growth of ice crystals within the concrete matrix.

**Table 3.4. The cumulative mass loss (oz/yd²) for the investigated silanes***

| No. of cycles | Control | SIL1 | SIL2 | SIL3 | SIL4 |
|---|---|---|---|---|---|
| 5 | 95.2 (3) | 0 | 0 | 0 | 0 |
| 10 | 212.9 (5) | 0 | 0 | 0 | 0 |
| 15 | – | 0.3 (2) | 0.3 (2) | 1.0 (3) | 0.1 (1) |
| 20 | – | 0.8 (2) | 1.2 (2) | 2.4 (3) | 0.4 (1) |
| 25 | – | 3.1 (3) | 3.9 (3) | 6.8 (4) | 1.6 (2) |
| 30 | – | 10.0 (3) | 12.0 (3) | 18.1 (4) | 5.1 (2) |
| 35 | – | 25.1 (4) | 29.8 (4) | 35.2 (5) | 17.0 (3) |
| 40 | – | 36.9 (5) | 40.7 (5) | 44.4 (5) | 34.7 (5) |

* The numbers in parentheses are the visual rating

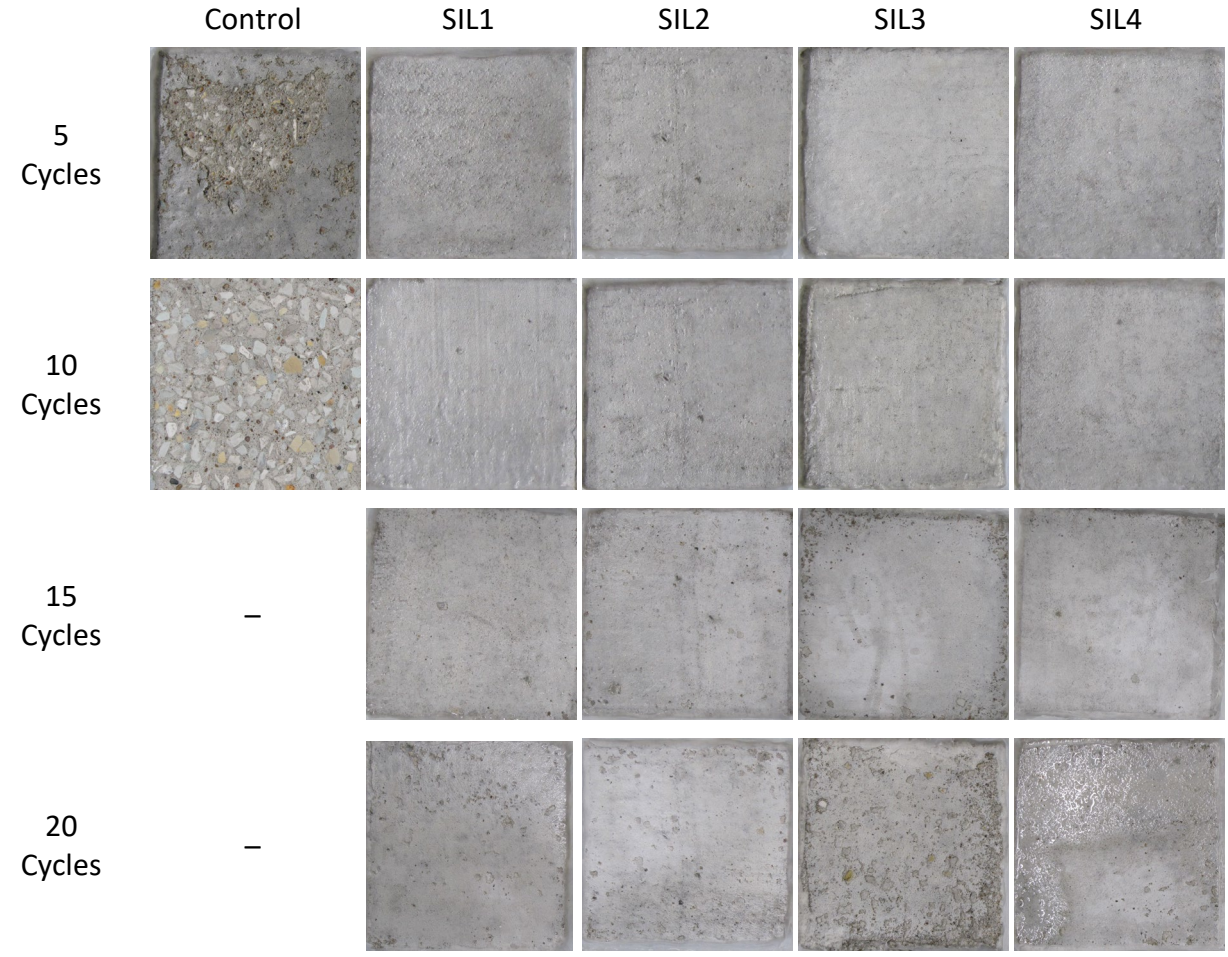

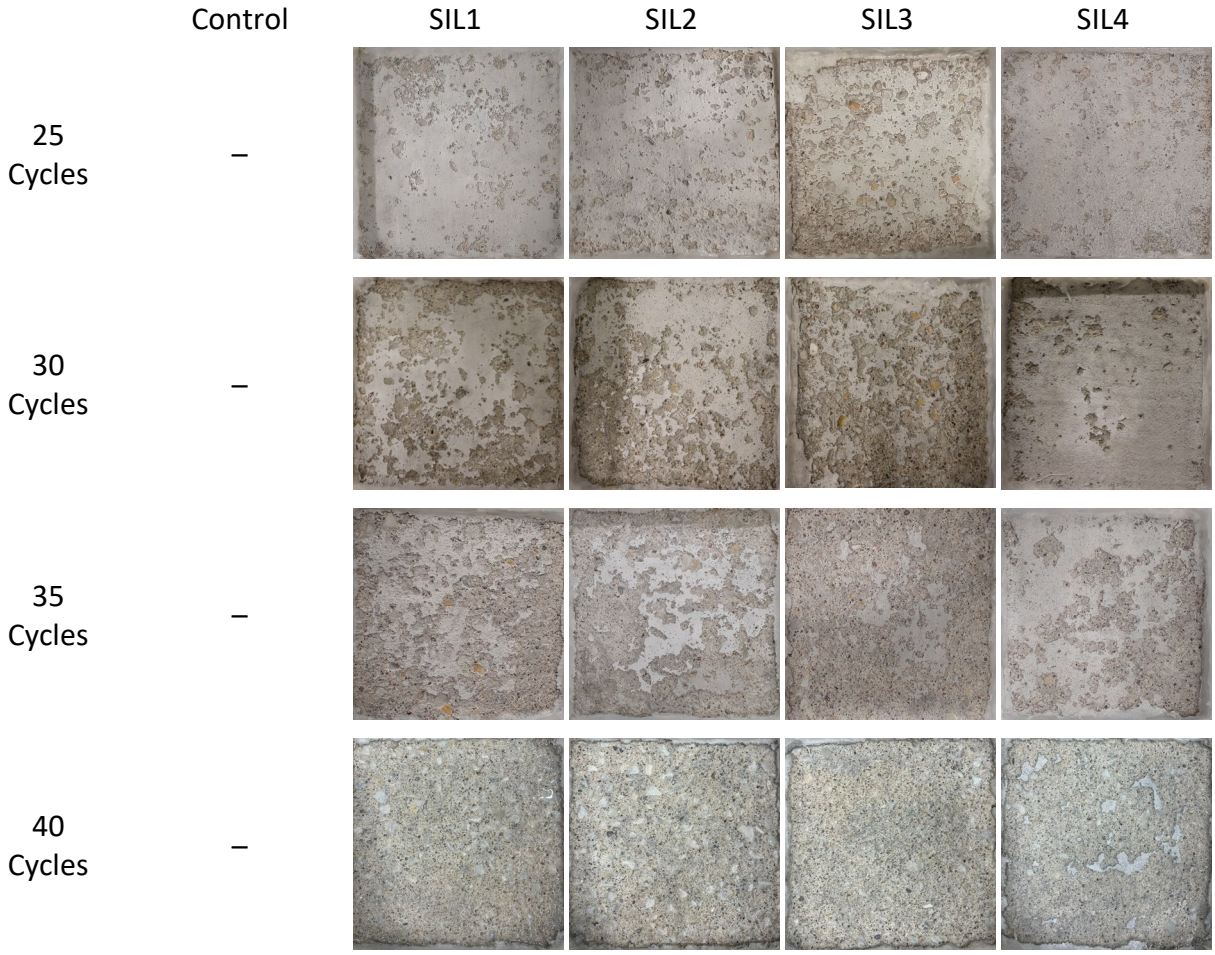


**Figure 3.4. Surface scaling progression at 5 cycles intervals**

Comparing the performance of different silane formulations (Figure 3.5), SIL4 exhibited the best performance due to a higher degree of hydrophobicity associated with its branched alkyl groups, in contrast to the linear-chain structure of SIL1 (silicic ester). SIL1 experienced nearly twice the cumulative scaling mass loss after 25 freeze-thaw cycles. SIL2, which contains a similar active ingredient (isobutyl-triethoxy) but is manufactured by a different supplier, demonstrated lower resistance to surface scaling than SIL4, with mass loss approximately 2.5 times higher after 25 cycles. SIL3 exhibited the poorest performance, with mass loss increasing by 420% relative to SIL4 after 25 cycles. Although the chemical composition of SIL3 was not fully disclosed by the manufacturer, an indication using gas chromatography suggested that methyl-trimethoxy is likely the primary functional group. Therefore, the reduced scaling resistance of SIL3 could be attributed to its lower hydrophobicity.

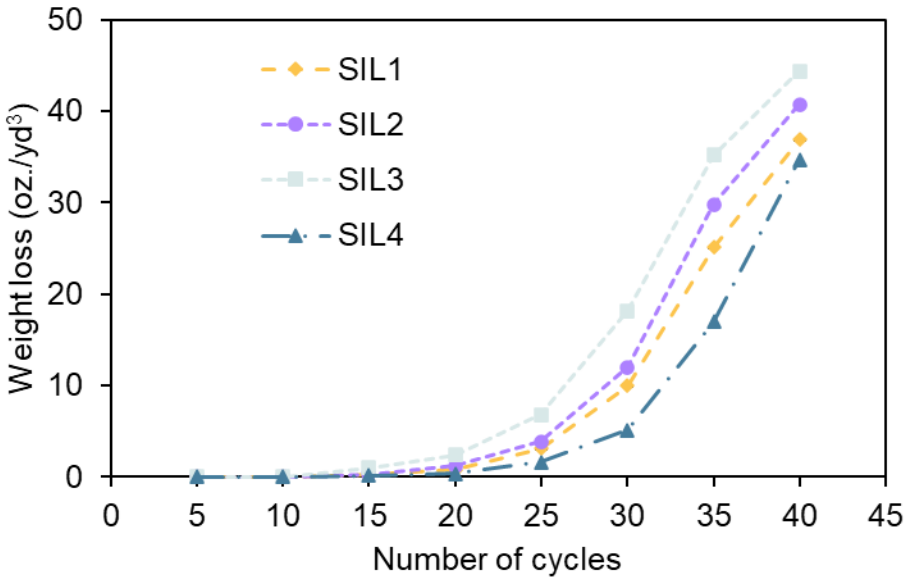


**Figure 3.5. Weight loss (oz/yd³) vs. number of cycles**

#### 3.2.3.3 Conclusions

Surface impregnation of concrete with silicone-based compounds effectively mitigates surface scaling of bridge decks exposed to de-icing chemicals. Among the silane formulations evaluated, performance in descending order was: SIL4, SIL1, SIL2, and SIL3. The results indicate that the chemical nature plays a critical role in reducing scaling. Additionally, silane products with similar active ingredients from different manufacturers exhibited variable performance, likely due to differences in pH, catalysts, solvents, or the overall reaction environment during application.

### 3.2.4 Bulk Electrical Conductivity

#### 3.2.4.1 Procedure of the Test

To evaluate the effect of silane surface treatment on the electrical conductivity of concrete under varying internal moisture conditions, three sets of measurements were performed on 4 in. × 8 in. cylindrical specimens a) Cylinders were tested following 28 days of moist curing in a controlled curing chamber, $S_0$ b) Cylinders were air-dried for 7 days, treated with silane (as described in Section 3.1), and then allowed to cure in ambient air for an additional 7 days, $S_1$, c) Cylinders were submerged in water for 7 days following silane curing, $S_2$. Silane was applied to the top and bottom surfaces of the cylinders, perpendicular to the direction of current flow, see Figure 3.6.a. The cylindrical lateral surface was left untreated to allow water penetration when specimens were submerged. For each measurement, specimens were mounted in a voltage cell using silicone rubber, and current flow was recorded under a 60 V potential difference applied for 1 min, see Figure 3.7. A damp cloth was used to prevent moisture loss, except during measurements conducted under dry conditions. Bulk electrical conductivity was calculated using Equation 2:

$$\sigma = K \frac{I_1}{V} \frac{L}{D^2}$$

Where:

σ = bulk electrical conductivity, mS/m

$I_1$ = current at 1 min, mA

V = applied voltage, V

L = average length of specimen, mm

D = average diameter of specimen, mm

K = conversion factor = 1273.2

**Equation 3.2. Bulk electrical conductivity of concrete**

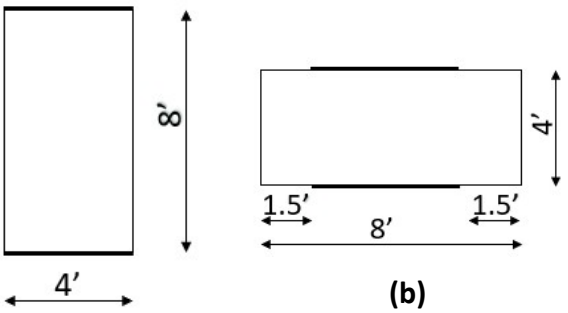


**Figure 3.6. Silane application (a) bulk conductivity (b) surface resistivity**


**Figure 3.7. Bulk conductivity test measurements**

### 3.2.4.2 Discussion of the Results

Figure 3.8 presents the electrical conductivity results for the different moisture conditions, moist-cured $S_0$, air-dried $S_1$, and submerged $S_2$, expressed in terms of weight loss as a percentage of the total mass of the moist-cured concrete. The results consistently demonstrate that drying of concrete leads to a reduction in electrical conductivity under all tested

conditions. With respect to the influence of silane impregnation, silane-treated specimens exhibited a pronounced decrease in electrical conductivity after drying and subsequent submersion in water for seven days, relative to untreated control specimens. Although the treated and untreated cylinders did not reach identical hygroscopic states, due to silane application on the top and bottom surfaces restricting moisture ingress and limiting saturation compared to the controls, the effect of silane treatment on reducing electrical conductivity was clearly evident. For specimens subjected to extended drying (14 days of air drying under laboratory conditions), silane-treated concrete continued to exhibit lower conductivity than untreated concrete; however, the difference between treated and untreated specimens was substantially reduced. Despite the limited number of measurements, the results indicate that continued drying significantly decreases concrete conductivity, whereas the influence of silane treatment becomes less pronounced under prolonged dry conditions.

Comparing the performance of different silane formulations, the measured electrical conductivity increased in the following order: SIL1, SIL4, SIL3, and SIL2. This trend suggests that SIL1 and SIL4 may be more effective in limiting ionic mobility through the concrete pore structure in salt-exposed environments. The relatively high conductivity observed for SIL2 was unexpected and may be attributable, at least in part, to a higher initial conductivity of the concrete substrate prior to treatment.

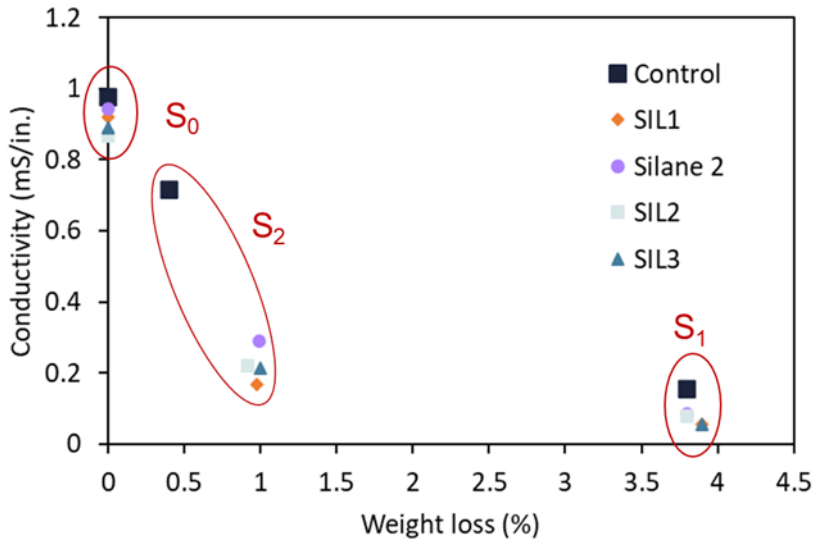


**Figure 3.8. The electrical bulk conductivity (mS/in.) for the different moisture conditions**

### 3.2.4.3 Conclusions

Surface treatment of concrete with silane substantially reduced electrical conductivity. Among the evaluated formulations, performance in increasing order was SIL1, SIL4, SIL3, and SIL2. These results indicate that silane surface treatment has the potential to enhance the service life of bridge decks by lowering concrete conductivity and reducing ionic mobility, particularly chloride ions from de-icing chemicals, thereby decreasing the risk of reinforcement corrosion.

### 3.2.5 Surface Resistivity of Concrete (AASHTO T358)

#### 3.2.5.1 Procedure of the Test

The surface resistivity of concrete was measured using a Wenner four-point probe with an electrode spacing of 1.5 in. For each test condition, three cylindrical specimens were cast and cured for 28 days. After curing, the circumference of the top surface of each cylinder was permanently marked at four quadrants, and these reference marks were extended along the cylindrical surface. An additional reference mark was placed at the mid-height of each specimen to ensure consistent electrode positioning during measurements. Following the initial drying period, silane was applied to the central portion of each specimen, as illustrated in Figure 3.6.b. The outer portions of the cylinder, 1.5 in. at each end along the longitudinal axis, were left uncoated. Surface resistivity measurements were performed under the following conditions: a) after 28 days of moist curing in a controlled curing chamber; b) after 7 days of air drying under ambient laboratory conditions, followed by silane treatment and an additional 7 days of air curing; and c) after submersion in water for 7 days, followed by drying periods of 30 min, 2 h, 10 h, 1 day, 3 days, and 7 days. For each condition, a total of 12 resistivity measurements were obtained per specimen set, and the average value was reported.

#### 3.2.5.2 Discussion of the Results

Table 3.5. summarizes the surface resistivity results obtained prior to submerging the specimens in water. For the untreated concrete, surface resistivity increased by a factor of 3.9 at 42 days compared to the moist-cured condition. This increase is attributed to the reduced degree of saturation within the internal pore structure of concrete. When comparing silane-treated and untreated specimens at 42 days, no resistivity measurements were obtained for the treated specimens thereby indicating the effect of concrete surface treatment on surface resistivity.

**Table 3.5. Surface resistivity results of coated and uncoated concrete prior to submersion**

| | Un-coated concrete moist-cured for 28 days | Un-coated dried concrete at the age of 35 days | Coated concrete at the age of 42 days |
|---|---|---|---|
| Control | 3.6 | 9.3 | 13.8 |
| SIL1 | 3.7 | 9.6 | N/A |
| SIL2 | 3.6 | 9.0 | N/A |
| SIL3 | 3.5 | 9.0 | N/A |
| SIL4 | 3.5 | 8.7 | N/A |

Figures 3.9 and 3.10 present the variation of surface resistivity and specimen mass loss with time during the post-submergence drying period. Initially, the silane-treated specimens exhibited greater mass loss than the uncoated specimens, indicating a lower degree of internal saturation attributable to the presence of the hydrophobic silane layer. The uncoated specimens showed an increasing drying rate up to approximately 3 days, primarily due to rapid moisture loss from the concrete surface. In contrast, for the silane-treated specimens, the hydrophobic surface layer resulted in a drier near-surface region, requiring water molecules to

migrate over a longer internal path before evaporating. This mechanism reduced the rate of mass loss during the early stages of drying. Notably, although the silane-treated concrete initially exhibited a lower degree of saturation, the uncoated specimens dried more rapidly and eventually exceeded the treated specimens in cumulative mass loss after approximately 3 days. This behavior demonstrates that the hydrophobic layer retards water vapor transport during drying.

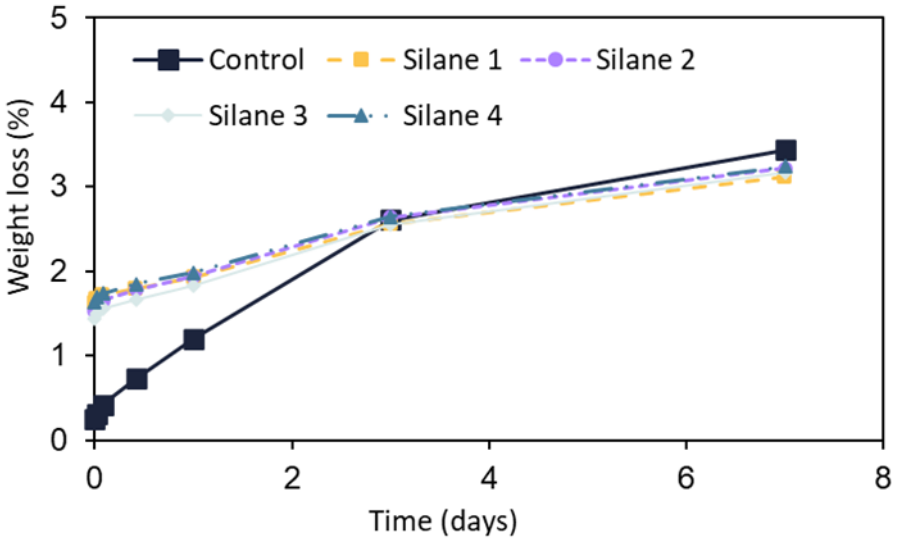


**Figure 3.9. Weight loss (%) vs. time (days)**

With respect to electrical resistivity, the silane-treated specimens initially exhibited higher resistivity values compared to the control specimens. However, after approximately 3 days of drying, the resistivity of the treated specimens decreased relative to the uncoated concrete. This trend is attributed to the initially lower saturation level of the treated specimens, followed by the retarding influence of siloxane-based products. The electrical resistivity was also found to be dependent on the chemical composition of the hydrophobic layer. The silicic ester (SIL1) produced higher resistivity values than the isobutyl triethoxy silanes (SIL2 and SIL4). In contrast, SIL3 resulted in reduced resistivity. Importantly, the observed resistivity trends correlate well with the long-term chloride penetration results, supporting the relationship between electrical properties of concrete and chloride ingress resistance. It should be noted that resistivity measurements obtained after 14 and 28 days exhibited significant variability and were therefore excluded from further analysis.

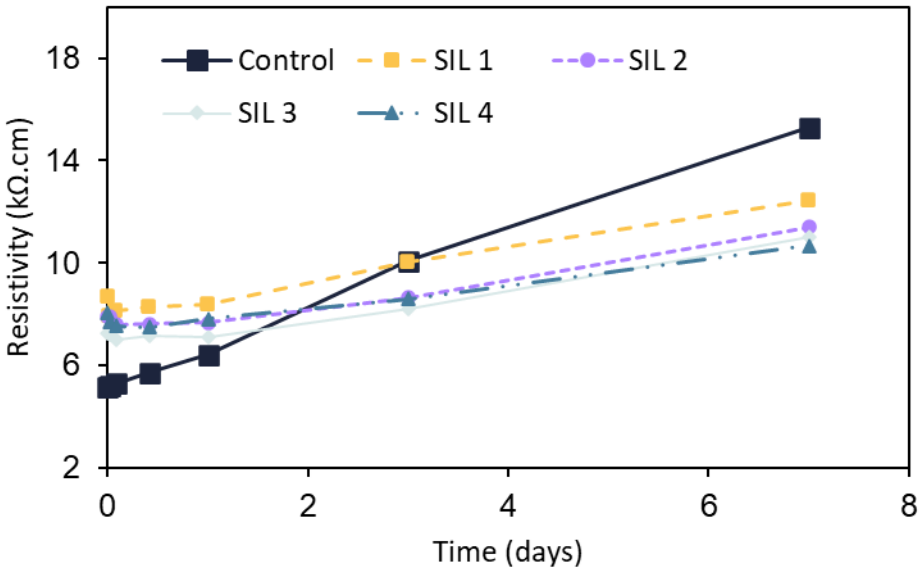


**Figure 3.10. Surface resistivity (kΩ.cm) vs. time (days)**

#### 3.2.5.3 Conclusions

Silicone-based surface treatments increase the surface resistivity of concrete. The magnitude of improvement is dependent on the moisture condition of the concrete substrate. Among the evaluated products, the silicic ester exhibited the highest surface resistivity, followed by the isobutyl-triethoxy silanes. In contrast, SIL3 showed the lowest performance in terms of resistivity enhancement.

### 3.2.6 Rate of Absorption (ASTM C1585)

#### 3.2.6.1 Procedure of the Test

Sorptivity is a measure of the rate of water uptake in concrete resulting from capillary suction through its porous network. This transport mechanism plays a critical role in concrete durability, as it contributes to the ingress of aggressive agents associated with deterioration processes such as chloride-induced corrosion, sulfate attack, and alkali-silica reaction. For this test, duplicate standard cylindrical specimens were prepared and cured as described in Section 3.2. The cylindrical surface of each specimen was sealed with an epoxy coating to ensure one-dimensional water absorption during testing. From each cylinder, the top 2 in. disk was cut, and oven-dried at a controlled temperature of 120 °F for 3 days. It should be mentioned that conditioning the specimens at 120°F in a desiccator containing a potassium bromide solution as shown in Figure 3.11, resulted in a reduction in specimen mass after 6 h. Therefore, this conditioning procedure was replaced with oven drying at the same temperature. Following drying, the specimens were stored in sealed containers and allowed to cool to room temperature. To minimize moisture loss from the bottom surface during testing, a loosely attached plastic bag was secured around the specimen. The prepared top surface of each specimen was then placed in contact with water maintained at a depth of 0.04–0.12 in. (1–3 mm) above the concrete surface, See Figure 3.12. Changes in specimen mass were recorded

after 60 s, 1 min, 5 min, 10 min, 20 min, and 30 min; subsequently at hourly intervals up to 6 h; then daily up to 7 days, with a final reading taken after 9 days of water exposure. The absorption was calculated using Equation (3):

$$I = \frac{m_t}{a \times d}$$

Where:

I = Absorption in in.

$m_t$ = change in weight in oz

a = the exposed area of the specimen in $in.^2$

d = density of water in $oz/in.^3$

**Equation 3.3. The absorption of concrete (in.)**

**Figure 3.11. Conditioning of the sample using potassium bromide at 120 °F as per ASTM C1585**

**Figure 3.12. Rate of absorption test**

### 3.2.6.2 Discussion of the Results

Figure 3.13. illustrates the absorption behavior of treated and untreated concrete surfaces as a function of the square root of time after initial contact with water. All specimens exhibited a characteristic bilinear absorption response, corresponding to the initial and secondary stages of capillary suction. The application of silane to the concrete surface was effective in significantly reducing capillary absorption. The initial and secondary sorptivity coefficients were determined from the slopes of the best-fit linear regressions that minimized the sum of squared errors. The calculated values are presented in Table 3.6. Based on these results, SIL4 and SIL1 demonstrated the highest effectiveness in reducing water absorption, followed by SIL2, while SIL3 exhibited the lowest performance.

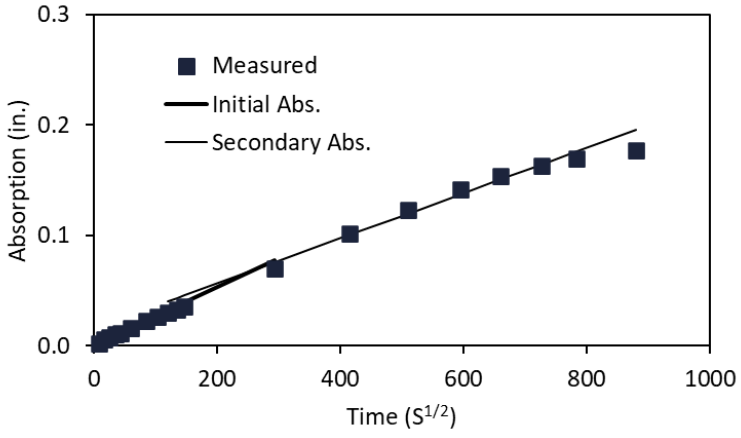


**(a)**

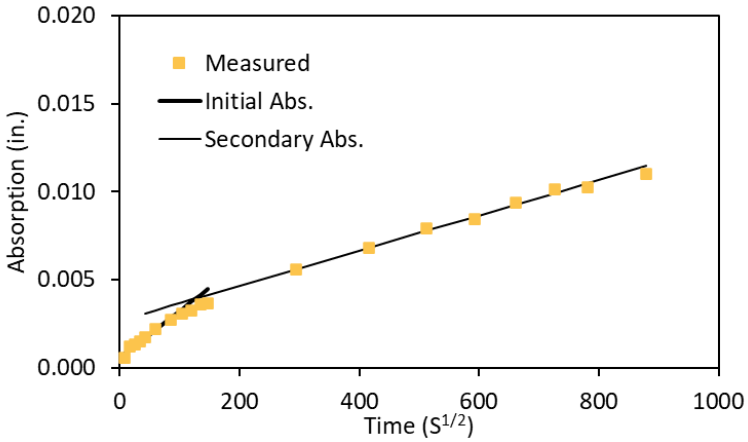
0.020
0.015
0.010
0.005
0.000
Absorption (in.)
Measured
Initial Abs.
Secondary Abs.
0
200
400
600
800
1000
Time (S^1/2)

**(b)**

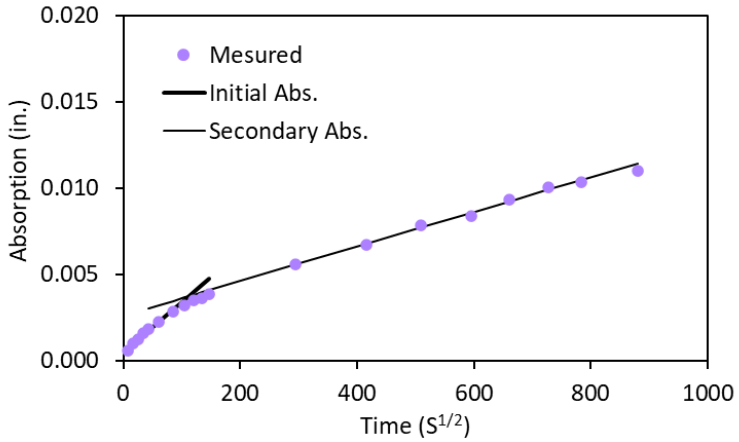
0.020
0.015
0.010
0.005
0.000
Absorption (in.)
Mesured
Initial Abs.
Secondary Abs.
0
200
400
600
800
1000
Time (S^1/2)

**(c)**

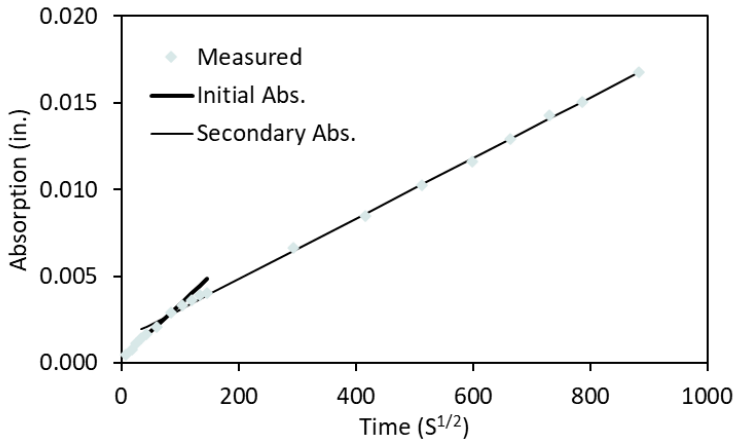
0.020
0.015
0.010
0.005
0.000
Absorption (in.)
Measured
Initial Abs.
Secondary Abs.
0
200
400
600
800
1000
Time (S^1/2)

**(d)**

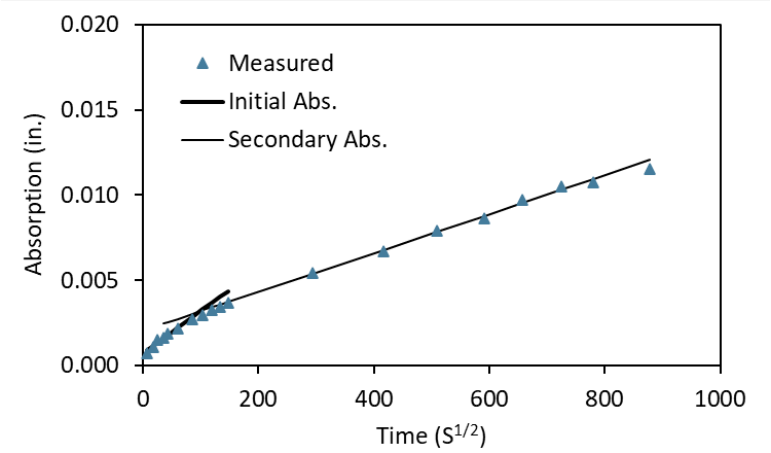


**(e)**

**Figure 3.13. Absorption characteristics of the different silanes (a) un-treated concrete (b) SIL 1 treated concrete (c) SIL2 treated concrete (d) SIL3 treated concrete (e) SIL4 treated concrete**

**Table 3.6. Initial and secondary absorption of the different silanes**

| | $S_i$ (in./$s^{1/2}$) | S.D | $S_S$ (in./$s^{1/2}$) | S.D |
|---|---|---|---|---|
| Control | $2.6x10^{-4}$ | $2.9x10^{-6}$ | $2.1x10^{-4}$ | $6x10^{-6}$ |
| SIL1 | $2.7x10^{-5}$ | $9x10^{-7}$ | $1.1x10^{-5}$ | $1.7x10^{-5}$ |
| SIL2 | $3.2x10^{-5}$ | $3.8x10^{-6}$ | $1.1x10^{-5}$ | $1.0x10^{-5}$ |
| SIL3 | $3.3x10^{-5}$ | $1.8x10^{-6}$ | $1.9x10^{-5}$ | $1.2x10^{-5}$ |
| SIL4 | $2.5x10^{-5}$ | $4x10^{-7}$ | $9x10^{-6}$ | $3.9x10^{-5}$ |

#### 3.2.6.3 Conclusions

Silane surface treatment was found to reduce capillary suction in concrete, which may contribute to improved resistance to deterioration mechanisms such as freeze-thaw cycling, surface scaling, chloride-induced corrosion, and sulfate attack. Based on the results of this study, the relative effectiveness of the evaluated silane products in reducing concrete sorptivity is ranked as follows: SIL4, SIL1, SIL2, and SIL3.

### 3.2.7 The Apparent Chloride Diffusion Coefficient (ASTM C1556)

#### 3.2.7.1 Procedure of the Test

Diffusivity refers to the transport of chloride ions into concrete driven by a concentration gradient. The chloride diffusion test was conducted in accordance with ASTM C1556 and is summarized as follows: a) Test cylinders were cured for 28 days in a standard moist curing chamber b) After curing, the cylinders were allowed to dry and were then cut to a depth of 75 mm using a water-cooled diamond saw c) All surfaces except the top exposure surface were sealed with an epoxy resin to ensure one-dimensional chloride ingress d) The exposed top surface of each specimen was treated with the designated silane product and allowed to cure under typical laboratory conditions for 7 days e) Following silane curing, the specimens were immersed with the treated surface exposed to a sodium chloride (NaCl) solution having a

concentration of 165 g/L for a period of 90 days f) After the exposure period, specimens were removed from the solution, excess surface moisture was blotted, and the exposed surface was rinsed with water. The specimens were then allowed to dry for 24 h under laboratory conditions g) Chloride concentration profiles were obtained by mechanically removing and discarding the top 1 mm of concrete from the exposed surface. Then, powdered concrete samples were collected by drilling at successive depths from the exposed surface. The collected samples were analyzed for acid-soluble chloride content using a potentiometric titration method in accordance with ASTM C1152. It should be mentioned that in case of SIL2, only one specimen was considered for analysis because the epoxy coatings on the remaining specimens were partially damaged during testing, which could have affected the validity of the measurements.

#### 3.2.7.2 Discussion of the Results

The chloride ion concentration profiles for the unmodified and surface-modified concrete specimens are presented in Figure 3.14. As demonstrated previously, silane surface treatment is an effective method for reducing chloride diffusion into concrete. At a given depth, the measured chloride content for specimens treated with SIL1 and SIL4 is approximately similar, whereas SIL2 exhibited comparatively lower performance. SIL3 demonstrated the poorest performance in mitigating chloride penetration.

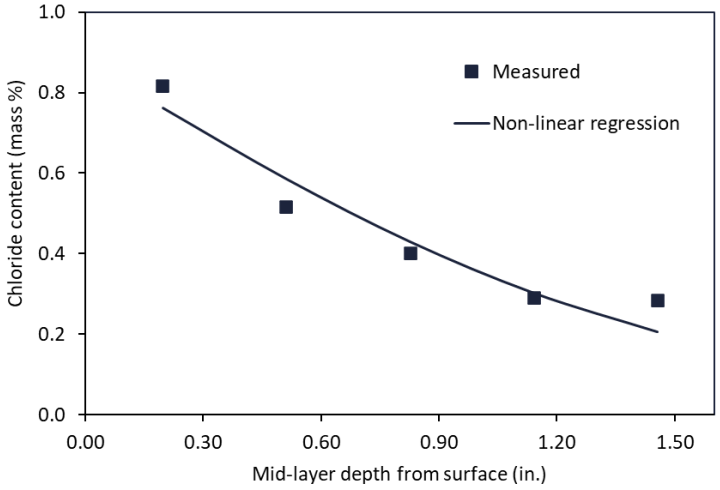


**(a)**

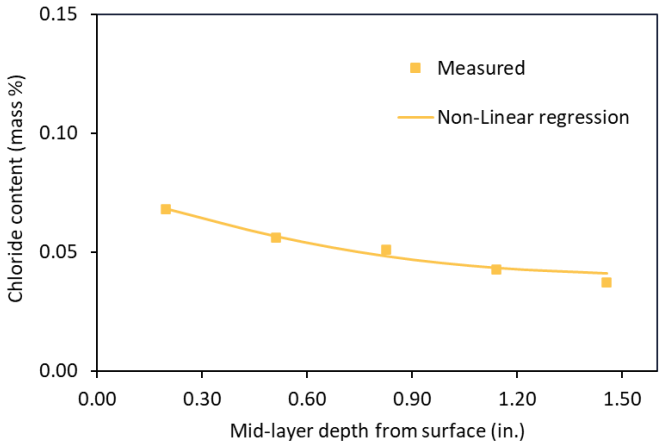
0.15
0.10
0.05
0.00
Chloride content (mass %)
Measured
Non-Linear regression
0.00
0.30
0.60
0.90
1.20
1.50
Mid-layer depth from surface (in.)

**(b)**

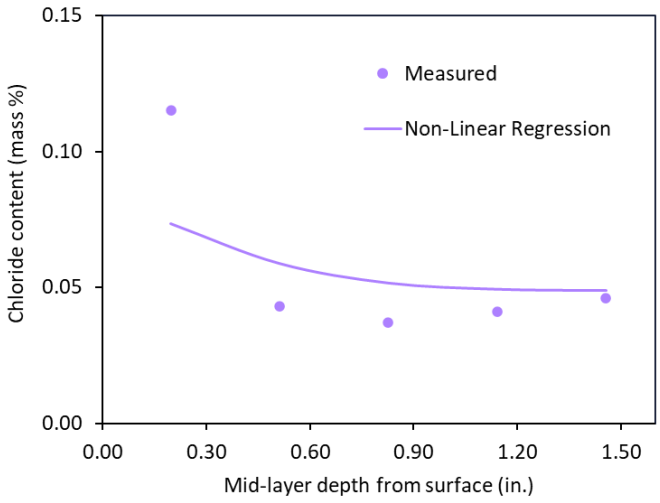
0.15
0.10
0.05
0.00
Chloride content (mass %)
Measured
Non-Linear Regression
0.00
0.30
0.60
0.90
1.20
1.50
Mid-layer depth from surface (in.)

**(c)**

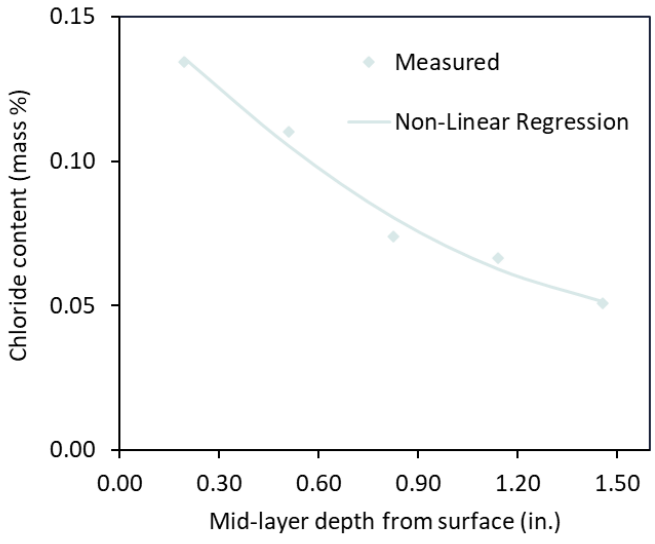
0.15
0.10
0.05
0.00
Chloride content (mass %)
Measured
Non-Linear Regression
0.00
0.30
0.60
0.90
1.20
1.50
Mid-layer depth from surface (in.)

**(d)**

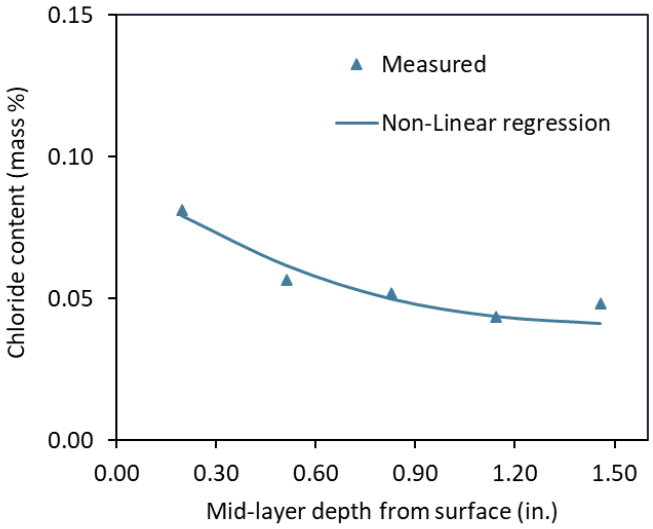


**(e)**

**Figure 3.14. Non-Linear regression analysis for the chloride profile for the different silanes**

**(a) un-treated concrete (b) SIL 1 treated concrete (c) SIL 2 treated concrete (d) SIL3 treated concrete (e) SIL4 treated concrete**

Figure 3.14 also presents the best-fit curves for chloride concentration as a function of depth based on Fick's second law of diffusion, obtained using non-linear regression analysis. The corresponding projected surface chloride concentration ($C_s$) and apparent chloride diffusion coefficient ($D_a$) values are summarized in Table 3.7. Compared to the unmodified concrete, specimens treated with SIL1, SIL2, SIL3, and SIL4 exhibited reductions in projected surface chloride concentration of approximately 92%, 90%, 81%, and 89.5%, respectively, and reductions in apparent chloride diffusion coefficient of approximately 63%, 83%, 39.5%, and 69.2%, respectively. SIL2 was among the best-performing silane treatments, however these results should be interpreted with caution because the measured chloride profile showed considerable scatter relative to the best-fit curve based on Fick's second law of diffusion, introducing greater uncertainty into the estimated diffusion parameters, see Figure 3.14.c. Although SIL1 exhibited a slightly higher apparent diffusion coefficient ($D_a = 19.78 \times 10^{-12}$ m²/s) compared to SIL4, it also showed the lowest projected surface chloride concentration ($C_s$ = 0.077%). This combination indicates superior overall performance of SIL1 in limiting chloride ingress.

**Table 3.7. Projected surface chloride (% mass) and apparent chloride diffusion coefficient (in.²/s) for the different silanes**

| | Projected Surface chloride $C_S$ (% mass) | Apparent chloride diffusion coefficient $D_a$ (in.²/s) |
|---|---|---|
| Control | 0.876 | $8.258 \times 10^{-8}$ |
| SIL1 | 0.077 | $3.067 \times 10^{-8}$ |
| SIL2* | 0.085 | $1.405 \times 10^{-8}$ |

| | Projected Surface chloride $C_S$ (% mass) | Apparent chloride diffusion coefficient $D_a$ (in.$^2$/s) |
|---|---|---|
| SIL3 | 0.156 | $4.997 \times 10^{-8}$ |
| SIL4 | 0.092 | $2.541 \times 10^{-8}$ |

* Only one sample was tested

#### 3.2.7.3 Conclusions

Among the evaluated treatments, SIL1 and SIL4 exhibited the best overall performance, showing similar chloride profiles with the lowest chloride concentrations at comparable depths. SIL3 showed poorer performance, with higher chloride contents and smaller reductions in diffusion parameters. SIL2 exhibited intermediate performance with respect to resistance to chloride penetration among the silane products evaluated. Quantitatively, SIL1 achieved the greatest reduction in projected surface chloride concentration (approximately 92%) and a significant reduction in apparent diffusion coefficient (approximately 63%). Although SIL1 exhibited a slightly higher $D_a$ than SIL4, it also had the lowest $C_s$, indicating superior overall resistance to chloride ingress. SIL4 also performed well, with reductions of approximately 89.5% in $C_s$ and 69.2% in $D_a$. Although SIL2 showed reductions of 90% in the projected surface chloride concentration and 83% in the apparent chloride diffusion coefficient, these estimates is not representative of its chloride barrier performance because of the considerable scatter in the measured chloride profile. SIL3 provided more limited improvement, with reductions of approximately 81% in $C_s$ and 39.5% in $D_a$.

### 3.2.8 Water Permeation Test

#### 3.2.8.1 Procedure of the Test

Water permeability is a critical parameter for assessing the long-term durability of concrete surfaces. Increased surface permeability facilitates the ingress of chlorides and other aggressive ions into the concrete matrix, which can accelerate material degradation and promote corrosion of reinforcing steel. An in-house device was built to measure the surface water permeability of concrete, as shown in Figure 3.15. The apparatus consists of a pressure chamber that was securely mounted to the surface of a 12 in. × 12 in. concrete slab using a rubber gasket to ensure a watertight seal. The chamber was filled with water, and the internal pressure increased to 100 kPa. As water permeated into the concrete, the pressure within the chamber decreased due to the surface permeability. To maintain the internal pressure at the target level, a micrometer-controlled piston was used to replace the volume of water absorbed by the concrete. Micrometer readings were recorded at elapsed times of 1, 2, 5, 10, and 20 min. The water flux at each interval, expressed in inches per second (in./s), was calculated using Equation 3.4.

$$Q = \frac{B \times (g_1 - g_2)}{Axt}$$

Where:

Q = water flux, in./sec

$g_1$ and $g_2$= initial and final micrometer readings, in.

B = the area of the micrometer pin, $in.^2$

A = the area of the pressurized concrete, $in.^2$

t= the time, sec.

**Equation 3.4. The flux of water inside the concrete**

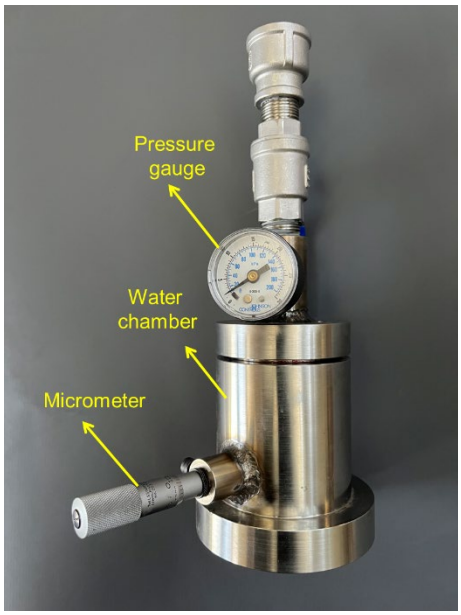


**Figure 3.15. Water permeability device**

### 3.2.8.2 Discussion of the Results

The micrometer readings and the corresponding water flux values (in./s) as a function of time are presented in Figures 3.16 and 3.17, respectively. Testing of the control specimens was discontinued when the micrometer gauge reached its full-scale capacity, indicating a high rate of water permeation through the untreated concrete surface. Application of silane sealers resulted in a substantial reduction in surface water permeability, with measured flux values approximately five to six times lower than those of the control concrete. Although minor variations were observed among individual silane products, the results indicate that isobutyltriethoxy silane treatments (SIL2 and SIL4) provided the most effective reduction in surface water permeability compared to the other sealers evaluated.

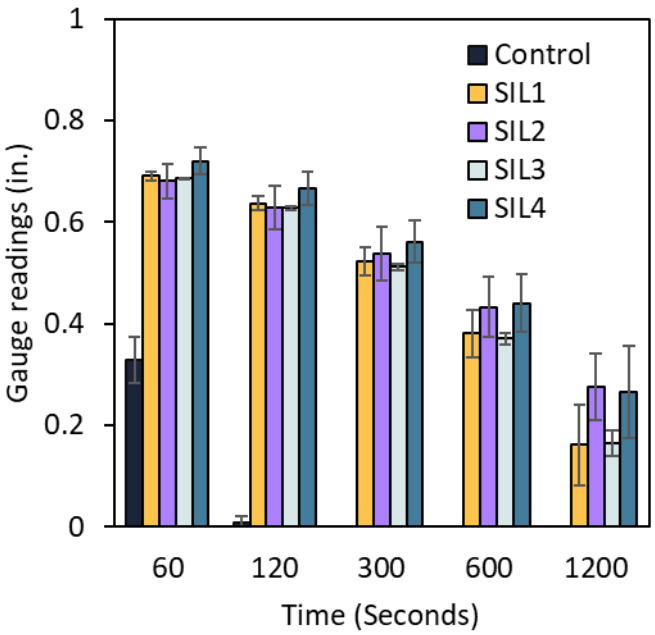


**Figure 3.16. Gauge readings (in.) vs. time (Sec.)**

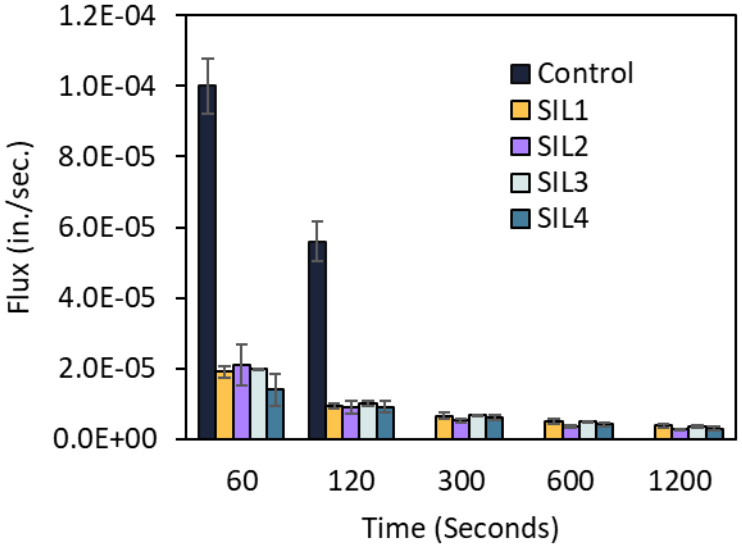


**Figure 3.17. Water flux (in./sec) vs. time**

### 3.2.8.3 Conclusions

The water permeation test was conducted to differentiate the performance of the silane treatments under investigation. The results exhibited considerable scatter, indicating limitations in the ability of the test method to consistently evaluate and rank the performance of the sealers. Despite this variability, the overall trend suggests that isobutyltriethoxy silane treatments demonstrated superior performance relative to the other sealers evaluated.

## 3.3 Summary

In summary, the performance of four silane products selected from the Missouri Department of Transportation (MoDOT) approved concrete sealers list was investigated. The silanes were evaluated based on salt absorption and desorption characteristics, chloride penetrability, frost-scaling resistance, surface and bulk electrical resistivity, rate of absorption, and water permeability. The cumulative findings are summarized in Table 3.8. Overall, Protectosil SH100 and SIL-ACT-ATS 200 outperformed the other products evaluated. Based on these results, both products were selected for use in the subsequent evaluation of nanocomposite coatings for concrete.

**Table 3.8. Summary of performance of silane sealers**

| | Protectosil SH100 | Protectosil S300 | Protectosil CIT | SIL-ACT-ATS 200 |
|---|---|---|---|---|
| Salt absorption (NCHRP Series II) | ●● | ●●●● | ● | ●●● |
| Chloride content (NCHRP Series II) | ● | ●●● | ●● | ●●●● |
| Long term chloride ion penetration (AASHTO T259) | ●●●● | ●● | ● | ●●● |
| Scaling resistance | ●●● | ●● | ● | ●●●● |
| Bulk conductivity | ●●●● | ● | ●● | ●●● |
| Surface resistivity AASHTO T358 | ●●● | ●● | ● | ●● |
| Rate of absorption ASTM C1585 | ●●● | ●● | ● | ●●●● |
| Apparent chloride diffusion coefficient ASTM C1556 | ●●●● | ●● | ● | ●●● |
| Water permeation | ● | ●● | ● | ●● |

* For Vapor transmission in accordance with NCHRP Series (II),No major differences were found between different silanes

# Chapter 4: Experimental Investigation of Silane-Nanoclay Composites

In this investigation, a silane-nanoclay composite was evaluated to assess the barrier characteristics associated with surface modification of concrete. The composite is intended to provide dual functionality: (a) pore lining and filling through the formation of silane reaction products, and (b) partial filling of near-surface pores by nanoclay particles. For this purpose, silane-nanoclay composites were prepared by intermixing nanoclay with a silicic ester at loading ratios of 2.5% and 5.0% by weight of silane. All mixtures were applied to concrete specimens produced using MoDOT Grade B1 concrete.

## 4.1 Overview of the Experimental Investigation

In this investigation, non-air-entrained concrete (MoDOT Grade B1), supplied by Wieberg Red-E-Mix, was used for all tests. The mixture proportions are provided in Table 4.1. The coarse aggregate consisted of crushed dolomitic stone with a nominal maximum size of 1 in. The aggregate had a water absorption of 0.7% and a specific gravity of 2.61. The fine aggregate consisted of natural river sand with a water absorption of 0.3% and a specific gravity of 2.61. A Type A water-reducing admixture was used to achieve a target slump of 6 in. Cement conforming to ASTM C595 Type IL was used in the mixture.

**Table 4.1. Concrete mix proportions (per cubic yard)**

| Cement<br>lb | Coarse Aggregates<br>lb | Sand<br>lb | Water<br>lb | Water Reducer<br>oz | Slump<br>in. | 28-day comp. strength<br>Psi |
|---|---|---|---|---|---|---|
| 629 | 1170 | 1880 | 260 | 3 | 6 | 5220 |

In this phase of the investigation, two silane products demonstrating improved performance, Protectosil SH100 and SIL-ACT-ATS 200, were selected for further evaluation. For consistency with the terminology used throughout this study, Protectosil SH100 and SIL-ACT-ATS 200 are hereafter referred to as SIL1 and SIL4, respectively. Surface-modified organophilic montmorillonite nanoclay, containing 25–30 wt.% trimethyl octadecyl ammonium chloride, was procured from Sigma-Aldrich and used in the preparation of nanocomposite coatings. The nanoclay had an average particle size of less than 20 μm, according to the manufacturer's specifications. A total of 140 specimens were cast and cured for 28 days, unless otherwise noted, in accordance with ASTM C31/C31M-25b. Prior to treatment, concrete surfaces were prepared by hydro-jetting (see Figure 4.1). The specimens were then conditioned under standard laboratory environmental conditions prior to application of the treatments. Figure 4.2 schematically illustrates the application procedure for both silane and silane-nanoclay composite systems. The silane-nanoclay composite was prepared by intermixing a predetermined mass of nanoclay with the silane at low speed for 5 min using a hand mixer. The mixture was subsequently ultrasonicated for 1 h using a Branson M2800 unit operating at a maximum power of 110 W (see Figure 4.3). The silane and silane-nanoclay composite treatments were applied by brushing to surface saturation. A total of three coats were applied,

with a 20 min interval between successive coats. Concrete specimens treated with neat silanes were cured under standard laboratory environmental conditions for 14 days prior to performance testing. Nanoclay exhibits pozzolanic activity, therefore Specimens treated with silane-nanoclay composite were cured under wet burlap for 7 days, followed by drying under laboratory environmental conditions for an additional 7 days. Figure 4.4 shows the post-treatment curing procedures for neat silane and silane-nanoclay treated-concrete.

**Figure 4.1. Concrete surface preparation by hydro-jetting**

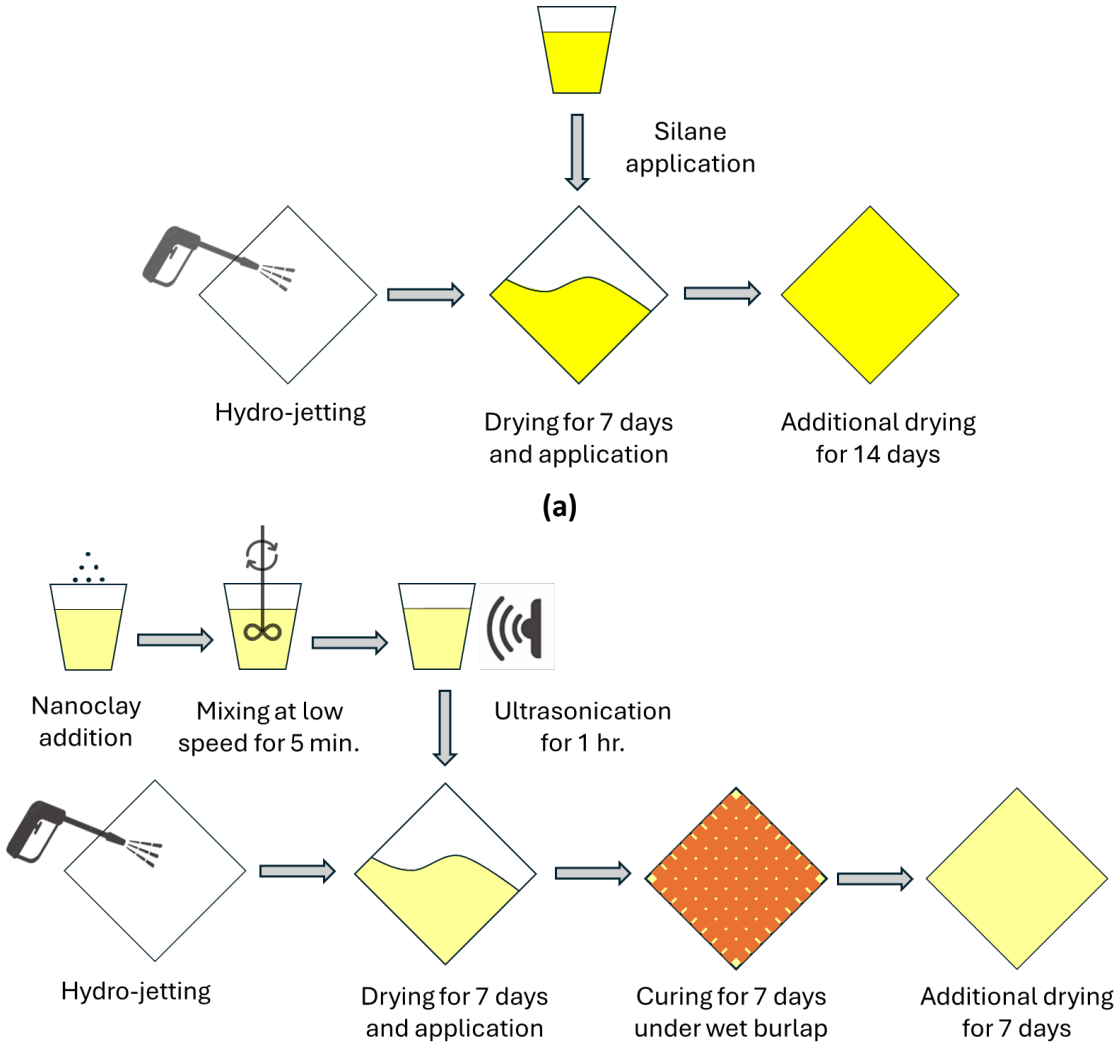


**Figure 4.2. Procedures for preparation of concrete specimens (a) neat silanes, and (b) silane-nanoclay composites**


**Figure 4.3. Ultrasonic bath used in this study**

**Figure 4.4. Post-treatment procedures for neat silanes and silane-nanoclay composites**

## 4.2 Performance Tests

### 4.2.1 Salt Absorption/Vapor Transmission Test

#### 4.2.1.1 Procedure of the Test

The test was conducted as previously described (see Section 3.3.1.1). The initial chloride content of the concrete, measured prior to submersion, was subtracted from the chloride measurements obtained for both the control and neat silane-treated specimens. Specimens treated with the silane-nanoclay composite were expected to have higher initial chloride content and were evaluated separately. This elevated baseline was expected due to the presence of ammonium chloride associated with the organophilic nanoclay, which is intercalated within the interlayer (gallery) spaces of the clay structure.

#### 4.2.1.2 Discussion of the Results

The absorption/desorption characteristics of the concrete are presented in Figure 4.5. Surface treatment significantly reduced the absorption of saline solution, with reductions of 84.7% and 83.4% observed for SIL1 and SIL4, respectively. Consistent with established behavior, silane treatments do not inhibit vapor transmission; therefore, moisture loss (desorption) proceeds without significant restriction in specimens treated with neat silanes.

For specimens treated with the silane-nanoclay composite, a slight increase in absorption was observed. However, a substantial increase in the rate of vapor loss was also recorded. This behavior may be attributed to saturation of the near-surface concrete layer with saline solution during exposure. Accelerated drying of the concrete surface layer increases its electrical resistivity and promotes the removal of excess moisture from the concrete cover zone over the reinforcement, which may contribute to reducing the risk of corrosion.

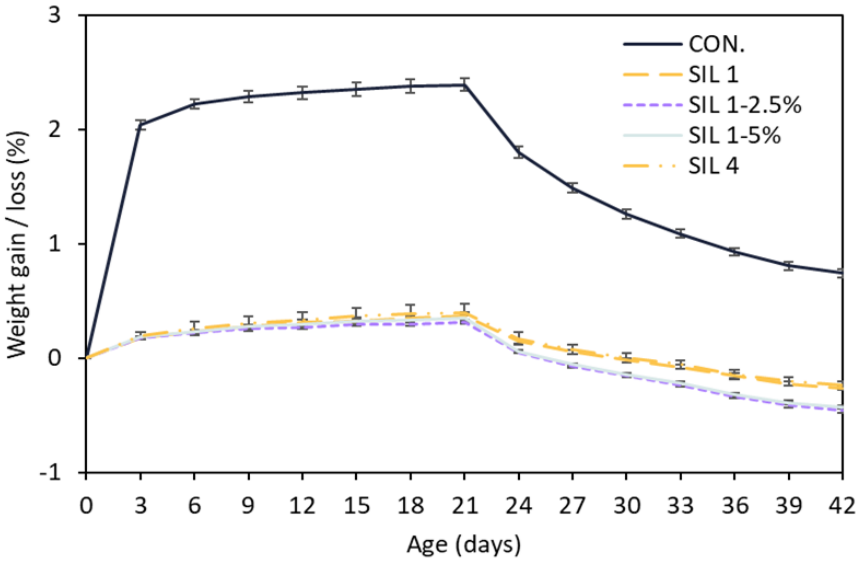


**Figure 4.5. Weight gain/loss (%) vs. time (days)**

Chloride contents are presented in Table 4.2. It should be noted that baseline chloride content of 0.0394% by weight of concrete was the same for all specimens, regardless of whether nanoclay was incorporated. Neat silane treatments reduced chloride penetration into the concrete by 81.9% and 77.7% for SIL1 and SIL4, respectively. In contrast, specimens treated with silane-nanoclay composites exhibited an increase in measured chloride content. Chloride concentrations reached 0.161% and 0.152% by weight of concrete for nanoclay loading ratios of 2.5% and 5%, respectively. The mechanism governing this behavior will be discussed later in this chapter (see Section 4.3.2).

**Table 4.2. The ion chloride content for untreated and silane treated concrete**

| Type | $Cl^-$ (%) |
|---|---|
| Control | 0.602±0.028 |
| SIL1 | 0.109±0.003 |
| SIL1-2.5% | 0.161±0.010 |
| SIL1-5% | 0.152±0.004 |
| SIL4 | 0.134±0.007 |

#### 4.2.1.3 Conclusions

In summary, both neat silanes and silane-nanoclay composites reduced saline solution absorption and chloride ingress by more than 75%. Among the treatments evaluated, SIL1 demonstrated superior performance. Silane-nanoclay composite treatments exhibited an increased rate of vapor loss, which is beneficial for reducing the risk of reinforcement corrosion by promoting drying of the concrete cover. The observed increase in measured chloride content associated with the nanocomposite treatments will be discussed in a subsequent section.

### 4.2.2 Wettability of Concrete

#### 4.2.2.1 Procedure of the Test

Wettability is defined as the ability of a solid concrete surface to be wetted by a liquid and is typically quantified by the contact angle. The contact angle is defined as the angle formed at the intersection of the solid-liquid and liquid-gas interfaces. Surfaces are classified as hydrophilic when the contact angle is less than 90°, and hydrophobic when the contact angle exceeds 90°. In this test, water droplets were carefully placed on the concrete surface, and the droplet profiles were captured using a standard resolution camera Canon EOS R100 (see Figure 4.6). The droplet profiles were analyzed using the low-bond axisymmetric drop shape analysis (LB-ADSA) plugin in ImageJ software. This method fits the experimental droplet profile to a theoretical curve based on the axisymmetric Young-Laplace equation. The contact angle was determined at the point where the theoretical curve best matched the experimental droplet outline. Five measurements were obtained for each specimen, and the average contact angle was reported.

**Figure 4.6. Contact angle measurement setup**

#### 4.2.2.2 Discussion of the Results

Figure 4.7 shows the droplet profile immediately upon placement on the concrete substrate and after allowing the droplet to settle for 5 min. Contact angle measurements are summarized in Table 4.3. For the reference (untreated) concrete, the contact angle decreased to below 60°, reflecting the higher surface energy of the substrate, which promotes spreading of water molecules across the surface. Following silane treatment, the contact angle increased to 87° for SIL1 and 99° for SIL4, indicating a reduction in surface energy and enhanced hydrophobicity. SIL4 imparted a greater degree of hydrophobicity due to the branched structure of its alkyl groups. For silane-nanoclay composite treatments, a slight increase in contact angle was observed; however, the improvement was marginal compared to neat silane treatments.

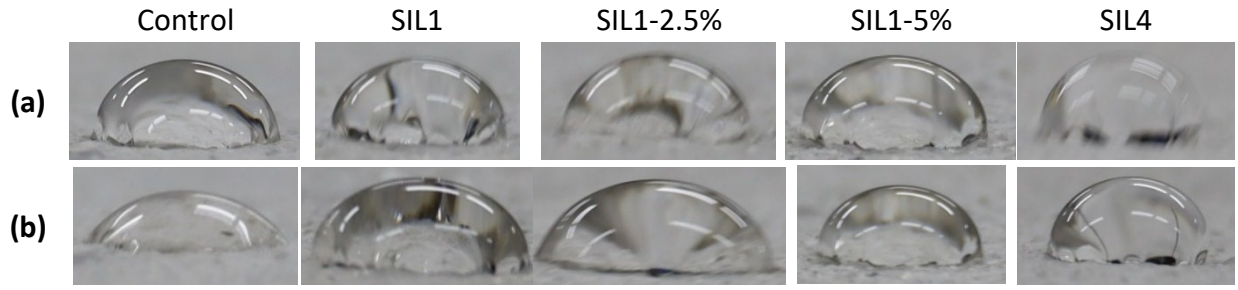


**Figure 4.7. Droplet shape (a) after contact with the surface (b) at t= 5 min after contact with the surface**

**Table 4.3. Contact angles for various surface treatment procedures**

| | Control | SIL1 | SIL1-2.5% | SIL1-5% | SIL4 |
|---|---|---|---|---|---|
| $T_0$ (min) | 81° | 97° | 95° | 94° | 104° |
| $T_5$ (min) | 58° | 87° | 91° | 90° | 99° |

#### 4.2.2.3 Conclusions

In this test, droplet profiles were captured for each surface treatment under investigation and analyzed using the LB-ADSA plugin in ImageJ, which fits the droplet profile to the axisymmetric Young-Laplace equation. All surface modification approaches resulted in a significant increase in contact angle compared to the untreated control concrete. Among the neat silane treatments, SIL4 exhibited a higher contact angle than SIL1. The addition of nanoclay did not produce a substantial increase in contact angle; the improvement observed was minimal and largely marginal.

### 4.2.3 Long Term Ion Chloride Penetration (AASHTO T259)

#### 4.2.3.1 Procedure of the Test

The test procedure follows the sequence described in Section 3.2.2.1.

#### 4.2.3.2 Discussion of the Results

Chloride contents as a function of depth from the exposed surface are presented in Table 4.4. The initial chloride content was 0.032% by weight of concrete. Both neat silane and silane-nanoclay composite treatments reduced chloride content relative to the reference specimens, with reduction percentages ranging from 47.8% to 74.2%. Among the neat silane treatments, SIL1 demonstrated greater resistance to chloride ingress compared to SIL4. The incorporation of nanoclay into the silane matrix resulted in a slight additional reduction in chloride content; however, the extent of improvement was modest. At a depth of 0.5–1.0 in., the reductions in chloride content were 68.4%, 74.2%, and 74.0% for SIL1, SIL1–2.5%, and SIL1–5%, respectively, relative to the control specimens. The influence of exposure conditions on the performance of silane-nanoclay composites is discussed in Section 4.3.

**Table 4.4. Chloride ion content (% by weight of concrete) vs. depth (in.) as per AASHTO T259**

| Depth | Control | SIL1 | SIL1-2.5% | SIL1-5% | SIL4 |
|---|---|---|---|---|---|
| 0.063-0.5 in. | 0.339 | 0.158 | 0.159 | 0.149 | 0.168 |
| 0.5-1.0 in. | 0.180 | 0.057 | 0.047 | 0.047 | 0.053 |
| 1.0-1.5 in. | 0.074 | 0.039 | 0.033 | 0.036 | 0.037 |

#### 4.2.3.3 Conclusions

In light of the results obtained, all surface treatment approaches evaluated in this study improved resistance to chloride ingress. Among the treatments, SIL1 demonstrated superior performance, consistent with earlier findings. Silane-nanoclay composite treatments provided a

slight improvement in chloride ingress resistance compared to neat silanes, likely due to enhanced barrier characteristics. However, the extent of this improvement was marginal.

### 4.2.4 Long Term Ion Chloride Penetration of Cracked Concrete (Modified AASHTO T259)

#### 4.2.4.1 Procedure of the Test

Triplicate concrete slabs, both untreated and treated, were fabricated and cured for 14 days in a controlled curing chamber. A saw-cut with a width of 1/12 in. and a depth of 5/8 in. was introduced into each slab, see Figure 4.8. The slabs were subsequently surface-impregnated with the corresponding silane or silane-nanoclay composite treatments. Following treatment, the top surface of each slab was abraded using a steel wire brush to simulate the effects of traffic on bridge deck surfaces. A dam was then constructed around the perimeter of each slab, and the specimens were ponded with a 3% NaCl solution by weight prepared with distilled water for a duration of 90 days. For chloride ion analysis, the upper 0.063 in. of the slab surface was ground, and powdered samples were collected according to the layout shown in Figure 4.9. Chloride ion content was determined using the acid digestion potentiometric method in accordance with AASHTO T 260. Chloride concentrations were assumed to be constant on both sides of the crack.

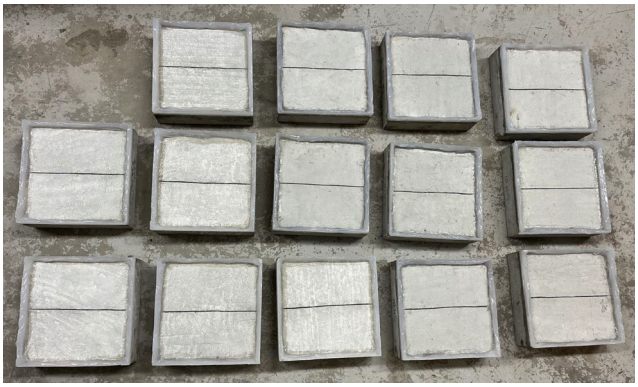

**(a)**

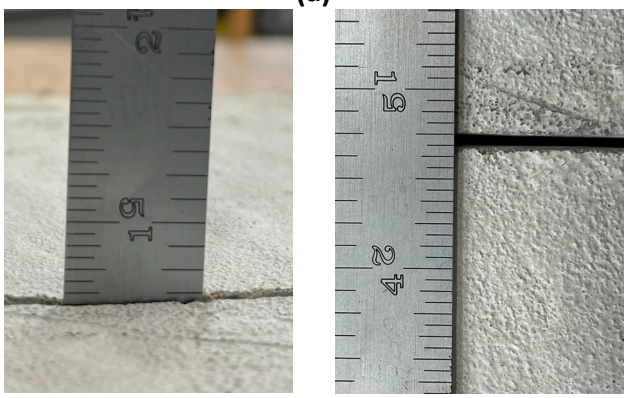

**(b)**

**Figure 4.8. Modified AASHTO T259 chloride penetration test (a) cracked samples before exposure (b) the depth and width of the crack**

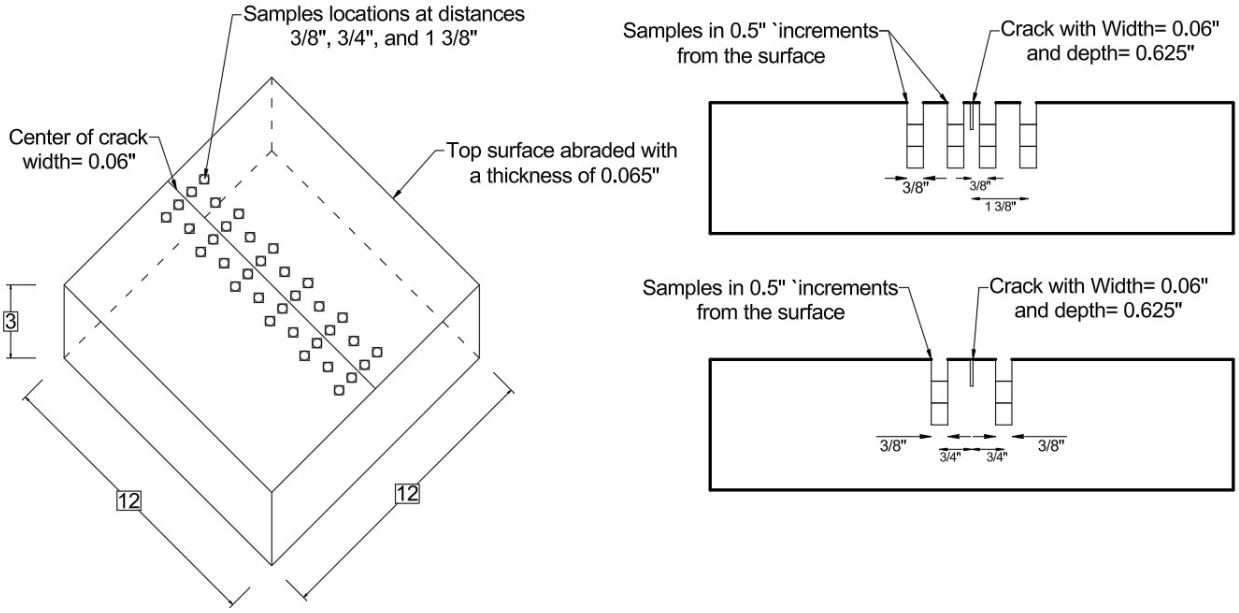


**Figure 4.9. Layout for chloride sampling for long-term chloride ion penetration of cracked concrete (All dimensions are in inches)**

#### 4.2.4.2 Discussion of the Results

Figure 4.10 illustrates chloride ion concentration as a function of depth at specified distances from the crack. Figure 4.11 presents chloride ion concentration as a function of distance from the crack at selected depths. In all figures, a dashed line indicates the baseline chloride content of 0.032%. The results demonstrate that surface treatments reduce chloride ingress through surface cracks and pavement joints compared to the untreated control specimens. The percentage reduction in chloride content ranges from 11.8% to 75.7%, depending on the location relative to the crack. In general, the effectiveness of the surface treatments increases with distance from the crack. For example, SIL1 reduced chloride content by 41.9%, 59.1%, and 75.8% at distances of 3/8 in., 3/4 in., and 1 1/12 in. from the crack, respectively. Comparing the performance of neat silane treatments, SIL1 consistently demonstrated greater resistance to chloride ingress than SIL4. At a distance of 3/8 in. from the crack, SIL1 reduced chloride content by 41.9%, 27.2%, and 40.5% at depths of 1/2 in., 1.0 in., and 1 1/12 in., respectively. Under the same conditions, SIL4 achieved reductions of 37.7%, 11.8%, and 28.8%. At a distance of 1 3/8 in. from the crack, the percentage reductions for SIL1 were 75.8%, 67.9%, and 29.5% at depths of 1/2 in., 1.0 in., and 1 1/2 in., respectively, while the corresponding reductions for SIL4 were 68.5%, 66.4%, and 34.4%.

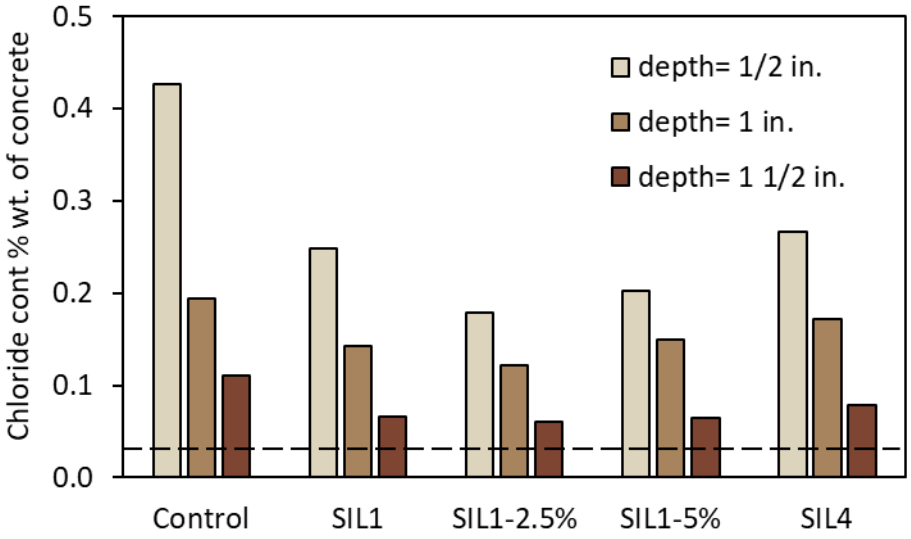
0.5
0.4
0.3
0.2
0.1
0.0
Chloride cont % wt. of concrete
depth= 1/2 in.
depth= 1 in.
depth= 1 1/2 in.
Control
SIL1
SIL1-2.5%
SIL1-5%
SIL4

**(a)**

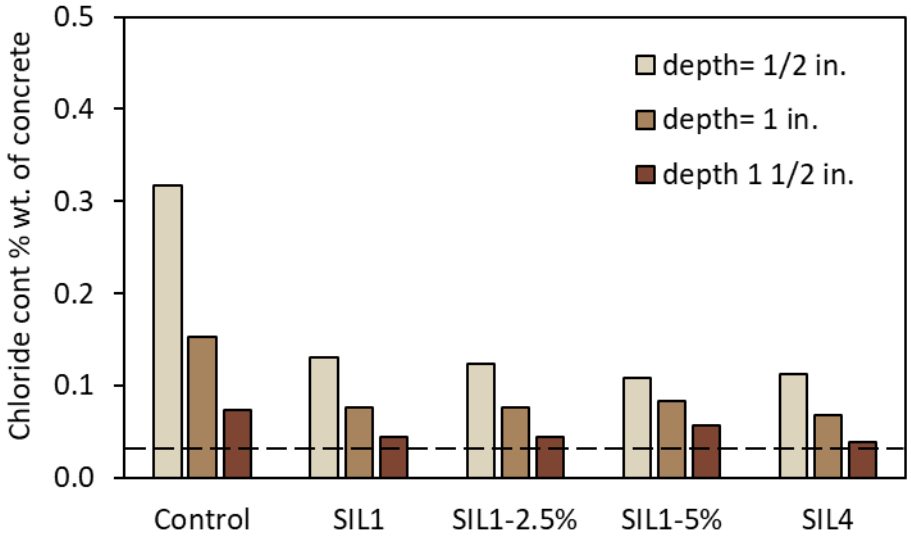
0.5
0.4
0.3
0.2
0.1
0.0
Chloride cont % wt. of concrete
depth= 1/2 in.
depth= 1 in.
depth 1 1/2 in.
Control
SIL1
SIL1-2.5%
SIL1-5%
SIL4

**(b)**

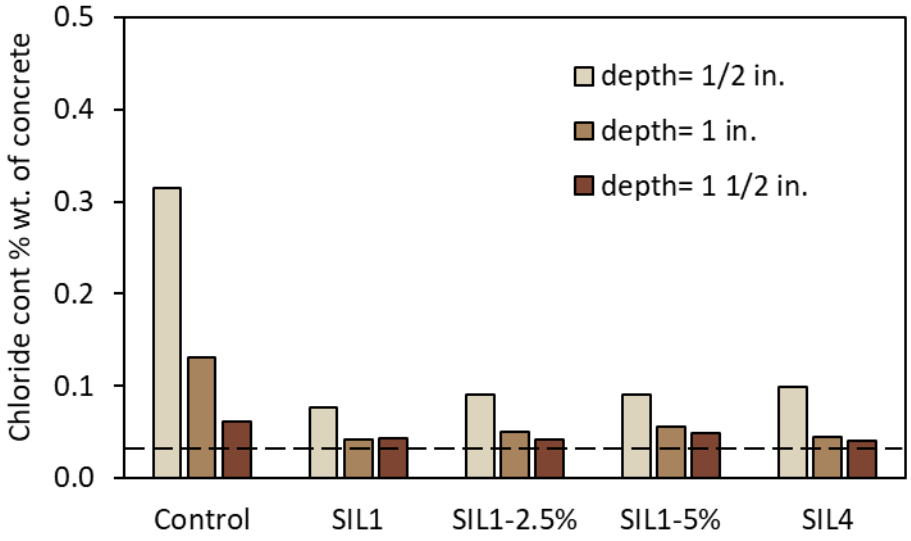


**(c)**

**Figure 4.10. Chloride ion content (% wt. of concrete) as function of depth (in.) at (a) distance= 3/8 in. (b) distance= 3/4 in. and (c) distance= 1 3/8 in. from the center of crack**

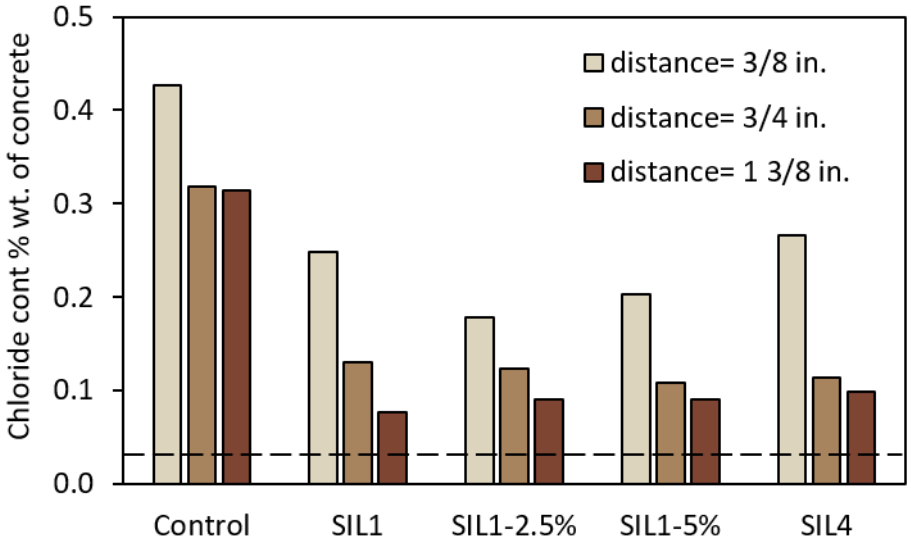


**(a)**

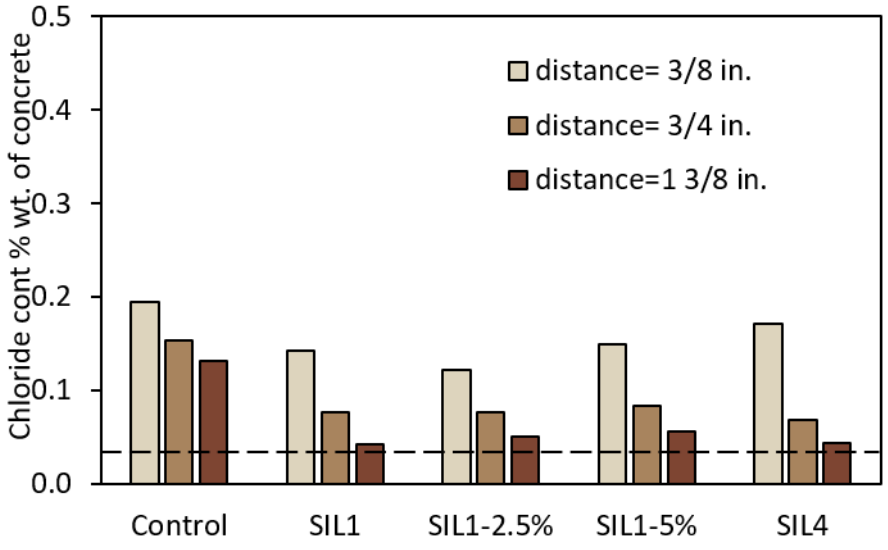


**(b)**

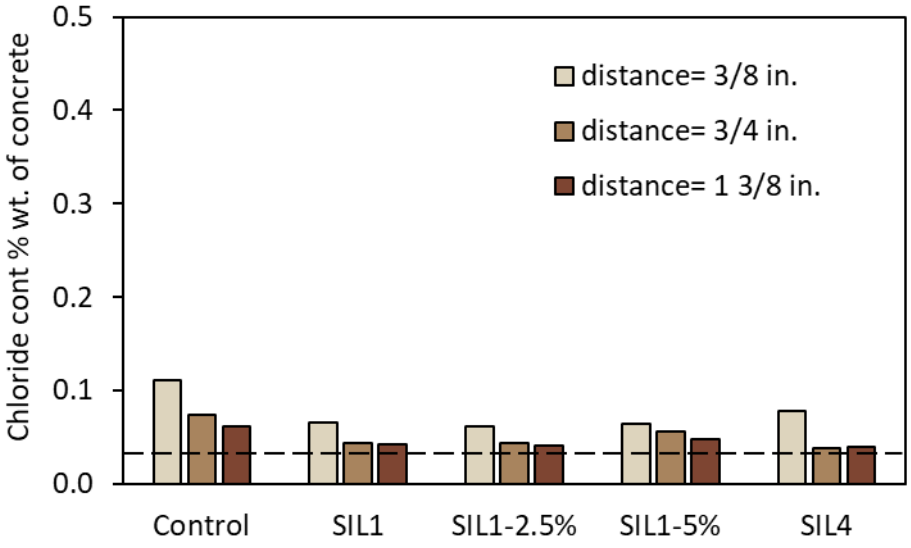


**(c)**

**Figure 4.11. Chloride ion content (% wt. of concrete) as function of distance (in.) from the crack (a) depth= 1/2 in. (b) depth 1 in. and (c) depth= 1 1/2 in.**

In general, silane-nanoclay composites reduce chloride ion penetration at all measured depths. For example, at a location 3/8 in. from the crack and a depth of ½ in., incorporation of nanoclay into the silane matrix reduced chloride content by 27.8% and 18.1% relative to neat silane at loading ratios of 2.5% and 5%, respectively. A minor inconsistency was observed at a depth of 1.0 in. and a distance of 3/8 in. from the crack. At this location, chloride contents of 0.142 and 0.149 were measured for SIL1 and SIL1–5%, respectively. This difference may be associated with the higher initial nanoclay content or localized interaction effects (e.g., adsorption of chlorides by nanoclay particles) during testing; however, this behavior is not conclusively

established. Similarly, at a depth of 1/2 in. and a distance of 1 3/8 in. from the crack, chloride content increased slightly from 0.076 for neat silane to 0.090 for the silane-nanoclay composite. Overall, the results indicate that silane-nanoclay composites used for surface treatment of concrete can form an effective barrier in cracked regions, thereby reducing chloride ingress into the concrete.

Figures 4.10. and 4.11. indicate that the relative effectiveness of surface treatments for concrete is most reliably evaluated near the crack, within a depth of approximately 1 in. under the test conditions of this study. The highest treatment efficiency occurs near the exposed surface and away from the crack. At greater depths, no appreciable variation in chloride content is observed, regardless of distance from the crack. Based on these observations, silane-nanoclay composites demonstrate the greatest effectiveness for crack sealing specifically at a loading ratio of 2.5%. For neat silanes, SIL1 exhibits better performance than SIL4 under the same conditions. These findings are consistent with the results presented earlier in Sections 3.2.2 and 4.2.3.

It is worth highlighting that chloride content in uncracked and cracked silane-nanoclay treated specimens at 3/8 in. from the crack show lower change in chloride content demonstrating notable ability in sealing the crack against further chloride ingress (see section 4.2.3.2).

#### 4.2.4.3 Conclusions

In this phase of the study, the effectiveness of silanes and silane-nanoclay composites in sealing surface cracks and pavement joints was evaluated. The results indicate that both silanes and silane-nanoclay composites reduce chloride ingress into the concrete. Among the neat silanes, SIL1 demonstrates better resistance compared to SIL4 in limiting chloride penetration. Silane-nanoclay composites exhibit higher performance, particularly at a loading ratio of 2.5%, relative to neat silane. Interestingly, when nanoclay is incorporated into the silane matrix, lower difference in chloride concentration was observed between cracked and uncracked concrete, suggesting effective mitigation of chloride ingress in the presence of surface cracks.

### 4.2.5 Scaling Resistance of Concrete

#### 4.2.5.1 Procedure of the Test

The test implemented as previously described in Section 3.2.3.1.

#### 4.2.5.2 Discussion of the Results

The cumulative mass loss (oz/yd$^2$), together with the visual rating, is presented in Table 4.5 and Figure 4.12 at 10-cycle intervals. The results clearly demonstrate the effect of silane and silane-nanoclay composite treatments on the scaling resistance of concrete. For neat silane treatments, prior results indicate that SIL4 provides greater resistance to scaling, which is attributed to the branched structure of its organofunctional group. Silane-nanoclay composites exhibit a non-uniform effect on scaling resistance. At a nanoclay loading of 2.5%, the specimens exhibit higher mass loss after 20 cycles compared to neat silane-treated concrete. However,

after 50 cycles, the cumulative mass loss decreases, falling below that of the neat silane-treated specimens by approximately 2.6 oz/yd². At a 5% nanoclay loading, the mass loss shows a pronounced increasing trend throughout the test duration, ultimately reaching a cumulative mass loss of approximately 3.2 oz/yd² higher than the control concrete. One possible explanation is that the presence of nanoclay may increase the local chloride concentration at the concrete surface. This concentration gradient can induce osmotic pressure, which may contribute to increased scaling and reduced durability of the treated concrete.

**Table 4.5. The cumulative mass loss (oz/yd²) and visual rating for neat silanes and silane-nanoclay composites***

| No. of cycles | Control | SIL1 | SIL1-2.5% | SIL1-5% | SIL4 |
|---|---|---|---|---|---|
| 10 | 41±3.9 (5) | 0 | 0 | 0 | 0 |
| 20 | 103±9.8 (5) | 1±0.3 (2) | 1±0.2 (3) | 3±0.5 (3) | 1±0.4 (2) |
| 30 | 127±19.6 (5) | 3±0.7 (3) | 2±0.8 (3) | 5±0.7 (3) | 2±0.4 (2) |
| 40 | 167±21.3 (5) | 8±1.4 (4) | 7±0.8 (3) | 10±2.8 (4) | 6±0.3 (3) |
| 50 | 195±25.2 (5) | 14±1.2 (4) | 11±2.0 (4) | 17±3.5 (4) | 12±0.4 (4) |

* The numbers in parentheses are the visual rating

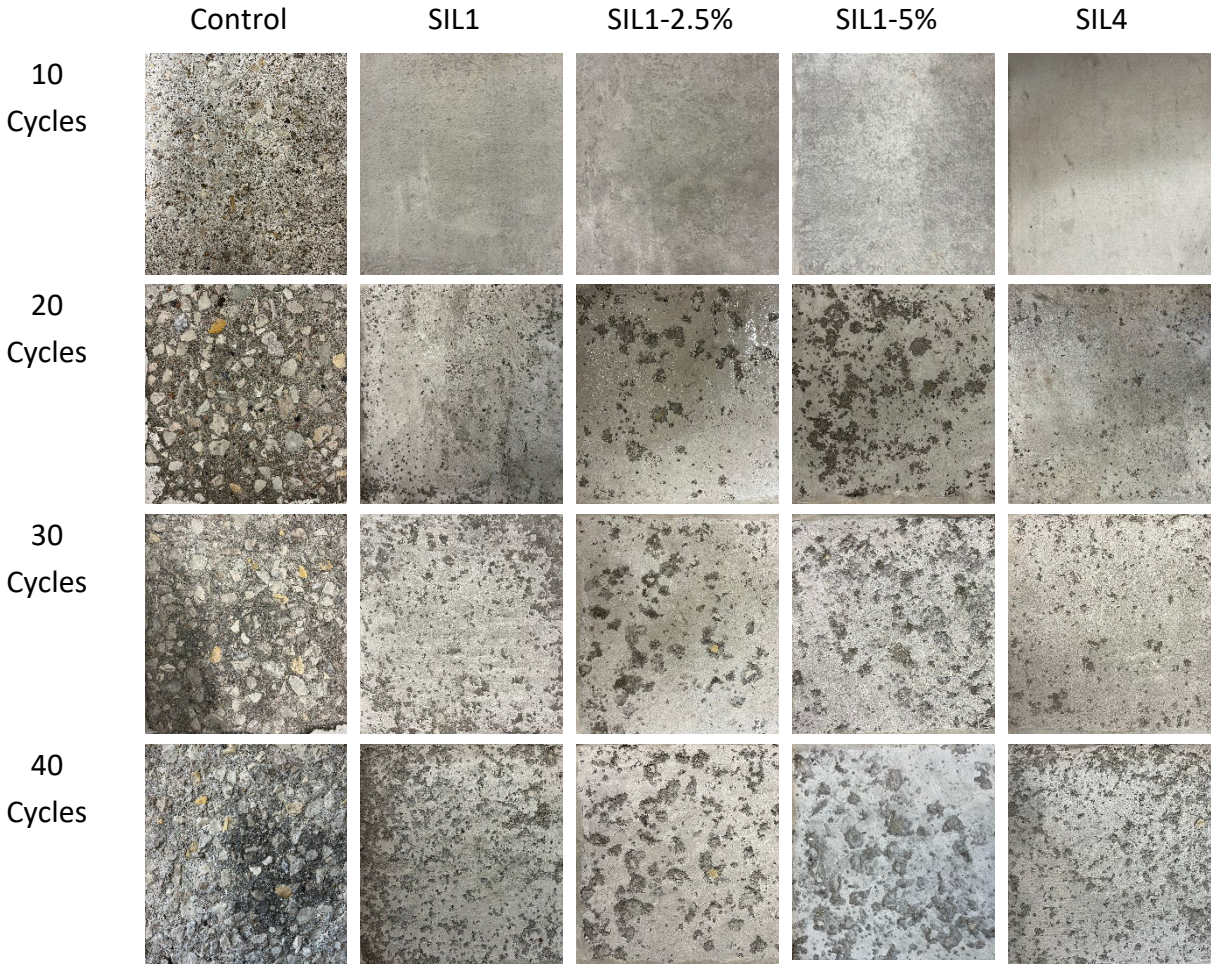


**Figure 4.12. Surface scaling progression at 10-cycle intervals**

#### 4.2.5.3 Conclusions

In summary, both neat silanes and silane-nanoclay composites reduce the scaling of concrete exposed to deicing chemicals. Among the neat silanes, SIL4 demonstrates greater retardation to surface scaling than SIL1. However, the incorporation of nanoclay appears to increase scaling deterioration. Although a marginal improvement was anticipated at a 2.5% nanoclay loading, the observed results do not consistently support this expectation.

### 4.2.6 Surface Resistivity of Concrete (AASHTO T358)

#### 4.2.6.1 Procedure of the Test

Surface resistivity measurements were conducted in accordance with the procedure described in Section 3.2.5.1. After casting and curing, eight indelible marks were placed uniformly around the circumference of each specimen, in addition to a centerline reference, as shown in Figure 4.13. The cylindrical specimens were then coated with the respective protective treatments. Initial measurements were obtained after curing and drying for 7 days. Subsequently, the specimens were immersed in water, and surface resistivity readings were recorded at the following intervals: 30 min, 3 h, 12 h, 24 h, 3 days, 7 days, 14 days, and 28 days. At each time interval, a total of 24 readings were collected and averaged to obtain a representative value for resistivity.


**(a)** **(b)**

**Figure 4.13. Marking for measurement of surface resistivity (a) top of the cylinder (b) side of the cylinder**

#### 4.2.6.2 Discussion of the Results

Figure 4.14 illustrates the increase in specimen mass as a function of time during water immersion. The silane-treated specimens exhibit reduced water uptake compared to the control concrete, indicating that the silane forms a hydrophobic boundary layer that limits moisture ingress. Among the treatments, SIL4 shows greater water uptake than SIL1. No significant difference in water absorption is observed for the silane-nanoclay composites relative to the neat silane-treated specimens.

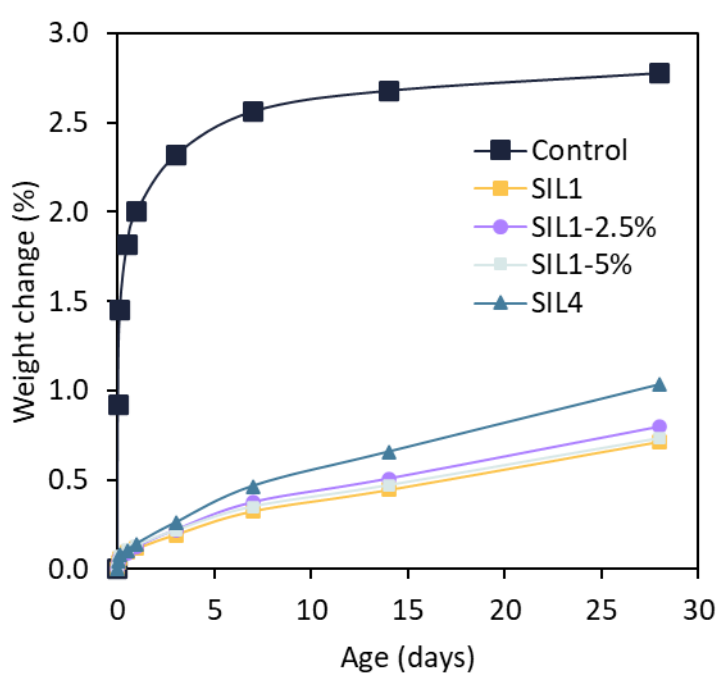


**Figure 4.14. Weight gain (%) vs. time (days)**

The surface resistivity results are presented in Figure 4.15. It should be noted that, immediately after submersion, the resistivity readings, particularly for SIL1-treated specimens, were highly variable and required more than 10 min to stabilize. For the control concrete, surface resistivity decreases significantly upon immersion and approaches a stable value after approximately 3 days. In contrast, both neat silane and silane-nanoclay composite specimens exhibit anomalous behavior. Upon initial immersion, resistivity increases despite concurrent water uptake, followed by a decrease after approximately 3 h of exposure. Concrete treated with SIL1 exhibits higher surface resistivity than that treated with SIL4. This observation is consistent with earlier findings that the hydrophobic surface layer influences electrical resistivity. In addition, SIL1-treated concrete appears to maintain a lower degree of saturation, which contributes to higher resistivity values.

For silane-nanoclay composites, a similar level of saturation is observed; however, resistivity is reduced relative to neat silane-treated concrete. This behavior may be attributed to the presence of well-dispersed nano particles, which can form conductive pathways within the silane layer and thereby decrease resistivity. At a nanoclay loading ratio of 5%, resistivity increases slightly, possibly due to particle agglomeration within the silane-nanoclay matrix. The observed reduction in resistivity associated with nanoclay incorporation should not be interpreted as a direct indication of reduced concrete durability.

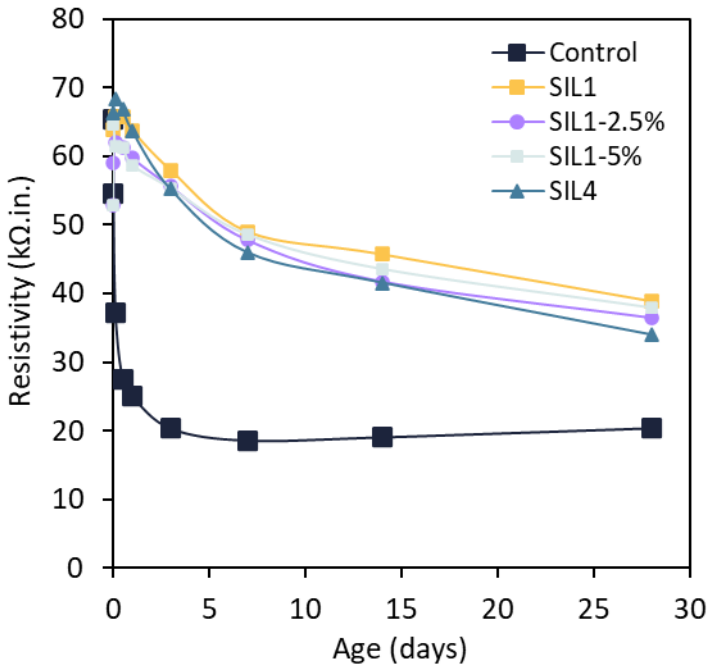


**Figure 4.15. Surface resistivity (KΩ.in.) vs. time (days)**

#### 4.2.6.3 Conclusions

Concrete surface resistivity is a key parameter for characterizing the penetrability of concrete and its susceptibility to the ingress and diffusion of aggressive agents. Surface modification significantly increases resistivity compared to unmodified concrete. Upon water exposure, the resistivity of unmodified concrete decreases rapidly whereas surface-treated concrete exhibits gradual reduction. Among the treatments, SIL1 shows higher resistivity, indicating improved resistance to ionic penetration in aggressive environments. The inclusion of nanoclay reduces resistivity. This behavior may be attributed to the formation of conductive pathways within the silane layer that connect to the underlying substrate, thereby facilitating electrical conduction.

### 4.2.7 Bulk Conductivity of Concrete

#### 4.2.7.1 Procedure of the Test

Concrete resistivity was measured on cylindrical specimens using a uniaxial configuration with two plate electrodes applied to the top and bottom surfaces. Electrical contact was established using saturated sponges, as illustrated in Figure 4.16. Following curing and drying, as described in Section 4.1, the initial resistivity measurement was obtained prior to water immersion. Subsequently, uniaxial resistivity measurements were recorded at 30 min, 3 h, 12 h, 24 h, 3 days, 7 days, and 28 days after submersion. For each sealing material, measurements were conducted on three replicate cylinders, and the results were averaged.

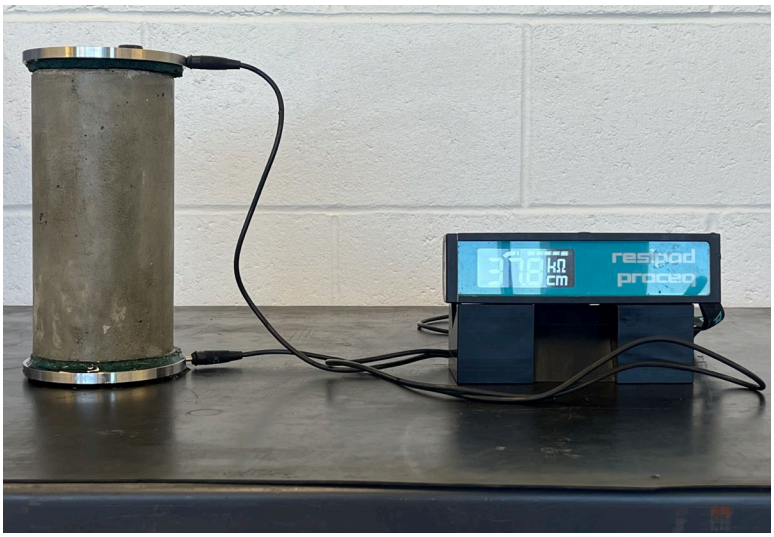

**Figure 4.16. Test arrangement for bulk (uniaxial) resistivity measurement**

#### 4.2.7.2 Discussion of the Results

Figure 4.17 presents the variation in specimen mass (weight gain) with time. The observed trend generally follows that of surface resistivity; however, the magnitude of weight gain is comparatively lower for SIL4-treated specimens.

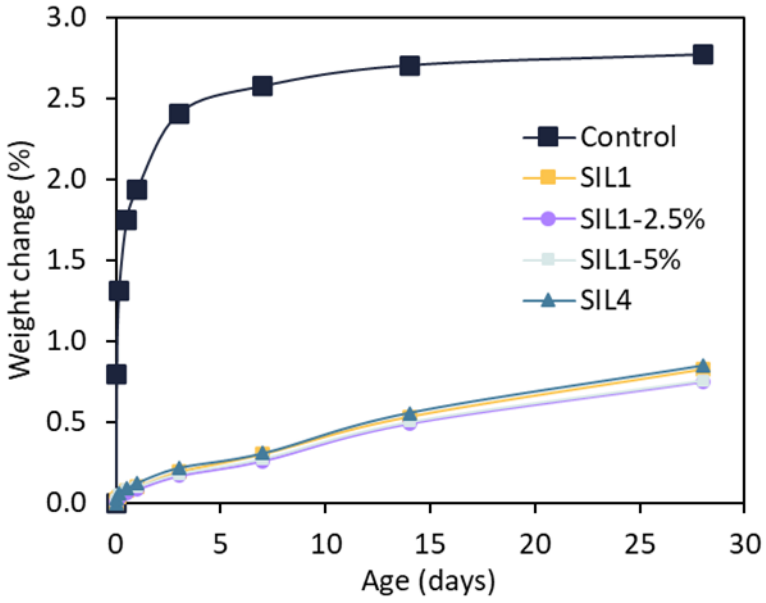


**Figure 4.17. Weight gain (%) vs. age (days)**

The variation of concrete resistivity with time is shown in Figure 4.18. The control (unmodified) concrete exhibits a rapid decrease in resistivity upon immersion, followed by stabilization after approximately 1 day. Silane treatment influences resistivity behavior. The silicic ester (SIL1) results in higher resistivity compared to isobutyltriethoxysilane (SIL4), indicating the effect of silane chemical composition on electrical properties. The inclusion of nanoclay significantly reduces bulk resistivity. This behavior may be influenced by the measurement configuration, as

the larger contact area associated with plate electrodes in the uniaxial test setup can increase sensitivity to conductive pathways within the treated layer.

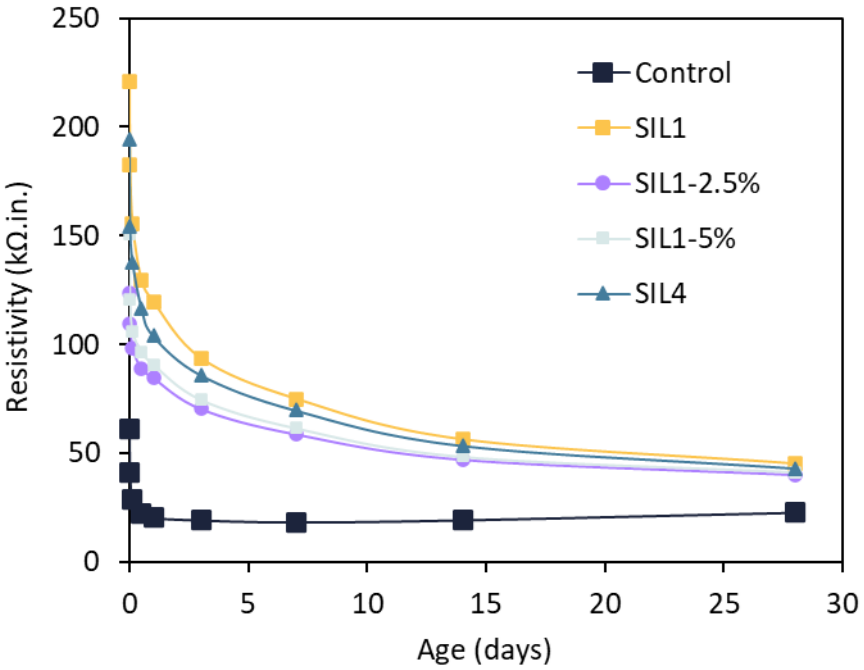


**Figure 4.18. Bulk resistivity (KΩ.in.) vs. age (days)**

#### 4.2.7.3 Conclusions

In summary, the bulk resistivity results exhibit trends similar to those observed for surface resistivity. For unmodified (control) concrete, resistivity decreases rapidly upon immersion and subsequently stabilizes at a near-constant value. Neat silane and silane-nanoclay composite treatments exhibit a comparable reduction pattern over time. Among the silanes, the silicic ester (SIL1) demonstrates higher resistivity, indicating improved resistance to ion mobility. The inclusion of nanoclay reduces resistivity. This behavior may be attributed to the formation of conductive pathways within the silane matrix that facilitate current flow between the surface layer and the underlying concrete substrate.

### 4.2.8 Resistance of Concrete to Freezing and Thawing

#### 4.2.8.1 Procedure of the Test

In this test, concrete specimens were subjected to freeze-thaw cycling and performance was evaluated based on mass loss, length change, and relative dynamic modulus of elasticity. Prismatic specimens measuring 4 in. × 3 in. × 16 in. were prepared. During preparation, gage studs were installed in accordance with ASTM C341/C341M for length change measurement. After 14 days of wet curing, the specimens were demolded and subjected to hydro-jetting to remove surface laitance. The specimens were then oven-dried at 165 °F for 5 days, followed by conditioning under typical laboratory environment for 2 days prior to application of the

respective neat silane and silane-nanoclay composite treatments, as described earlier in Section 4.1. Following treatment, specimens were exposed to cyclic freezing and thawing in accordance with ASTM C666 procedure (b). Each cycle consisted of reducing the temperature from 40 °F to 0 °F in 3 h (freezing phase in air), followed by increasing the temperature from 0 °F to 40 °F in 1 h (thawing phase in water). At intervals of 20 cycles, specimens were removed from the chamber and evaluated for mass change, length change, and relative dynamic modulus of elasticity, see Figures 4.19 and 4.20 for illustration. A length comparator and reference bar conforming to ASTM C490/C490M were used for length change measurements. An initial comparator reading was recorded prior to exposure, and subsequent length changes at each interval were calculated using Equation 4.1. The relative dynamic modulus of elasticity was determined using ultrasonic pulse velocity measurements obtained at three locations along each specimen. The relative dynamic modulus was calculated using Equation 4.2 below.

$$L_c = \frac{(L_2 - L_1)}{L_g} \times 100$$

Where:

$L_c$ = Length change after C cycles of freezing and thawing, %

$L_1$ = Length comparator reading at 0 cycles

$L_2$ = Length comparator reading at C cycles

$L_g$ = Effective gauge length between the innermost ends of the gage studs as shown in the mold diagram in specification C490

**Equation 4.1. Length change after C cycles of freezing and thawing**

$$P_c = \frac{v_c}{v_0} \times 100$$

Where:

$P_c$ = Relative dynamic modulus of elasticity after C cycles of freezing and thawing, %

$v_c$ = Ultra-sound pulse velocity at 0 cycles, in./sec.

$v_0$ = Ultra-sound pulse velocity at C cycles, in./sec.

**Equation 4.2. Relative dynamic modulus of elasticity after C cycles of freezing and thawing**

**Figure 4.19. Length change measurement using comparator**

**Figure 4.20. Ultra-sound pulse velocity for the determination of the relative dynamic modulus of elasticity**

#### 4.2.8.2 Discussion of the Results

The results of the accelerated freeze-thaw testing, including mass change, length change, and relative dynamic modulus of elasticity, are summarized in Table 4.6. The progression of damage at 20-cycle intervals is presented in Figure 4.21. Failure criteria were defined as any of the following: (a) mass loss exceeding 3%, (b) length increase exceeding 0.1%, or (c) relative dynamic modulus of elasticity falling below 60%. For mass change measurements, a positive value indicates an increase in mass due to water absorption within the concrete pore structure, whereas a negative value indicates mass loss resulting from scaling or material deterioration. For length change measurements, a positive value indicates expansion relative to the initial length (at 0 cycles), while a negative value indicates contraction.

**Table 4.6. The results of accelerated freeze-thaw testing for mass change, length change, and relative dynamic of elasticity**

| | | CONTROL | SIL1 | SIL1 - 2.5% | SIL1 - 5% | SIL4 |
|---|---|---|---|---|---|---|
| 20 cycles | $W_C$ (%) | 2.950 | 0.392 | 0.238 | 0.237 | 0.269 |
| | $L_C$ (%) | 0.028 | -0.010 | -0.005 | -0.007 | -0.007 |
| | $P_C$ (%) | 90.3 | 98.5 | 96.3 | 97.9 | 93.9 |
| 40 cycles | $W_C$ (%) | 3.542 | 0.518 | 0.289 | 0.294 | 0.329 |
| | $L_C$ (%) | 0.102 | -0.005 | -0.003 | -0.004 | -0.004 |
| | $P_C$ (%) | 69.7 | 99.3 | 99.8 | 96.9 | 95.4 |
| 60 cycles | $W_C$ (%) | 0.587 | 0.614 | 0.369 | 0.373 | 0.420 |
| | $L_C$ (%) | 0.283 | 0.000 | 0.002 | -0.001 | -0.003 |
| | $P_C$ (%) | 41.0 | 99.3 | 97.0 | 97.8 | 93.3 |
| 80 cycles | $W_C$ (%) | -6.030 | 0.620 | 0.385 | 0.380 | 0.458 |
| | $L_C$ (%) | 0.564 | 0.002 | 0.001 | -0.003 | -0.003 |
| | $P_C$ (%) | 15.8 | 101.6 | 97.8 | 96.3 | 90.5 |
| 100 cycles | $W_C$ (%) | – | 0.702 | 0.448 | 0.423 | 0.502 |
| | $L_C$ (%) | – | 0.003 | 0.000 | -0.005 | -0.005 |
| | $P_C$ (%) | – | 99.1 | 99.2 | 97.8 | 91.7 |
| 120 cycles | $W_C$ (%) | – | 0.822 | 0.499 | 0.472 | 0.560 |
| | $L_C$ (%) | – | 0.010 | 0.003 | -0.001 | -0.004 |
| | $P_C$ (%) | – | 98.5 | 97.9 | 95.6 | 89.8 |
| 140 cycles | $W_C$ (%) | – | 1.019 | 0.580 | 0.523 | 0.621 |
| | $L_C$ (%) | – | 0.038 | 0.015 | 0.008 | 0.011 |
| | $P_C$ (%) | – | 95.7 | 92.2 | 98.3 | 88.4 |
| 160 cycles | $W_C$ (%) | – | 1.068 | 0.665 | 0.644 | 0.747 |
| | $L_C$ (%) | – | 0.097 | 0.026 | 0.004 | 0.027 |
| | $P_C$ (%) | – | 90.6 | 94.5 | 92.4 | 91.4 |
| 180 cycles | $W_C$ (%) | – | -3.526 | 0.514 | 0.715 | 0.857 |
| | $L_C$ (%) | – | 0.198 | 0.048 | 0.011 | 0.058 |
| | $P_C$ (%) | – | 88.5 | 95.2 | 95.9 | 90.0 |
| 200 cycles | $W_C$ (%) | – | – | 0.672 | 0.840 | 1.016 |
| | $L_C$ (%) | – | – | 0.093 | 0.029 | 0.136 |
| | $P_C$ (%) | – | – | 93.1 | 93.2 | 89.1 |
| 220 cycles | $W_C$ (%) | – | – | 0.799 | 0.990 | 1.170 |
| | $L_C$ (%) | – | – | 0.126 | 0.050 | 0.177 |
| | $P_C$ (%) | – | – | 88.2 | 92.3 | 81.7 |
| 240 cycles | $W_C$ (%) | – | – | – | 1.217 | – |

| | | CONTROL | SIL1 | SIL1 - 2.5% | SIL1 - 5% | SIL4 |
|---|---|---|---|---|---|---|
| | $L_C$ (%) | – | – | – | 0.106 | – |
| | $P_C$ (%) | – | – | – | 92.5 | – |

For the untreated (control) concrete, an increase in the number of freeze-thaw cycles results in progressive expansion (length increase) and a significant reduction in the relative dynamic modulus of elasticity. Based on the defined failure criteria, the control specimens fail after 40 cycles. Silanes and silane-nanoclay composites exhibit increases in both mass and length with increasing cycles; however, these changes are substantially lower than those observed in the control concrete. In addition, the relative dynamic modulus of elasticity for surface-treated specimens does not show significant degradation over time. Failure in these specimens is typically associated with localized deterioration along specimen edges rather than uniform internal damage. Neat silane treatments provide improved resistance to freeze-thaw deterioration. Specimens treated with SIL1 and SIL4 withstand 180 and 200 cycles, respectively, before reaching the failure criteria. The incorporation of nanoclay further enhances freeze-thaw resistance. The number of cycles to failure increases to approximately 220 and 240 cycles for nanoclay loadings of 2.5% and 5%, respectively, compared to 180 cycles for neat silane-treated concrete. For neat silane-treated concrete at 200 cycles, the mass loss, length change, and relative dynamic modulus of elasticity reach approximately 4.11%, greater than 0.2%, and 84.4%, respectively. In contrast, silane-nanoclay composite specimens with a 5% loading exhibit no appreciable damage at comparable exposure levels, see Figure 4.22. This improved performance may be attributed to the ability of nanoclay to refine the pore structure, thereby reducing water ingress and internal saturation of the concrete. This, in turn, mitigates damage associated with repeated freeze-thaw cycling.

#### 4.2.8.3 Conclusions

Neat silane and silane-nanoclay composite treatments significantly improve the resistance of concrete to repeated freeze-thaw cycles compared to untreated (control) concrete. The length change criterion (0.1%) was generally observed to govern failure. Based on the number of cycles to failure, the resistance of the tested systems increases in the following order: Control < SIL1 <SIL4 <SIL1–2.5% < SIL1–5%. The corresponding number of cycles to failure is 40, 180, 200, 220, and 240 cycles, respectively. The incorporation of nanoclay enhances freeze-thaw resistance, likely due to the development of a denser near-surface microstructure. This reduces moisture ingress and limits internal saturation, thereby mitigating damage associated with cyclic freezing and thawing.

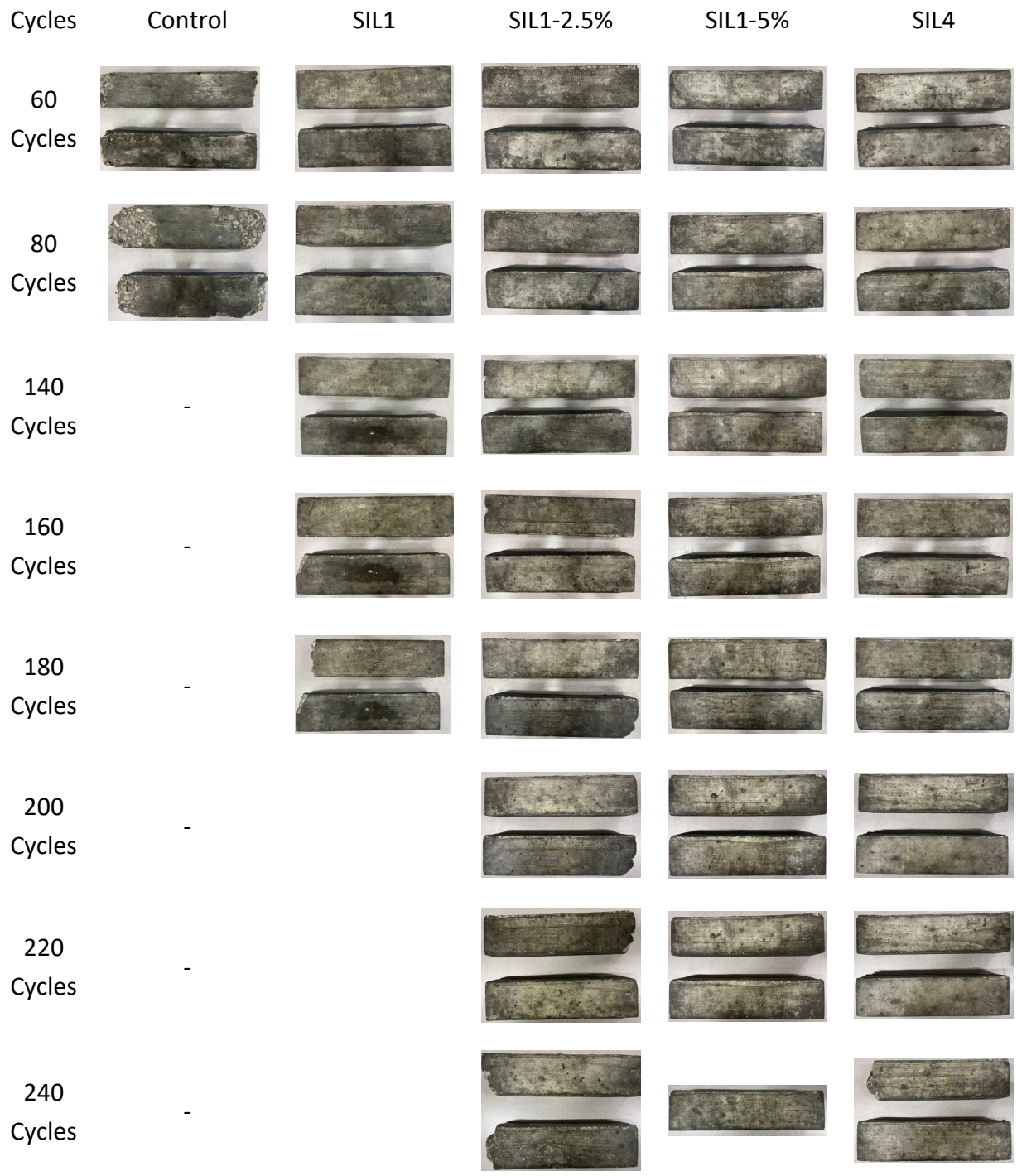


**Figure 4.21. The progression of damage at 20-cycles interval during accelerated freeze-thaw testing**

**Figure 4.22. Neat silane and silane-nanoclay coated concrete with 5% loading ratio after 200 freeze-thaw cycles**

## 4.2.9 Rate of absorption (ASTM C1585)

### 4.2.9.1 Procedure of the Test

The test was conducted in accordance with the sequence described in Section 3.2.6.1.

### 4.2.9.2 Discussion of the Results

Figure 4.23 illustrates the characteristic bilinear absorption behavior observed for both treated and untreated concrete, corresponding to the initial and secondary capillary suction phases. The calculated initial and secondary absorption coefficients are summarized in Table 4.7. Overall, surface treatment significantly reduces capillary suction, with absorption coefficients decreasing by approximately one order of magnitude compared to untreated concrete. For neat silane treatments, SIL1 exhibits an initial absorption coefficient 11% higher than SIL4; however, the secondary absorption coefficient decreases by 4%. In contrast, silane-nanoclay composites increase both initial and secondary absorption coefficients relative to neat silane-treated concrete. Specifically, for nanoclay loadings of 2.5% and 5%, the initial absorption coefficient increases by 43.1% and 11.4%, respectively, while the secondary absorption coefficient increases by 89.8% and 38.0%, respectively. The observed increase in absorption associated with nanoclay incorporation, particularly at the 2.5% loading level, is not fully understood and is the subject of ongoing investigation.

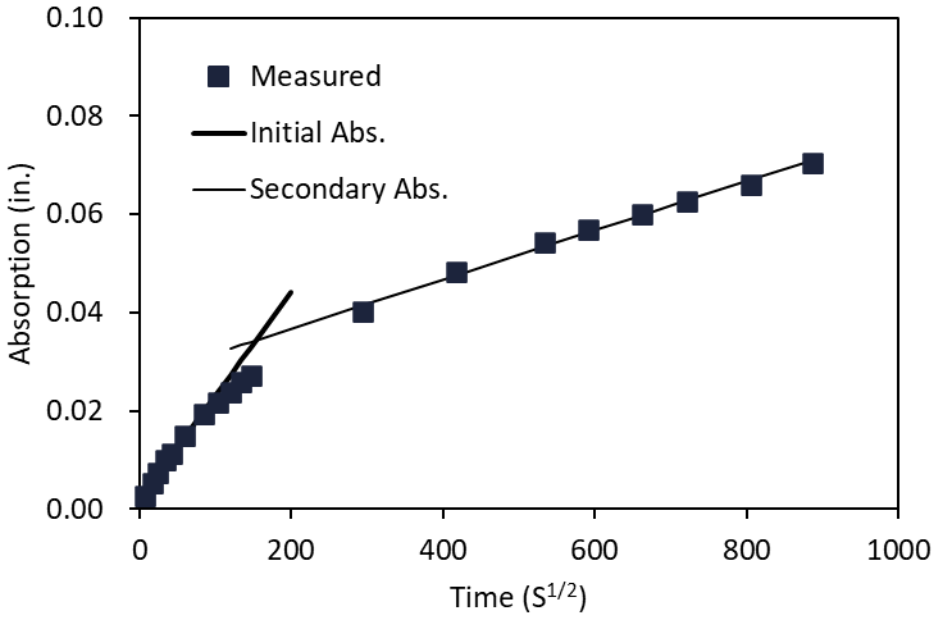
0.10
0.08
0.06
0.04
0.02
0.00
Absorption (in.)
Measured
Initial Abs.
Secondary Abs.
0
200
400
600
800
1000
Time (S^1/2)

**(a)**

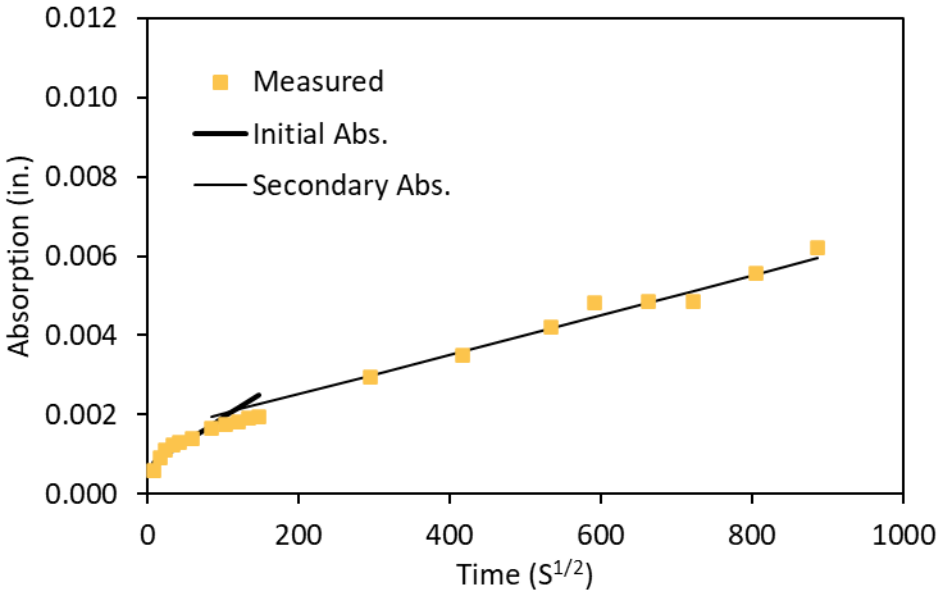
0.012
0.010
0.008
0.006
0.004
0.002
0.000
Absorption (in.)
Measured
Initial Abs.
Secondary Abs.
0
200
400
600
800
1000
Time (S^1/2)

**(b)**

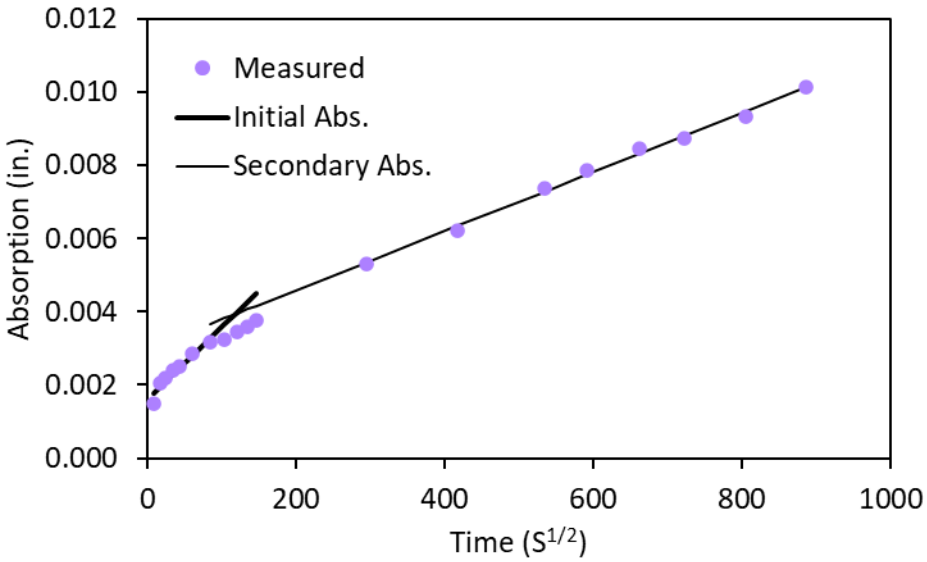
0.012
0.010
0.008
0.006
0.004
0.002
0.000
Absorption (in.)
Measured
Initial Abs.
Secondary Abs.
0
200
400
600
800
1000
Time (S^1/2)

**(c)**

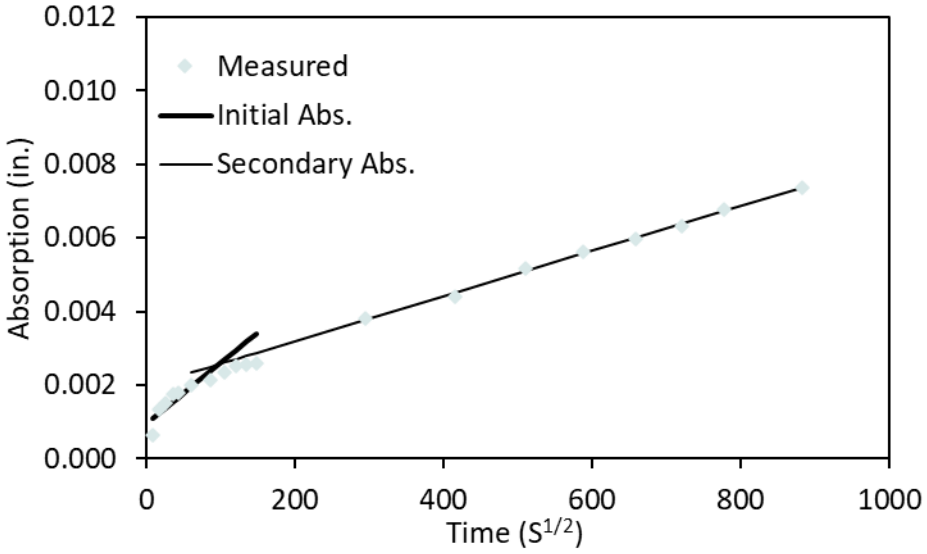
0.012
0.010
0.008
0.006
0.004
0.002
0.000
Absorption (in.)
Measured
Initial Abs.
Secondary Abs.
0
200
400
600
800
1000
Time (S^1/2)

**(d)**

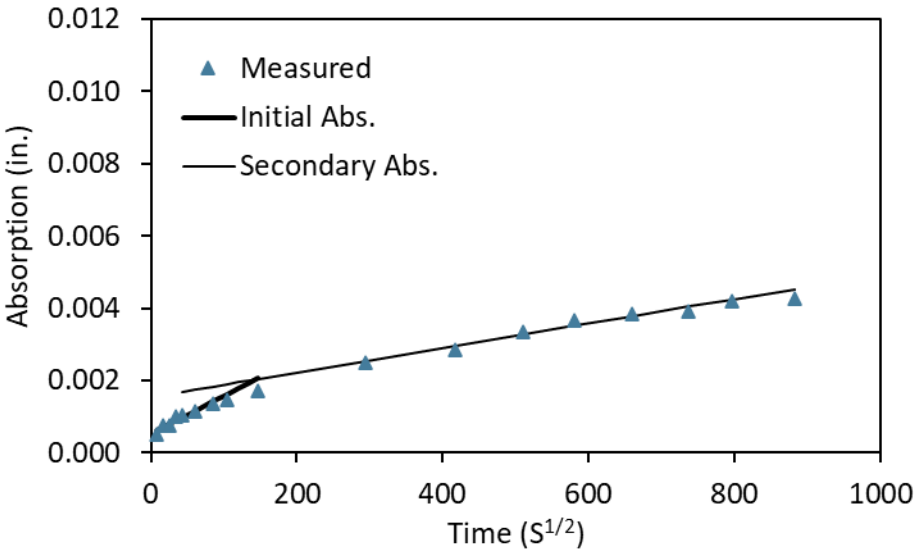


**(e)**

**Figure 4.23. Absorption characteristics of neat silanes and silane-nanoclay composites (a) un-treated concrete (b) SIL 1 treated concrete (c) SIL1-2.5% treated concrete (d) SIL1-5% treated concrete (e) SIL4 treated concrete**

**Table 4.7. Initial and secondary absorption coefficients for neat silanes and silane-nanoclay composites**

| | $S_i$ (in./$s^{1/2}$) | S.D | $S_S$ (in./$s^{1/2}$) | S.D |
|---|---|---|---|---|
| Control | $1.65 \times 10^{-4}$ | $4.61 \times 10^{-5}$ | $5.00 \times 10^{-5}$ | $4.15 \times 10^{-8}$ |
| SIL1 | $1.24 \times 10^{-5}$ | $1.70 \times 10^{-7}$ | $4.26 \times 10^{-6}$ | $7.21 \times 10^{-7}$ |
| SIL1-2.5% | $1.78 \times 10^{-5}$ | $1.85 \times 10^{-6}$ | $8.06 \times 10^{-6}$ | $1.54 \times 10^{-8}$ |
| SIL1-5% | $1.38 \times 10^{-5}$ | $2.83 \times 10^{-6}$ | $5.85 \times 10^{-6}$ | $2.55 \times 10^{-7}$ |
| SIL4 | $1.11 \times 10^{-5}$ | $7.09 \times 10^{-5}$ | $4.47 \times 10^{-6}$ | $1.08 \times 10^{-6}$ |

#### 4.2.9.3 Conclusions

Neat silanes and silane-nanoclay composites are effective in limiting the ingress of external fluids into concrete through capillary suction. Surface treatment reduces capillary suction by approximately one order of magnitude compared to untreated concrete. Among the neat silanes, SIL4 exhibits lower sorptivity than SIL1, consistent with previous findings. However, the incorporation of nanoclay, particularly at a 2.5% loading, results in a noticeable increase in capillary suction compared to neat silane-treated concrete. The underlying mechanism of this behavior is not yet fully understood and is currently under investigation.

### 4.2.10 Water Permeation Test

#### 4.2.10.1 Procedure of the Test

The test details and procedures were described in Section 3.2.8.1. For every specimen, two test arrangements were employed in which the tested portion of the slab was varied; a) Micrometer readings and the corresponding induced water flux within the concrete (in./s) were measured after 5 min under a constant pressure of 100 kPa b) Time-dependent flow measurements were recorded at 1, 2, 5, 10, and 20 min.

#### 4.2.10.2 Discussion of the Results

Micrometer readings and corresponding water flux (in./s) at each time interval are presented in Figures 4.24 and 4.25 for test arrangements (a) and (b), respectively. It should be noted that the test results exhibit considerable variability; therefore, they cannot be used to assess the relative performance of the different treatments. Testing of the control (untreated) concrete was discontinued after 5 min due to the high rate of water flux through the specimen.
Both neat silanes and silane-nanoclay composites reduce pressurized water flow through the concrete compared to the control specimens. Among the neat silanes, only minor differences are observed, although SIL4 shows a slightly lower water flux than SIL1. The incorporation of nanoclay does not consistently reduce water flux. The general trend indicates an initial increase in flux, followed by a reduction at later time intervals.

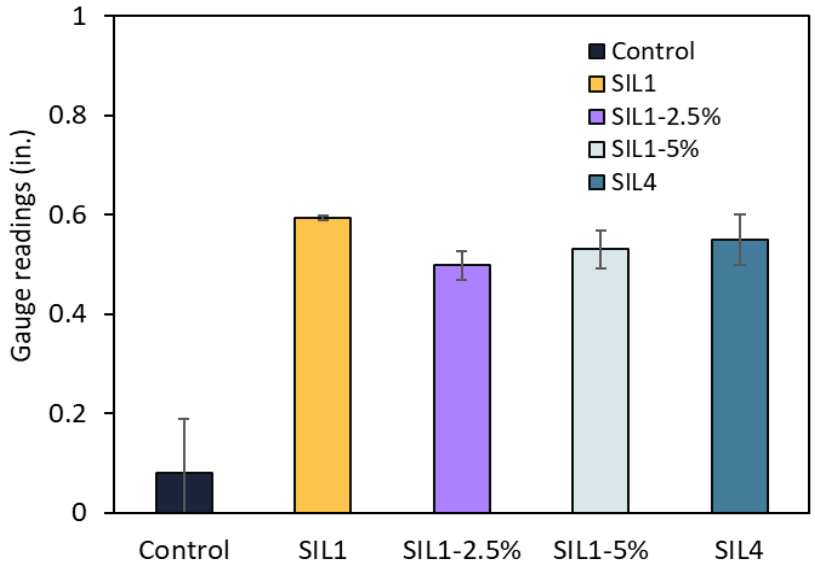


**(a)**

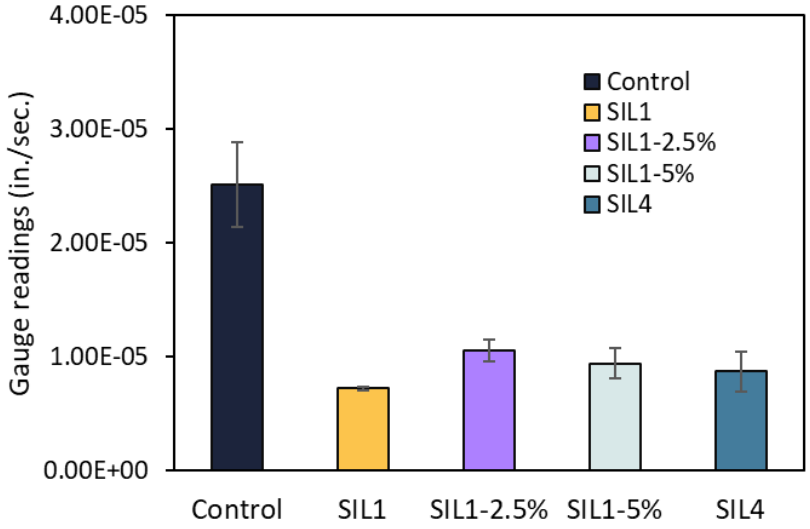


**(b)**

**Figure 4.24. Water permeation results after 5 min. (a) gauge readings (in.) (b) water flux (in./sec)**

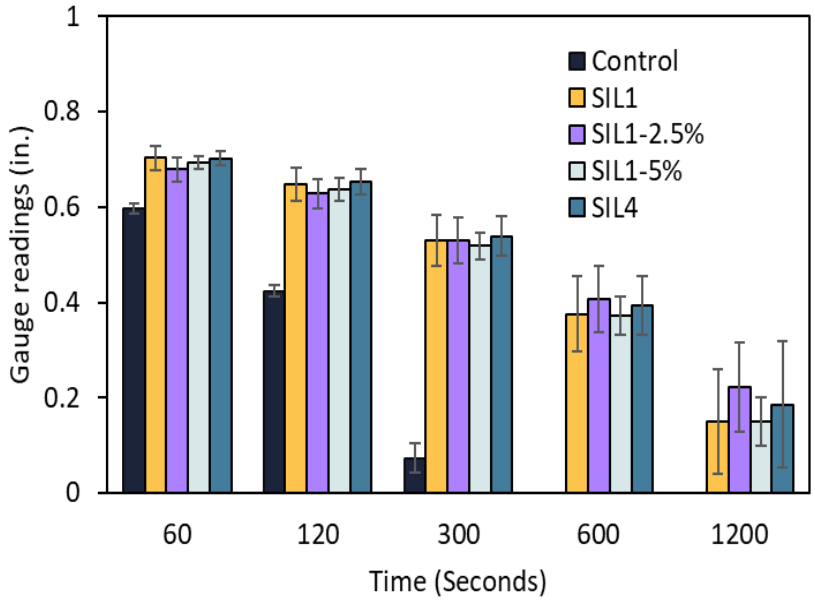


**(a)**

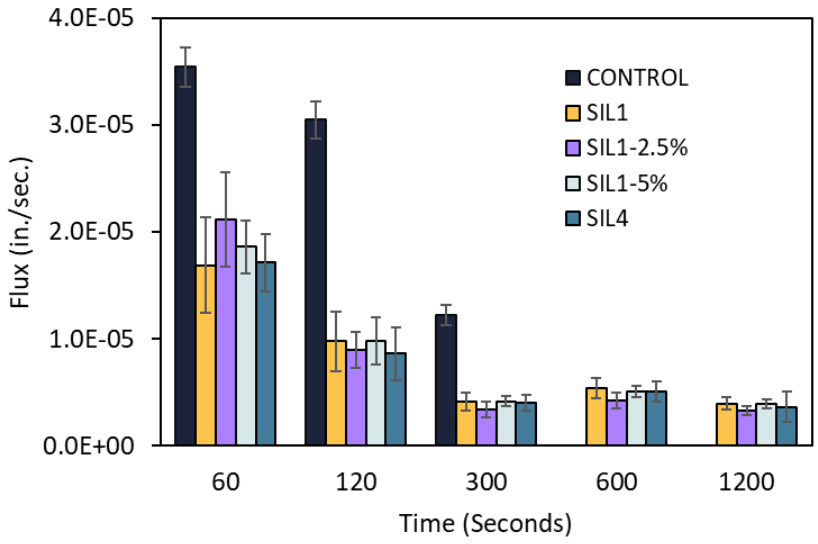


**(b)**

**Figure 4.25. Water permeation results after 5 min. (a) gauge readings (in.) (b) water flux (in./sec)**

#### 4.2.10.3 Conclusions

The water permeation performance of concrete treated with neat silanes and silane-nanoclay composites was evaluated. Surface treatment reduces pressurized water flow through concrete; however, it does not completely prevent water permeation. Only minor differences are observed among the treatments, and these variations are considered negligible. The incorporation of nanoclay into the silane matrix does not result in a measurable improvement in resistance to water permeation. It should be noted that the test results exhibit significant variability. Accordingly, the permeation tests are not considered sufficient, on their own, to reliably distinguish the relative performance of surface treatments.

## 4.3 Characterization of Silane-Nanoclay Composites

### 4.3.1 Methodology

To examine the surface morphology before and after treatment with silane and silane-nanoclay composites, scanning electron microscopy (SEM) was performed on fractured pieces obtained from the near-surface region of the concrete specimens using a Thermo Scientific Prisma E system. Prior to imaging, all samples were coated with a gold/palladium layer using a sputter coater. The SEM was operated in high-vacuum mode at an accelerating voltage of 20 kV.

X-ray diffraction (XRD) analysis was conducted on powdered samples collected from the surface layer of SIL1, SIL1–2.5%, and SIL1–5% specimens following completion of the frost scaling test. XRD patterns were obtained using Cu Kα radiation (λ = 1.5418 Å). The instrument was operated

at 45 kV and 40 mA. Data was collected over a 2θ range of 15° to 50°, with a step size of 0.025° and a scan rate of 2°/min.

High-resolution X-ray diffraction (HR-XRD) and Fourier transform infrared spectroscopy (FT-IR) were performed on nano powder samples treated with a 3% NaCl solution (see next section). For HR-XRD, diffraction patterns were obtained under similar operating conditions, over a 2θ range of 0.5 to 10°, with a scan rate of 0.5°/min. FT-IR analysis was conducted using a Nicolet iS50 FT-IR spectrometer equipped with an attenuated total reflectance (ATR) accessory. The instrument utilizes a DLaTGS detector and a KBr beam splitter. Spectra were acquired over the mid-infrared range of 400 to 4000 $cm^{-1}$.

### 4.3.2 Results and Discussion

SEM micrographs of the control, neat silane-treated concrete, and silane-nanoclay-treated concrete with a 5% nanoclay loading are presented in Figure 4.26. No appreciable improvement in microstructure was observed for silane-treated concrete compared to untreated concrete. However, at a 5% nanoclay loading, the treated surface was denser, with a greater proportion of surface voids filled by nanoclay particles.

s

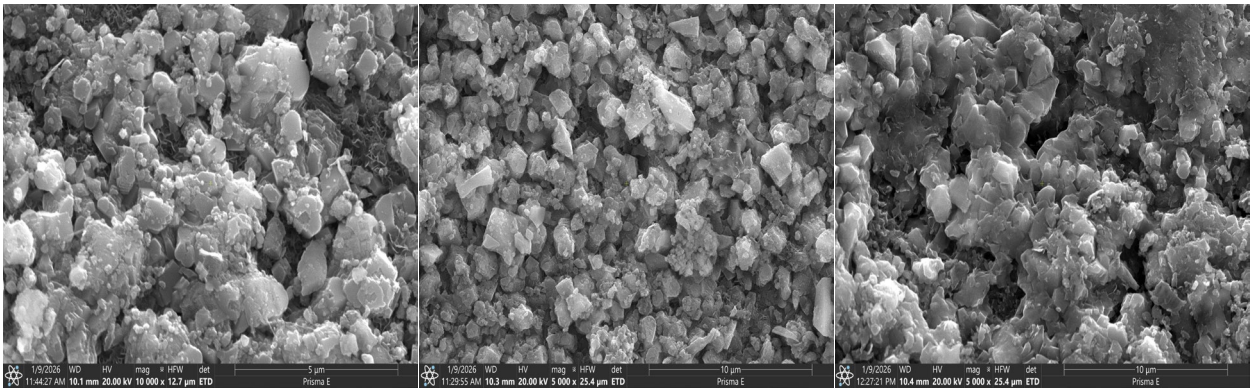

**(a)** **(b)** **(c)**

**Figure 4.26. SEM micrographs for (a) untreated, (b) neat silane, and (c) silane-nanoclay composite at loading ratio of 5%**

The X-ray diffraction (XRD) patterns obtained from powdered samples collected from the near-surface zone after salt frost exposure are presented in Figure 4.27. It was hypothesized that a higher concentration of calcium chloride in the near-surface region of silane-nanoclay-treated concrete, compared to neat silane-treated concrete, could contribute to the observed reduction in resistance to salt frost scaling. However, no crystalline calcium chloride phases were detected in the XRD patterns. These results suggest that the accumulation of calcium chloride in the near-surface zone is not the primary mechanism responsible for the observed deterioration in scaling resistance.

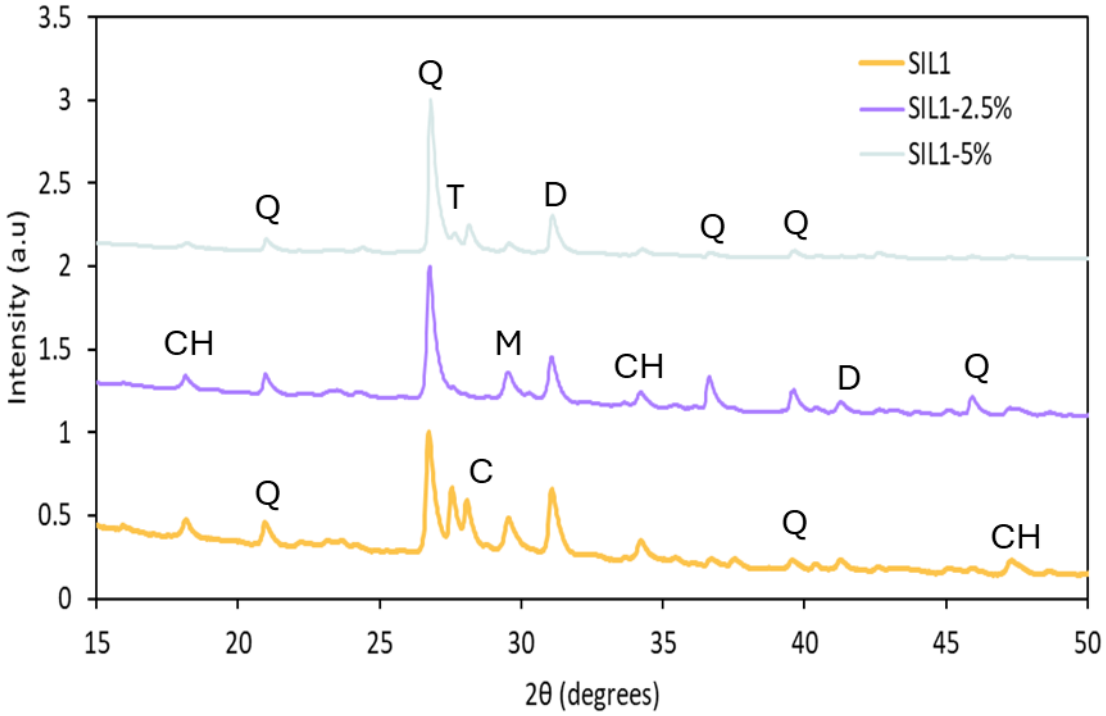


**Figure 4.27. XRD patterns for neat silane and silane-nanoclay composites (Q=Quartz, D=Dolomite, T=Ettringite, C=Calcite, M=Margarite, CH=Calcium hydroxide)**

Figure 4.28 illustrates the experimental setup in which a predetermined amount of nanoclay used in this study was dispersed in graduated cylinders containing tap water, 3% NaCl solution, 4% $CaCl_2$ solution, and 15% NaCl solution. The suspensions were allowed to stand undisturbed for 48 h. The results indicate that the nanoclay gradually loses its intercalated organic modifier and settles to the bottom of the cylinder, with the extent of settling dependent on the ionic strength of the solution.

**Figure 4.28. Settled nanoclay after 48 h of dispersion in (from right to left) tap water, 3% NaCl solution, 4% $CaCl_2$ solution, and 15% NaCl solution**

The settled mass from the 3% NaCl solution was collected, filtered, and washed with distilled water 10 times to remove residual salts, and then oven-dried at 105 ± 5 °C. High-resolution X-

ray diffraction (HR-XRD) patterns of the dried mass and the nanoclay as received are presented in Figure 4.29. No significant peak shift was observed, suggesting that removal of the organic modifier did not measurably alter the basal spacing of the clay. Fourier transform infrared (FT-IR) spectra of the dried mass and untreated nanoclay are shown in Figure 4.30. An intense peak at approximately 1012 $cm^{-1}$, corresponding to Si-O-Si stretching vibrations, is observed. In addition, the Si-O-Si bending peak shifts from 456 $cm^{-1}$ to 439 $cm^{-1}$, which may indicate partial detachment of the organic modifier from the clay structure. These observations are currently under investigation.

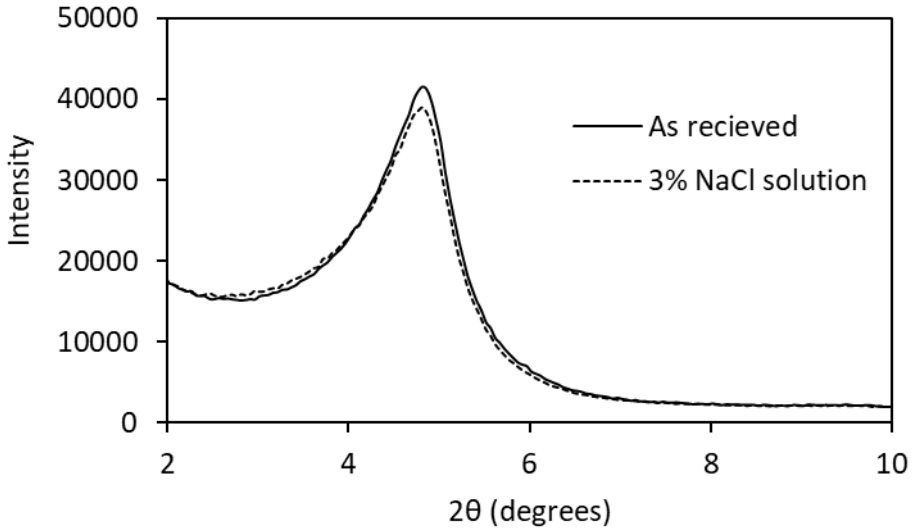


**Figure 4.29. HR-XRD for the nanoclay as received and after treatment with 3% NaCl solution**

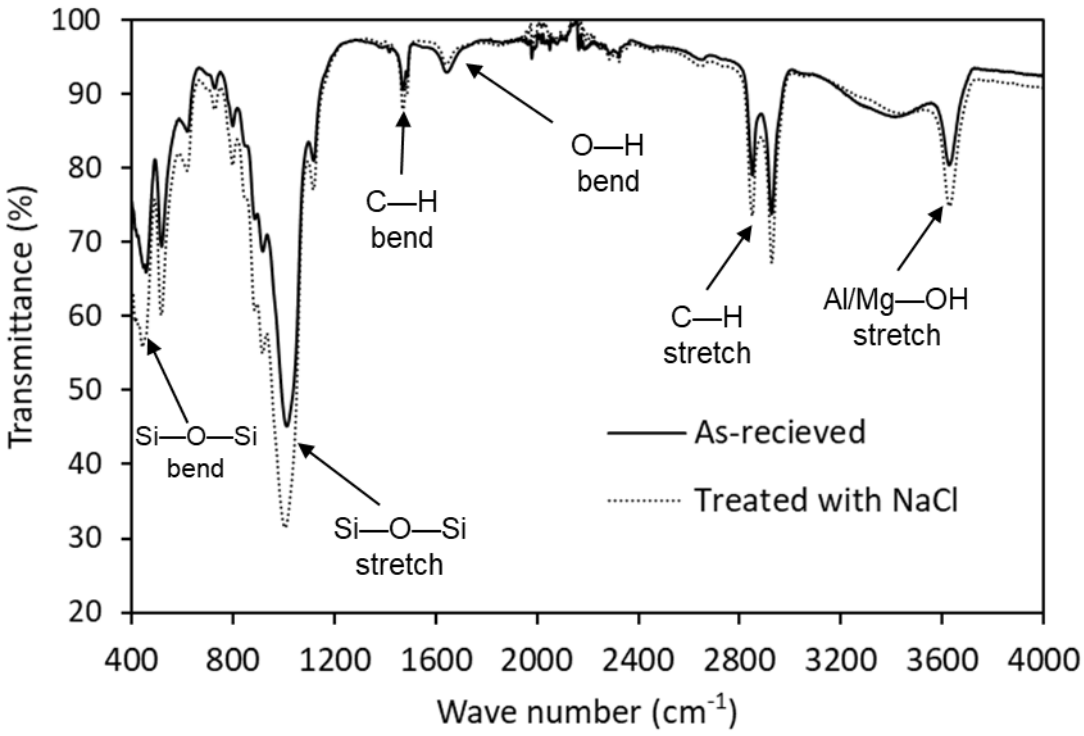


**Figure 4.30. FT-IR spectrum for the nanoclay as received and after treatment with 3% NaCl solution**

### 4.3.3 Conclusions

Silane-nanoclay composites densify the near-surface layer of concrete, which can enhance durability by forming a barrier to the ingress of external agents. X-ray diffraction (XRD) results do not indicate the presence of crystalline calcium chloride in the near-surface zone after salt-frost scaling. This could suggest that salt crystallization is not the primary mechanism governing the observed deterioration of silane-nanoclay-treated concrete. However, preliminary results indicate that the effectiveness of this barrier may be reduced due to deintercalation of the organic modifier from the interlayer galleries of the nanoclay.

## 4.4 Summary

In summary, the performance of silane-nanoclay composites was evaluated and compared with that of neat silane sealers, specifically Protectosil SH100 and SIL-ACT-ATS 200, which demonstrated best performance. The silane-nanoclay composites were evaluated based on salt absorption and vapor transmission, chloride penetration, surface and bulk resistivity, resistance to surface scaling, resistance to rapid freeze-thaw cycling, rate of absorption (sorptivity), and water permeability. The findings are summarized in Table 4.8. Both silane products exhibited excellent performance. However, Protectosil SH100 demonstrated higher resistance to chloride ion penetration, whereas SIL-ACT-ATS 200 showed higher resistance to frost scaling and freeze-thaw cycling. Silane-nanoclay composites appear to be more vulnerable under aggressive

conditions characterized by high ionic strength. This could be clearly anticipated with increased deterioration of silane-nanoclay composite at a loading ratio of 5% during frost scaling test.

**Table 4.8. Summary of performance of neat silanes and silane-nanoclay composites**

| | Protectosil SH100 | Protectosil SH100–2.5% Nanoclay | Protectosil SH100–5.0% Nanoclay | SIL-ACT-ATS 200 |
|---|---|---|---|---|
| Salt absorption NCHRP Series II | ●● | ●●● | ●●● | ● |
| Vapor transmission NCHRP Series II | ● | ●● | ●● | ● |
| Chloride content NCHRP Series II | ●●●● | ● | ●● | ●●● |
| Wettability | ● | ● | ● | ●● |
| Long term chloride ion penetration AASHTO T259 | ●● | ●●● | ●●● | ● |
| Long term chloride ion penetration on cracked concrete modified AASHTO T259 | ●● | ●●●● | ●●● | ● |
| Scaling resistance | ●● | ●●● | ● | ●●●● |
| Surface resistivity AASHTO T358 | ●●●● | ●● | ●●● | ● |
| Bulk resistivity | ●●●● | ● | ●● | ●●● |
| Resistance of concrete to rapid freezing and thawing | ● | ●●● | ●●●● | ●● |
| Rate of absorption ASTM C1585 | ●●● | ● | ●● | ●●●● |

* For water permeation test, no general trends were found between neat silanes and silane-nanoclay composites

# Chapter 5: Estimation of Service Life of Silanes and Silane-Nanoclay Composites

This chapter presents the estimation of the service life of silane sealers and silane-nanoclay composites used for concrete protection. The objective is to provide MoDOT with a reliable basis for scheduling the reapplication of surface treatments on bridge decks. The service life of concrete sealers is estimated based on a performance criterion that limits chloride concentration at the level of reinforcing steel to below the threshold required to initiate chloride-induced corrosion. The estimation of service life for neat silanes and silane-nanoclay composites follows the methodology developed under the Strategic Highway Research Program Project (SHRP) C-103 and referenced in NCHRP-209. It should be noted that the SHRP-based methodology is primarily intended to assess the effectiveness of treatments in protecting reinforcing steel against corrosion. It does not account for other deterioration mechanisms, such as damage due to freeze-thaw cycling or frost scaling.

## 5.1 30-Week Ion Chloride Penetration Test

For the purpose of service life estimation, a long-term chloride ion penetration test was conducted in accordance with AASHTO T259 on both control and surface-treated concrete specimens. The test procedure followed the sequence described in Section 3.2.2.1. Specimens were exposed for 30 weeks prior to chloride content analysis, during which the exposure solution was periodically replaced to maintain consistent test conditions.

The results of the 30-week chloride ion penetration test are presented in Table 5.1. For comparison, Figure 5.1 presents a bar chart of chloride penetration results at 12 and 30 weeks of exposure. The results indicate that incorporation of nanoclay into the silane matrix enhances performance over extended exposure periods. Although specimens treated with silane-nanoclay composites exhibited high initial rate of chloride ingress, the rate decreased over time relative to neat silane treatments.

**Table 5.1. Chloride content profile vs. depth after 30-week exposure as per AASHTO T259**

| Depth | CONTROL | SIL1 | SIL1-2.5% | SIL1-5% | SIL4 |
|---|---|---|---|---|---|
| 0.063 – 0.5in. | 0.482 | 0.253 | 0.199 | 0.206 | 0.286 |
| 0.25-0.75 in. | 0.322 | 0.152 | 0.141 | 0.134 | 0.165 |
| 0.5-1.0 in. | 0.256 | 0.123 | 0.087 | 0.089 | 0.135 |
| 0.75-1.25 in. | 0.194 | 0.078 | 0.065 | 0.058 | 0.068 |
| 1.0-1.5 in. | 0.147 | 0.050 | 0.046 | 0.040 | 0.054 |

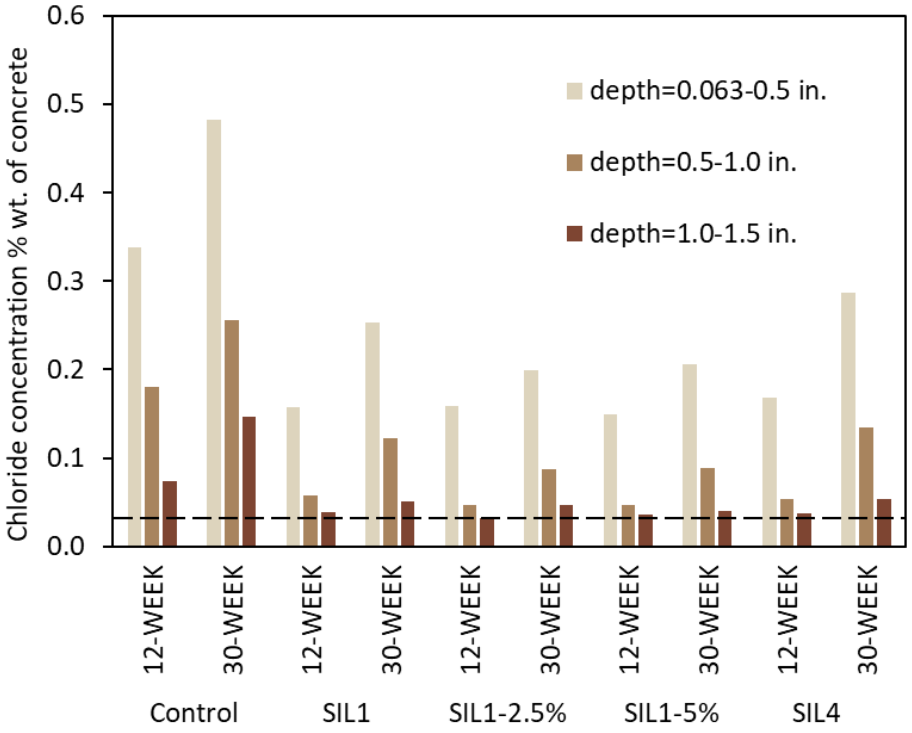


**Figure 5.1. Chloride ion content (% wt. of concrete) as function of depth (in.)**

## 5.2 Estimation of the Service Life

The estimation of service life, in accordance with Strategic Highway Research Program, is based on the analytical solution to Fick's Second Law of Diffusion, as presented in Equation 5.1.

$$C_0^{'} = \frac{C_{(x,t)}}{\left[1 - \text{erf}\frac{x}{2\sqrt{D_C.t}}\right]}$$

Where:

$C_0^{'}$= the equilibrium chloride concentration resulting from chloride leakage from the sealed zone of concrete (lb./yd$^3$)

$C_{(x,t)}$ = the chloride concentration threshold necessary to initiate corrosion from the surface of concrete layer (lb./yd$^3$)

x = depth of the cover of the shallowest 2.5 percent of the reinforcing steel (in.)

erf = the error function of the computed value of the argument

$D_C$= the field effective diffusion coefficient (in.$^2$/year)

t= the expected useful life of the bridge (year)

**Equation 5.1: The analytical solution of the differential equation of Fick's second law of diffusion**

First, the average chloride concentration corresponding to the threshold for initiation of reinforcement corrosion was determined. Subsequently, an equivalent exposure time ($t_{eq}$) for untreated concrete was estimated using the results presented in Table 5.1, assuming an environmental chloride diffusion coefficient of 0.12 in.²/year, representative of highway conditions in the state of Missouri.

The average allowable equilibrium surface chloride concentration ($C_o$–eq) was then calculated, assuming a linear increase in chloride concentration leaked from the concrete surface layer over the service life, see Equation 5.2 below.

$$C_{0\text{-}eq}=C_{0\text{-}total}\left(\frac{t_{eq}}{t}\right)$$

Where:

$C_{0\text{-}eq}$= the average equilibrium chloride concentration at time $t_{eq}$ (Ib/yd$^3$)

$C_{0\text{-}total}$ = the total chloride concentration at time t which equals two times the average chloride concentration $C'_0$ (Ib./yd$^3$)

$t_{eq}$= the equivalent field time that corresponds to 30 weeks of ponding of untreated specimens by using the environmental effective diffusion constant $D_C$ (year)

t= the expected useful life of the bridge (year)

**Equation 5.2. The average allowable equivalent chloride concentration (Ib/yd³)**

A leakage factor, representing the resistance to chloride ingress provided by the surface treatment relative to untreated concrete, was determined for each treatment at a depth of 0.25–0.75 in. An allowable leakage factor was subsequently determined as the ratio of the equivalent chloride concentration ($C_o$–eq) at the end of the equivalent exposure time (t_eq) to the field chloride concentration ($C_o$), which was taken as 3.9 Ib/yd³ based on Missouri highway practice. Finally, the estimated service life ($t_{sl}$) was calculated using Equation (5.3).

$$t_{sl}=t_{eq}\left(\frac{LR_{allowed}}{LR}\right)$$

Where:

$t_{sl}$= the estimated service life (year)

$t_{eq}$= the equivalent field time that corresponds to 30 weeks of ponding of untreated specimens by using the environmental effective diffusion constant $D_C$ (year)

$LR_{allowed}$= the allowable leakage factor

LR = the leakage factor for each surface treatment

**Equation 5.3. The estimated service life for the surface treatment**

The estimated service life values for neat silanes and silane-nanoclay composites are presented in Table 5.2. The results indicate that service life increases with improved resistance of the

surface treatment to chloride ingress, noting that other deterioration mechanisms were not considered in this analysis. SIL1 and SIL4 exhibited estimated service lives of 5.4 and 5.0 yr, respectively. The incorporation of nanoclay resulted in an increase of approximately 1.0 yr compared to neat silane (SIL1-treated concrete). These results should be interpreted within the context of the assumptions and methodology adopted in this study as there was a decrease in performance in harsh environment.

**Table 5.2. Estimated service life of neat silanes and silane-nanoclay composites***

| | SIL1 | SIL1-2.5% | SIL1-5% | SIL4 |
|---|---|---|---|---|
| $C'_0$ (lb/yd$^3$) | 1.11 | 1.11 | 1.11 | 1.11 |
| $C_{0\text{-total}}$ (lb/yd$^3$) | 2.21 | 2.21 | 2.21 | 2.21 |
| $LR_{allowed}$ | 22.17 | 22.17 | 22.17 | 22.17 |
| $t_{eq}$ (year) | 11.52 | 11.52 | 11.52 | 11.52 |
| $C_{0\text{-eq}}$ (lb/yd$^3$) | 0.51 | 0.51 | 0.51 | 0.51 |
| LR | 47.06 | 43.78 | 41.63 | 51.29 |
| $t_{sl}$ (year) | 5.4 | 5.8 | 6.1 | 5.0 |

* Assumptions: $C_0$=3.9 lb/yd$^3$, $D_c$=0.12 in.$^2$/year, the density of concrete for the conversion of chloride content from % wt. to kg/m$^3$=3916 lb/yd$^3$ in accordance with AASHTO T259.

## 5.3 Summary

Estimation of sealer service life is a critical parameter in the material selection process and in life-cycle cost analysis. In this study, the estimated service life of neat silanes ranged between 5.0 to 5.4 yr. The incorporation of nanoclay increased the estimated service life to 5.8 and 6.1 yr for loading ratios of 2.5% and 5.0%, respectively. It should be noted that service life estimates based on SHRP C-103 procedure may be misleading when applied to silane-nanoclay composites. Although the addition of nanoclay improves resistance to chloride ingress under the conditions evaluated, it may also accelerate deterioration due to frost scaling, particularly at the 5.0% loading ratio, and increase chloride uptake when exposed to high-concentration saline solutions compared to neat silanes. Accordingly, the results presented herein should be interpreted within the limitations of the adopted methodology. The service life estimates are based solely on chloride ion penetration testing conducted in accordance with AASHTO T259 for the determination of equivalent time and leakage factor.

# Chapter 6: Field Evaluation of the Performance of Silanes for Treatment of Bridge Decks

In this chapter, four bridges in the state of Missouri were selected to evaluate the field performance of silane as a surface impregnation treatment for bridge decks. All bridges were recently constructed and represent a range of average daily traffic (ADT) levels, from 630 to 8,430 vehicles per day. Field performance of the silane treatment was assessed based on depth of penetration, static contact angle, chloride penetration resistance, and water absorption.

## 6.1 Bridges Selection

For the purposes of this field investigation, four bridges were selected. Two bridges are located in eastern Missouri, while the remaining two are located in western Missouri, see Figures 6.1–6.5. Information obtained from Missouri Department of Transportation (MoDOT) records, including bridge location, bridge condition, geometric characteristics (length and width), and timing of silane application, is summarized in Table 6.1. All four bridges were constructed between 2017 and 2018 and received an initial silane treatment shortly after construction. Subsequent reapplication intervals ranged from 3 to 7 yr across the bridges.

**Table 6.1. Bridges selected for field investigation**

| Bridge Number | A8380 | A0964 | A8495 | A8499 |
|---|---|---|---|---|
| Latitude Dec Deg | 38.855 | 38.567236 | 37.805025 | 36.621594 |
| Longitude Dec Deg | -90.871389 | -90.440019 | -94.275081 | -94.180114 |
| Year Built/Reconstructed | 2018 | 2017 | 2017 | 2018 |
| ADT | 8430 | 7558 | 630 | 1742 |
| Deck Rating | 7 | 8 | 8 | 8 |
| Structure Length | 217.5 | 255.8 | 120.7 | 257.5 |
| Structure Width | 56.7 | 80.7 | 26.5 | 28.5 |
| Year of 1$^{st}$ application | 2018 | 2017 | 2018 | 2019 |
| Year of 2$^{nd}$ application | 2021 | 2020 | 2024 | 2025 |

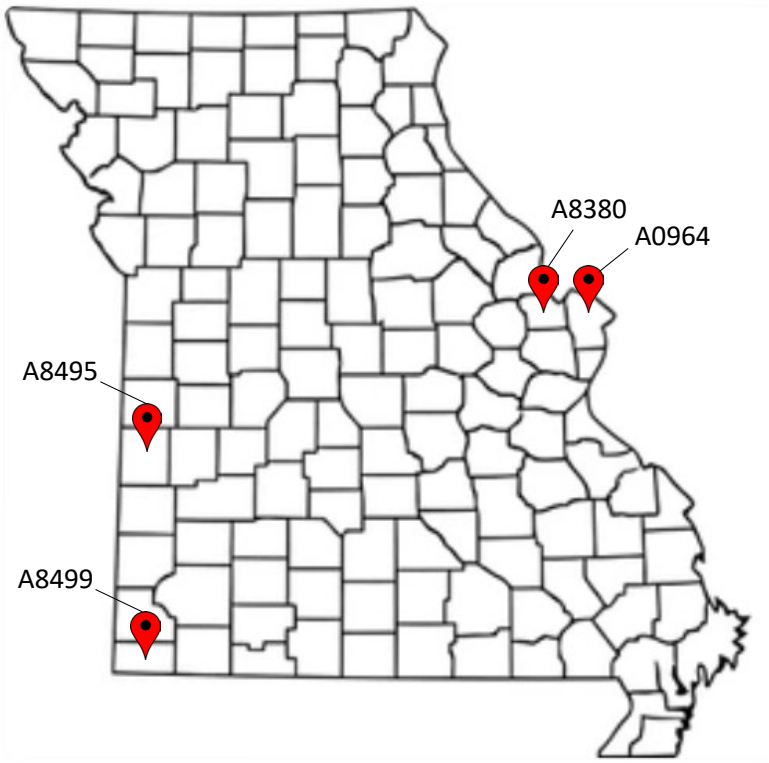


**Figure 6.1. The locations of bridges**


**Figure 6.2. Aerial photograph for bridge A8380 and the core locations**

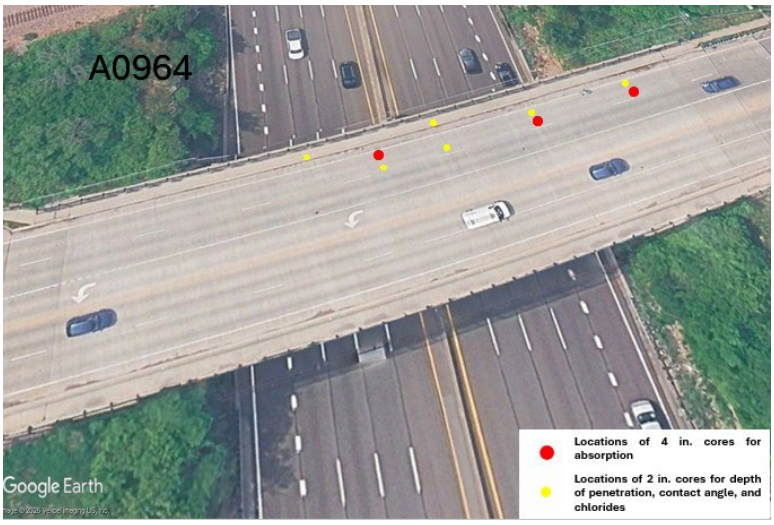


**Figure 6.3. Aerial photograph for bridge A0964 and the core locations**


**Figure 6.4. Aerial photograph for bridge A8495 and the core locations**


**Figure 6.5. Aerial photograph for bridge A8499 and core locations**

## 6.2 Samples Extraction

For each bridge, a minimum of nine core samples were extracted for field evaluation. Core diameters were 3 5/8 in. for water absorption testing and 1 5/8 in. for depth of penetration, static contact angle, and chloride penetration testing. Figure 6.6 presents representative core samples obtained from bridge A8499.

The length of the extracted cores varied depending on the specific test requirements. Table 6.2 summarizes the core samples, including their locations within each bridge, dimensions, test type, and physical condition.

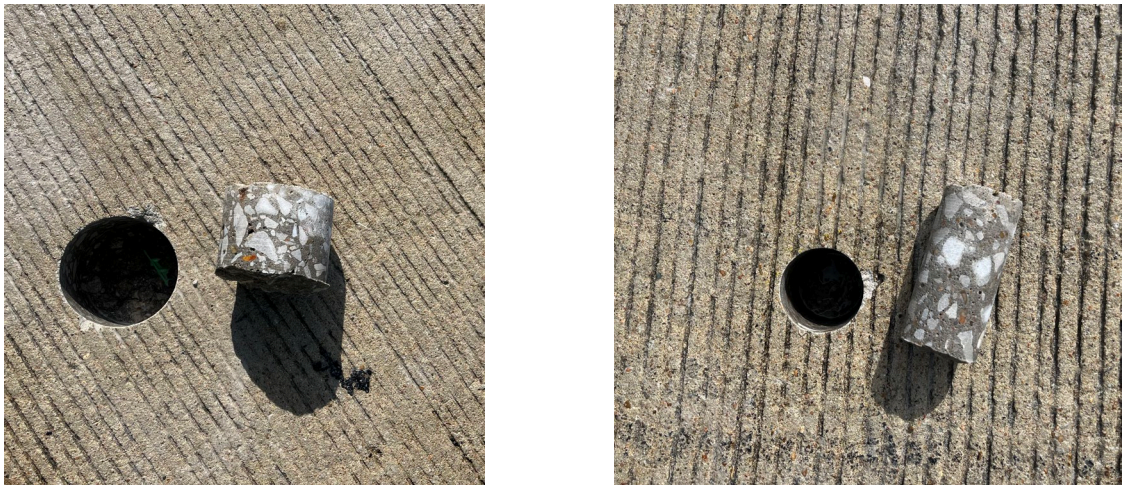

**(a)** **(b)**

**Figure 6.6. Examples of cores extracted from bridge A8499 (a) 3 5/8 in. core (b) 1 5/8 in. core**

**Table 6.2. The locations, dimensions, test type, and physical condition of the extracted cores**

| Bridge | Sample | Location | Dimensions (in.) | Test type | Physical condition |
|---|---|---|---|---|---|
| A8380 | TL-4-1 | Traffic lane | 3 5/8 x 3 1/8 | Absorption | Adequate |
| A8380 | TL-4-2 | Traffic lane | 3 5/8 x 3 5/8 | Absorption | Adequate |
| A8380 | TL-4-3 | Traffic lane | 3 5/8 x 2 7/8 | Absorption | adequate |
| A8380 | TL-2-1 | Traffic lane | 1 5/8 x 4 9/16 | Chloride analysis | Adequate |
| A8380 | TL-2-2 | Traffic lane | 1 5/8 x 3 9/16 | Chloride analysis | Adequate |
| A8380 | TL-2-3 | Traffic lane | 1 5/8 x 3 1/4 | Chloride analysis | Adequate |
| A8380 | TL-2-4 | Traffic lane | 1 5/8 x 3 1/4 | Contact angle and depth of penetration | Adequate |
| A8380 | SH-2-1 | Shoulder | 1 5/8 x 4 5/8 | Chloride analysis | Adequate |
| A8380 | SH-2-2 | Shoulder | 1 5/8 x 4 5/8 | Contact angle and depth of penetration | Adequate |
| A0964 | TL-4-1 | Traffic lane | 3 5/8 x 4 1/2 | Absorption | Two bars 3/4 in. in diameter located at distances of 2 1/4 in. and 3 in. |
| A0964 | TL-4-2 | Traffic lane | 3 5/8 x 4 3/16 | Absorption | Two bars 3/4 in. in diameter located at distances of 1 7/8 in. and 2 3/4 in. |
| A0964 | TL-4-3 | Traffic lane | 3 5/8 x 3 7/8 | Absorption | one bar 3/4 in. in diameter located at distance of 2 1/4 in. |
| A0964 | TL-2-1 | Traffic lane | 1 5/8 x 5 1/8 | Chloride analysis | Adequate |
| A0964 | TL-2-2 | Traffic lane | 1 5/8 x 4 15/16 | Chloride analysis | Adequate |
| A0964 | TL-2-3 | Traffic lane | 1 5/8 x 4 1/4 | Chloride analysis | Adequate |
| A0964 | TL-2-4 | Traffic lane | 1 5/8 x 1 5/8 | Contact angle and depth of penetration | Adequate |
| A0964 | SH-2-1 | Shoulder | 1 5/8 x 3 3/8 | Chloride analysis | Adequate |
| A0964 | SH-2-2 | Shoulder | 1 5/8 x 3 | Contact angle and depth of penetration | Adequate |
| A8495 | TL-4-1 | Traffic lane | 3 5/8 x 3 | Absorption | Adequate |
| A8495 | TL-4-2 | Traffic lane | 3 5/8 x 3 | Absorption | Adequate |
| A8495 | TL-4-3 | Traffic lane | 3 5/8 x 2 ¾ | Absorption | Adequate |
| A8495 | TL-2-1 | Traffic lane | 1 5/8 x 3 ¼ | Chloride analysis | Adequate |
| A8495 | TL-2-2 | Traffic lane | 1 5/8 x 3 | Chloride analysis | Adequate |

| Bridge | Sample | Location | Dimensions (in.) | Test type | Physical condition |
|---|---|---|---|---|---|
| A8495 | TL-2-3 | Traffic lane | 1 5/8 x 2 7/8 | Contact angle and depth of penetration | Adequate |
| A8495 | SH-2-1 | Shoulder | 1 5/8 x 3 3/4 | Chloride analysis | Adequate |
| A8495 | SH-2-2 | Shoulder | 1 5/8 x 2 3/8 | Contact angle and depth of penetration | Adequate |
| A8499 | TL-4-1 | Traffic lane | 3 5/8 x 3 | Absorption | Adequate |
| A8499 | TL-4-2 | Traffic lane | 3 5/8 x 2 3/4 | Absorption | Shows a slight indication of inadequate compaction |
| A8499 | TL-4-3 | Traffic lane | 3 5/8 x 2 3/4 | Absorption | Shows a slight indication of inadequate compaction |
| A8499 | TL-2-1 | Traffic lane | 1 5/8 x 3 5/8 | Chloride analysis | Adequate |
| A8499 | TL-2-2 | Traffic lane | 1 5/8 x 3 1/2 | Chloride analysis | Adequate |
| A8499 | TL-2-3 | Traffic lane | 1 5/8 x 3 1/8 | Contact angle and depth of penetration | Adequate |
| A8499 | SH-2-1 | Shoulder | 1 5/8 x 3 1/8 | Chloride analysis | Adequate |
| A8499 | SH-2-2 | Shoulder | 1 5/8 x 3 3/8 | Chloride analysis | Adequate |
| A8499 | SH-2-3 | Shoulder | 1 5/8 x 2 1/4 | Contact angle and depth of penetration | Adequate |

## 6.3 Performance Tests

### 6.3.1 Depth of Penetration

#### 6.3.1.1 Procedure of the Test

To determine the depth of silane penetration, core specimens with a nominal diameter of 2 in. (51 mm) were split using a concrete saw under dry conditions. The freshly exposed surface was polished using 500 grit sandpaper and then thoroughly cleaned with ethanol. A predetermined amount of navy-blue dye was mixed with water, and the specimen was immersed in the dye solution for 1.0 h. The dye preferentially stains non-silane-impregnated regions of the concrete while leaving silane-treated regions unstained. This contrast provides a visual indication of the depth of silane penetration. The penetration depth was measured at 8 locations along the exposed surface, and the average value was reported.

#### 6.3.1.2 Results and Discussion

Figure 6.7 graphically shows examples for the depth of silane penetration measured on core samples extracted from the different bridges. The average penetration depths are summarized in Table 6.3. All bridges exhibited a measurable and effective silane-treated layer. Bridge A8380 which received silane treatment in 2021 exhibited lower penetration depths compared to Bridges A0964, A8495 and A8499. The depth of silane penetration is influenced by several factors, including the water-to-cement ratio (w/c) of the concrete, substrate alkalinity, moisture condition of the concrete surface, and the timing and method of application. Assuming similar substrate and application conditions, these results suggest that silane effectiveness gradually decreases with time.

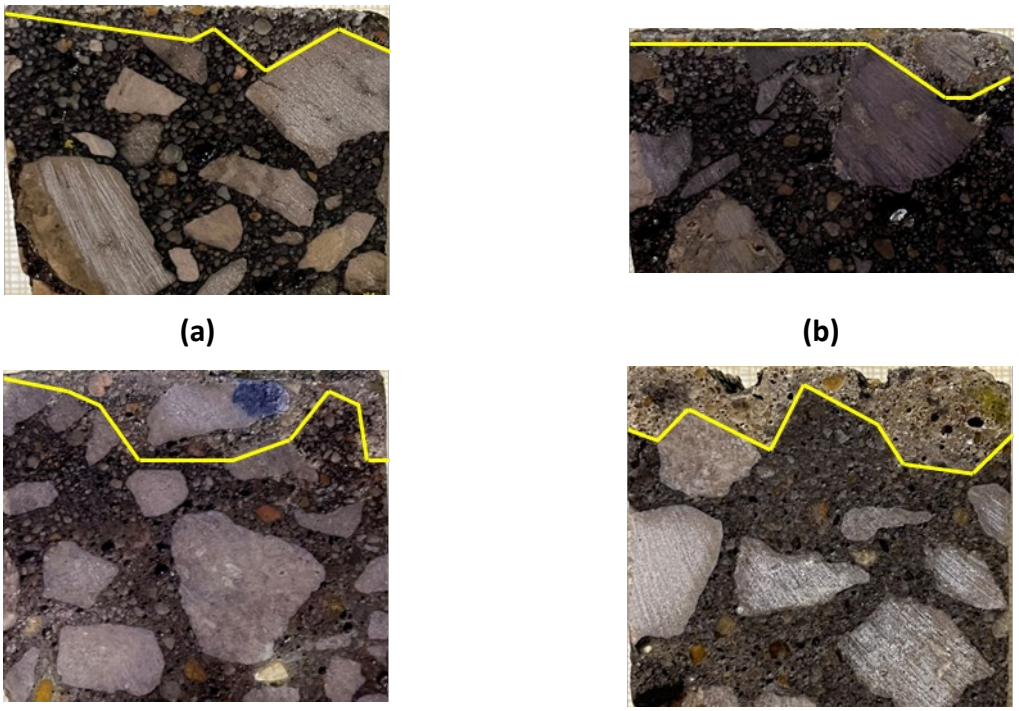

**(a)** **(b)**

**(c)** **(d)**

**Figure 6.7. Measuring the depth of penetration for (a) A8380 Bridge (b) A0964 Bridge (c) A8495 and (d) A8499 Bridge**

**Table 6.3. The depth of penetration measurement (in.)**

| Bridge | Depth of penetration (in.) |
|---|---|
| A8380 | 0.25 |
| A0964 | 0.34 |
| A8495 | 0.35 |
| A8499 | 0.33 |

### 6.3.2 Static Water Contact Angle

#### 6.3.2.1 Procedure of the Test

The static water contact angle was measured using a ramé-hart contact angle goniometer. Concrete specimens were split using a concrete saw in a dry condition. Then, the samples were placed on a leveled goniometer stage, and the optical system and illumination were adjusted to obtain a clear, high-contrast image of the solid-liquid interface. A sessile water droplet of approximately 10 µl was dispensed on the concrete surface by gently touching the droplet to the surface. The droplet was allowed to stabilize for 1 min then left and right contact angles were measured and averaged for each droplet. Measurements were taken at the surface-impregnated layer. At least three measurements were taken, and the average values were reported.

#### 6.3.2.2 Results and Discussion

The water contact angles are given in Table 6.4 below. The contact angles are higher for bridges A8380 and A8499 which showed similar degree of hydrophobicity. For bridges A0964 and A8495, the contact angle diminished to 47.8° and 50.4° respectively. Although the surface of bridge A0964 showed higher hydrophilicity in comparison to bridge A8495, the extent was irrelevant.

**Table 6.4. The water contact angle measurements (degrees)**

| Bridge | Contact angle (degrees) |
|---|---|
| A8380 | 60.7 |
| A0964 | 47.8 |
| A8495 | 50.4 |
| A8499 | 58.8 |

### 6.3.3 Chloride Ion Content (ASTM C1152)

#### 6.3.3.1 Procedure of the Test

In this test, core specimens with a nominal diameter of 2 in. were sectioned into 0.5 in. disks, as shown in Figure 6.8. The upper 0.25 in. (6.4 mm) layer was removed and discarded. Each disk was then ground into a fine powder using a disk mill for approximately 1 min (see Figure 6.9). A representative 0.35 oz (10 g) sample of the powdered sample was analyzed for acid-soluble chloride content using a potentiometric titration method in accordance with ASTM C1152.


(a) (b)

**Figure 6.8. Concrete core 2 in. nominal diameter for chloride content determination (a) before sectioning and (b) after sectioning**


**Figure 6.9. Disk mill used for grinding in chloride content determination**

#### 6.3.3.2 Results and Discussion

The chloride content (% by weight of concrete) at various depths is presented in Figure 6.10. The deck surface of bridge A8380 showed minimal penetrability by chloride ions. On contrary, the deck of bridge A0964 showed substantial chloride accumulation in the near surface zone.. In addition, for bridge deck A8499, the chloride concentration remains comparable to that of bridge A8350. Bridge A8495 has the highest chloride levels overall. The chloride ions

penetrated deeply beyond the near surface zone into the bulk concrete indicating deficient protective barrier.

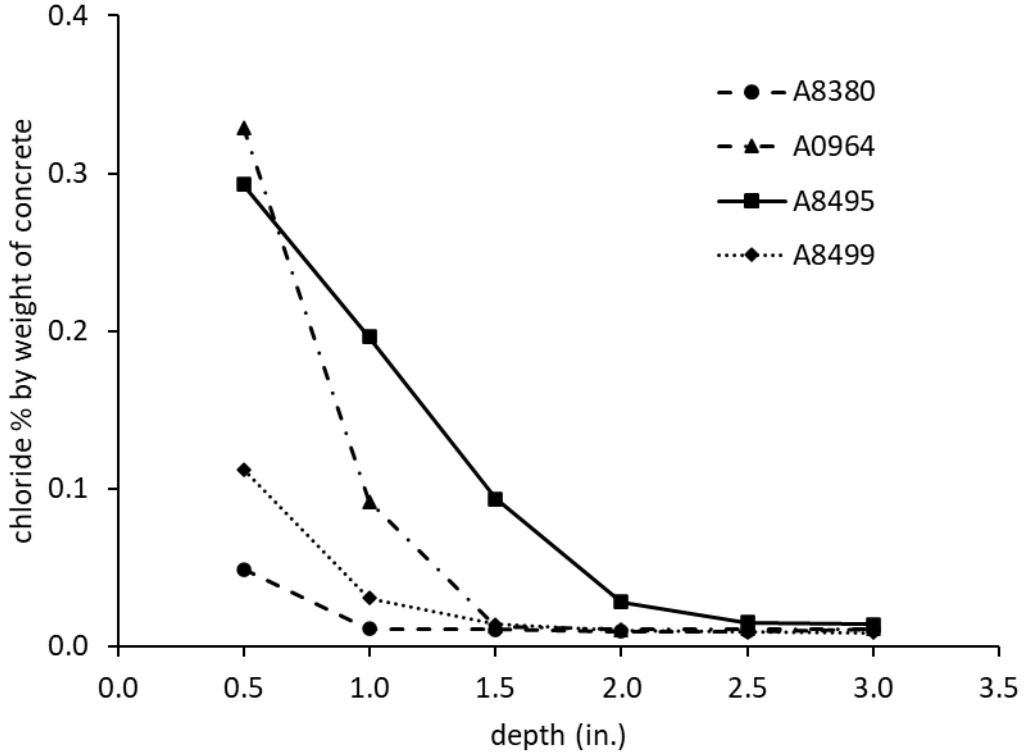


**Figure 6.10. Chloride content (%wt. of concrete) vs. depth (in.) for different bridges.**

### 6.3.4 Rate of Absorption (ASTM C1585)

#### 6.3.4.1 Procedure of the Test

The test was conducted in accordance with the procedure described in Section 3.2.6.1.

#### 6.3.4.2 Results and Discussion

The rate of absorption of each silane-treated bridge deck (in.) as a function of square root of time ($s^{1/2}$) is depicted in Figure 6.11. For the concrete deck surface of bridge A8350, the rate of capillary suction exhibits a marked reduction in capillary rise indicating the presence of a functional water repellent barrier. Comparatively, the deck surface of bridge A0964 shows a slightly higher absorption rate. The test specimens from bridges A8495 and A8499 show large scatter and higher rates of water absorption demonstrate that absorption due to capillary suction is highly sensitive to the testing locations across the bridge deck.

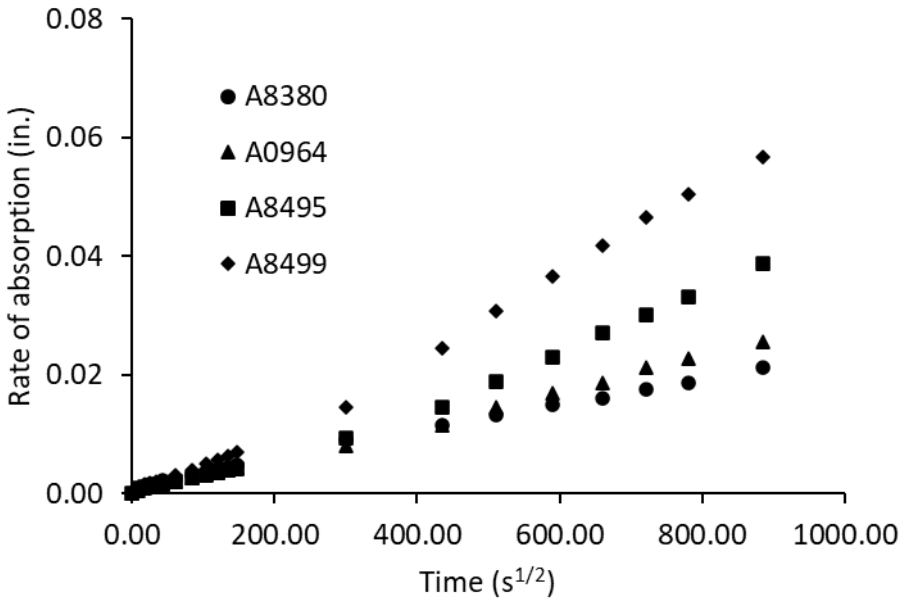


**Figure 6.11. Rate of absorption of the bridges**

## 6.4 Summary

This field investigation utilized core samples extracted from four bridge decks, two located in western Missouri and two in eastern Missouri. The evaluation results are summarized in Table 6.5. These findings may assist in selecting appropriate rehabilitation methods for the bridges investigated. For Bridges A8380 and A0964, continued protection using silane surface impregnation appears to be appropriate. For Bridge A0964, electrochemical chloride extraction (desalination) may also be considered to reduce the chloride concentration in the near-surface concrete before reapplication of the silane treatment. For Bridge A8495, the concrete substrate exhibited a high level of chloride contamination, and silane surface treatment is not expected to provide adequate protection against further chloride ingress because of the high absorption rate of the concrete. Therefore, it is recommended that the contaminated concrete cover be removed to below the level of the reinforcing steel. The removed concrete should then be replaced with sound, uncontaminated concrete, followed by the application of a silane surface treatment. Bridge A8499 exhibited inconsistent behavior relative to the other bridges. This bridge received a recent silane treatment. It is recommended that chloride accumulation in the concrete be monitored annually before a rehabilitation method is selected.

**Table 6.5: Summary of the field investigation results**

| | A8350 | A0964 | A8495 | A8499 |
|---|---|---|---|---|
| Penetration depth | ● | ●● | ●● | ●● |
| Static contact angle | ●● | ● | ● | ●● |
| Chloride ion penetration | ●●●● | ●● | ● | ●●● |
| Rate of absorption | ●●●● | ●●● | ●● | ● |

# Chapter 7: Conclusions/Recommendations

This study was conducted to evaluate the performance of neat silane sealers and silane-nanoclay composites for surface impregnation of bridge decks. The investigation included both laboratory and field components. Performance was assessed based on static contact angle, depth of penetration, chloride ion penetration in both cracked and uncracked concrete, chloride diffusivity, surface and bulk resistivity, resistance to frost scaling under deicing chemicals, resistance to rapid freeze-thaw cycling, sorptivity, and water permeability. Characterization of the silane-nanoclay composites was conducted using scanning electron microscopy (SEM), X-ray diffraction (XRD), and Fourier transform infrared spectroscopy (FTIR).

Based on the findings of this investigation, the following conclusions and recommendations are drawn:

- Protectosil SH100 (SIL1) and SIL-ACT-ATS 200 (SIL4) showed the best performance among the sealers evaluated. However, Protectosil SH100 is recommended for applications where chloride ion ingress is the main deterioration mechanism, whereas SIL-ACT-ATS 200 is more suitable for environments where freeze-thaw cycling and surface scaling are the dominant mechanisms of deterioration.

- Protectosil CIT (SIL3) performed the least among all silanes investigated. In comparison, Protectosil S300 exhibited improved performance with respect to chloride resistance, scaling resistance, and reduction of capillary water absorption.

- Surface resistivity measurements obtained under saturated conditions correlated well with chloride ion penetration. Accordingly, surface resistivity may be considered as a viable tool for routine quality control and assessment of chloride barrier performance in silane-treated concrete.

- Silane-nanoclay composites demonstrated improved resistance to freeze-thaw deterioration and slightly enhanced resistance to chloride penetration, particularly after long-term exposure to a 3% NaCl solution. However, it resulted in increased weight loss at higher nanoclay loading ratios (5%) during frost scaling and significantly greater chloride infiltration under high NaCl concentrations. These findings indicate that the performance of silane-nanoclay composites is influenced by the ionic strength of the exposure environment. Based on these observations, further investigation is recommended for silane-nanoclay composites incorporating nanoclays with different organic modifiers and particle sizes other than those used in this study.

- Silane–nanoclay composites demonstrated improved crack-sealing capability, as evidenced by their ability to effectively reduced chloride ingress in cracked concrete

- The estimated service life of Protectosil SH100 and SIL-ACT-ATS 200 was 5.4 and 5.0 yr, respectively. For silane-nanoclay composites, the estimated service life was 5.8 and 6.1 yr for loading ratios of 2.5% and 5.0%, respectively. These estimates for silane-nanoclay composites should be considered with caution because the validity of the SHRP C-103

procedure to silane-nanoclay composites was not demonstrated. In addition, the system exhibited poor performance in surface scaling and higher susceptibility to chloride ions infiltration in aggressive environments.

# Chapter 8: References


AASHTO, T259. " Standard method of test for resistance of concrete to chloride ion penetration." *American Association of State Highway and Transportation Officials* (2002).

AASHTO, T260. “Standard method of test for sampling and testing for chloride ion in concrete and concrete raw materials." *American Association of State Highway and Transportation Officials* (1997).

AASHTO, TP95. "Standard method of test for surface resistivity indication of concrete’s ability to resist chloride ion penetration." *AASHTO Provisional Standards* (2011): 78-86.

Adil, Goran, John T. Kevern, and Danny X. Xiao. "Influence of Penetrating Sealer on Performance of Concrete Joints." *ACI Materials Journal* 118, no. 5 (2021).

American Road & Transportation Builders Association. *2025 ARTBA Bridge Report*.

American Society of Civil Engineers. *2021 report card for America’s infrastructure: Bridges (2021)*.

ASTM, C. "Standard test method for acid-soluble chloride in mortar and concrete." *West Conshohocken, PA, ASTM International* (2012).

ASTM, C. "Standard test method for measurement of rate of absorption of water by hydraulic-cement concretes." *West Conshohocken, PA* (2013).

Azarsa, Pejman, and Rishi Gupta. "Electrical resistivity of concrete for durability evaluation: a review." Advances in Materials Science and Engineering 2017.1 (2017): 8453095.

Cady, Philip D. Sealers for portland cement concrete highway facilities. No. Project 20-5 FY 1992. (1994).

Carette, Jérôme, et al. "Advanced characterisation of the early age behaviour of bulk hydrophobic mortars." Construction and Building Materials 267 (2021): 120904.

Carter, Paul D. "Evaluation of dampproofing performance and effective penetration depth of silane sealers in concrete." Special Publication 151 (1994): 95-118.

Coppola, Luigi, et al. "Chloride diffusion in concrete protected with a silane-based corrosion inhibitor." Materials 13.8 (2020): 2001.

Dai, Jian-Guo, Y. Akira, F. H. Wittmann, H. Yokota, and Peng Zhang. "Water repellent surface impregnation for extension of service life of reinforced concrete structures in marine environments: The role of cracks." *Cement and Concrete Composites* 32, no. 2 (2010): 101-109.

Di Mundo, Rosa, et al. "Recent advances in hydrophobic and icephobic surface treatments of concrete." Coatings 10.5 (2020): 449.

Ganguly, Saheli, Kausik Dana, Tapas Kumar Mukhopadhyay, T. K. Parya, and Sankar Ghatak. "Organophilic nano clay: a comprehensive review." *Transactions of the Indian Ceramic Society* 70, no. 4 (2011): 189-206.

Gupta, Piyush, Vaibhav Sharma, and Garima Nagpal. "A comprehensive review of nano clay: From development and applications to research opportunities." *Environmental Progress & Sustainable Energy* 44, no. 6 (2025): e70055.

Issa, Ahmed A., and Adriaan S. Luyt. "Kinetics of alkoxysilanes and organoalkoxysilanes polymerization: a review." Polymers 11.3 (2019): 537.

Li, Guo, Jiang Yue, Chenhao Guo, and Yongsheng Ji. "Influences of modified nanoparticles on hydrophobicity of concrete with organic film coating." *Construction and Building Materials* 169 (2018): 1-7.

McCarter, W. J. "Assessing the protective qualities of treated and untreated concrete surfaces under cyclic wetting and drying." *Building and environment,* 31.6 (1996): 551-556.

Nagaoka, S., K. Nakayama, and M. Iwanami. "A basic study on the evaluation of the protective effect of silane-based impregnation on mortar using electrochemical impedance spectroscopy." Life-Cycle of Structures and Infrastructure Systems. CRC Press, 2023. 3388-3395.

Nguyen, Thang Duc. Development of silane/siloxane emulsions for application in building protection. Diss. Victoria University of Technology, (1996).

Pfeifer, Donald Wayne, and Mauro J. Scali. "Concrete sealers for protection of bridge structures." *NCHRP report* 244 (1981).

Sakr, M. R., and M. T. Bassuoni. "Silane and methyl-methacrylate based nanocomposites as coatings for concrete exposed to salt solutions and cyclic environments." *Cement and Concrete Composites* 115 (2021): 103841.

Scarfato, Paola, Luciano Di Maio, Maria Letizia Fariello, Paola Russo, and Loredana Incarnato. "Preparation and evaluation of polymer/clay nanocomposite surface treatments for concrete durability enhancement." *Cement and Concrete Composites* 34, no. 3 (2012): 297-305.

Tittarelli, Francesca, and Giacomo Moriconi. "The effect of silane-based hydrophobic admixture on corrosion of reinforcing steel in concrete." *Cement and Concrete Research* 38, no. 11 (2008): 1354-1357.

Uddin, Faheem. "Clays, nanoclays, and montmorillonite minerals." *Metallurgical and Materials Transactions A* 39, no. 12 (2008): 2804-2814.

Weyers, Richard E., Jerry Zemajtis, and Rick O. Drumm. "Service lives of concrete sealers." *Transportation research record* (1995):1490.

Wittmann, Folker H., P. Guo, and T. Zhao. "Influence of cracks on the efficiency of surface impregnation of concrete." *5th International Conference on Water Repellent Treatment of Building Materials Aedificatio Publishers*, 287-298 (2008).

Wong, Hong S., et al. "Hydrophobic concrete using wastepaper sludge ash." Cement and Concrete Research 70 (2015): 9-20.

Woo, Ricky SC, Honggang Zhu, Michael MK Chow, Christopher KY Leung, and Jang-Kyo Kim. "Barrier performance of silane–clay nanocomposite coatings on concrete structure." *Composites science and technology* 68, no. 14 (2008): 2828-2836.

Xiao, Danny X., Goran Adil, John Kevern, and Sam Owusu-Ababio. "Field performance of concrete pavement joints protected by silane sealer: Case study." *Journal of Performance of Constructed Facilities* 35, no. 6 (2021): 04021089.

Zheng, Meng, Lu Zhang, and Yakai Feng. "A review on silane and siloxane materials: Enhancing durability of cementitious materials through surface treatments." *Journal of Materials Science* 59, no. 23 (2024): 10119-10139.